International
Progress Report

IPR-02-12

Äspö Hard Rock Laboratory

Fracture network models in three dimensions for four 30m cubes located at a depth region of 380-500m at Äspö HRL

Pinnaduwa H.S.W Kulatilake
Jeong-Gi Um

Kulatilake & Associates

March 2002

Svensk Kärnbränslehantering AB
Swedish Nuclear Fuel
and Waste Management Co
Box 5864
SE-102 40 Stockholm Sweden
Tel +46 8 459 84 00
Fax +46 8 661 57 19

Äspö Hard Rock
Laboratory

Report no.	No.
IPR-02-12	F102K
Author	Date
Kulatilake, Um	01-12-03
Checked by	Date
Christer Andersson Rolf Christiansson	02-04-03
Approved	Date
Christer Svemar	02-04-09

Äspö Hard Rock Laboratory

Fracture network models in three dimensions for four 30m cubes located at a depth region of 380-500m at Äspö HRL

Pinnaduwa H.S.W Kulatilake
Jeong-Gi Um

Kulatilake & Associates

March 2002

Keywords: 3D-fracture network, DFN, Rock block

Abstract

The location of a rock mass volume termed the NGI's (Norwegian Geotechnical Institute's) box in the three-dimensional (3-D) space at the ÄSPÖ Hard Rock Laboratory is shown using the Rectangular Cartesian Coordinate data provided by the NGI. This box was divided into 480 blocks of 30m cubes. The NGI has provided the three-dimensional coordinates for the center of each cube. The orientation and location data given for the three boreholes KAS02, KA2598A and KA2511A are used to show the location of the boreholes in the three dimensional space with respect to the location of the NGI box. It was found that the borehole KA2511A only just touches the NGI box. The other two boreholes were found to intersect the NGI box. The lithology data provided for the boreholes KAS02 and KA2598A are used to select the following four 30m cubes from the NGI box, each having a different lithology which is given below: (a) NGI block number 409---Äspö diorite; (b) NGI block number 169----Småland granite; (c) NGI block number 5---fine grained granite; (d) NGI block number 49----a mixed lithology consisting of about 49% Småland granite, 22% Äspö diorite, 15% greenstone and 14% fine grained granite. The fracture data provided are used to develop and validate a stochastic 3-D fracture network model for each of the selected 4 NGI blocks.

Sammanfattning

Läget för bergvolymen benämnd NGI-volymen (Norges Geotekniska Institut) i Äspö Hard Rock Laboratory är presenterad i ett koordinatsystem erhållet av NGI. Volymen är indelad i 480 kubiska block med en kantlängd av 30 meter. Centrumkoordinaten för varje block är tillhandahållen av NGI. Inmätningsdata från de tre borrhålen KAS02, KA2598A och KA2511A har använts för att undersöka deras respektive läge i rymden i förhållande till NGI-volymen. Det visar sig att borrhålet KA2511A endast passerar en begränsad del av NGI-volymen medan de andra borrhålen penetrerar en större del av volymen. Den erhållna geologiska informationen från borrhålen KAS02 och KA2598A har använts för att välja ut fyra stycken 30 meters block ur NGI-volymen bestående av olika bergarter. De valda blocken och deras huvudsakliga bergarter är: (a) NGI block 409 -- Äspödiorit, (b) NGI block 169 -- Smålandsgranit, (c) NGI block 005 -- finkornig granit, NGI block 049 -- bestående av en blandad geologi med cirka 49% Smålandsgranit, 22% Äspödiorit, 15% grönsten och 14% finkornig granit. Erhållen data från sprickkarteringen användes för att bestämma och validera en stokastiskt 3-D sprickmodell för vart och ett av de 4 blocken ur NGI-volymen.

Table of Contents

ABSTRACT **i**

SAMMANFATTNING **iii**

1 INTRODUCTION **3**

2 SELECTION OF 4 CUBIC BLOCKS HAVING DIFFERENT LITHOLOGY **11**

3 AVAILABLE FRACTURE DATA FOR THE PROJECT **13**

4 STOCHASTIC 3-D FRACTURE NETWORK MODEL FOR ÄSPÖ DIORITE ROCK MASS (NGI BLOCK NUMBER 409) **17**

4.1 Number of Fracture Sets and Correction for Orientation Bias 17
4.2 Orientation Distribution for Each Fracture Set 26
4.3 Trace Length and Size Distributions for Each Fracture Set 34
4.4 Spacing Distribution and 1-D Fracture frequency for Each Fracture Set 34
4.5 1-D Fracture frequency in any Direction in 3-D 39
4.6 Mean Estimates for Block Size, Number of Blocks per Unit Volume and Number of Fractures per Unit Volume 39
4.7 Fracture System Generation in 3-D and Validation 44

5 STOCHASTIC 3-D FRACTURE NETWORK MODEL FOR SMÅLAND GRANITE ROCK MASS (NGI BLOCK NUMBER 169) **49**

5.1 Number of Fracture Sets and Correction for Orientation Bias 49
5.2 Orientation Distribution for Each Fracture Set 60
5.3 Trace Length and Size Distributions for Each Fracture Set 60
5.4 Spacing Distribution and 1-D Fracture frequency for Each Fracture Set 69
5.5 1-D Fracture frequency in any Direction in 3-D 71
5.6 Mean Estimates for Block Size, Number of Blocks per Unit Volume and Number of Fractures per Unit Volume 71
5.7 Fracture System Generation in 3-D and Validation 71

6 STOCHASTIC 3-D FRACTURE NETWORK MODEL FOR FINE-GRAINED GRANITE ROCK MASS (NGI BLOCK NUMBER 5) **79**

6.1 Number of Fracture Sets and Correction for Orientation Bias 79
6.2 Orientation Distribution for Each Fracture Set 88
6.3 Trace Length and Size Distributions for Each Fracture Set 88
6.4 Spacing Distribution and 1-D Fracture frequency for Each Fracture Set 95
6.5 1-D Fracture frequency in any Direction in 3-D 97
6.6 Mean Estimates for Block Size, Number of Blocks per Unit Volume and Number of Fractures per Unit Volume 97
6.7 Fracture System Generation in 3-D and Validation 99

7 STOCHASTIC 3-D FRACTURE NETWORK MODEL FOR NGI BLOCK NUMBER 49 **105**

7.1 Number of Fracture Sets and Correction for Orientation Bias 105
7.2 Orientation Distribution for Each Fracture Set 114
7.3 Trace Length and Size Distributions for Each Fracture Set 114
7.4 Spacing Distribution and 1-D Fracture frequency for Each Fracture Set 121
7.5 1-D Fracture frequency in any Direction in 3-D 123
7.6 Mean Estimates for Block Size, Number of Blocks per Unit Volume and Number of Fractures per Unit Volume 123
7.7 Fracture System Generation in 3-D and Validation 127

8 CONCLUSIONS **131**

REFERENCES **133**

1 Introduction

The Norwegion Geotechnical Institute (NGI) has selected a rock block volume located at a depth region of 380-500 m at Äspö Hard Rock Laboratory (HRL), Sweden. This block volume is termed as NGI's box. Table 1.1 provides the Rectangular Cartesian Coordinates of the corners of the NGI box. Figure 1.1 shows this box in three-dimensions. The box is 600m in length, 180m in width and 120m in height. This box is divided into 480 thirty-meter cubic blocks. Total height of the NGI box is separated into 4 layers, each layer of 30m thickness (top layer: 380-410m; 2nd layer from top: 410-440m; 3rd layer from top: 440-470m; bottom layer: 470-500m). In the length and width directions, the NGI box is divided into 20 and 6 cubes, respectively. The cubic blocks are numbered as shown in Figure 1.2 starting from the top northwest corner of the NGI box. As shown in Figure 1.2, the first layer has 120 cubic blocks. Similarly, the cubic blocks of the 2nd, 3rd and bottom layers are numbered in that order to end up with the number 480 at the bottom, southeast corner of the NGI box. NGI has provided the center coordinates for each cubic block of the NGI box (Table 1.2).

The objective of this study is to select 4 cubic blocks of 30m from the NGI box, each having a different lithology, and then to develop the fracture network in three dimensions for each of these cubes. In conducting this research, it was necessary to use only the information provided by SKB through given reports and data supplied through electronic files. These cubic blocks will be used in a later study to perform three-dimensional stress analysis to estimate strength and deformability of the rock blocks.

Table 1.1 Corner co-ordinates of NGI´s box model

	Northing, X (m)	Easting Y (m)	Z1 (m)	Z2 (m)
1	7342.515	1828.096	500	
2	7342.515	1828.096		380
3	7379.144	2426.977	500	
4	7379.144	2426.977		380
5	7162.851	1839.084	500	
6	7162.851	1839.084		380
7	7199.48	2437.965	500	
8	7199.48	2437.965		380

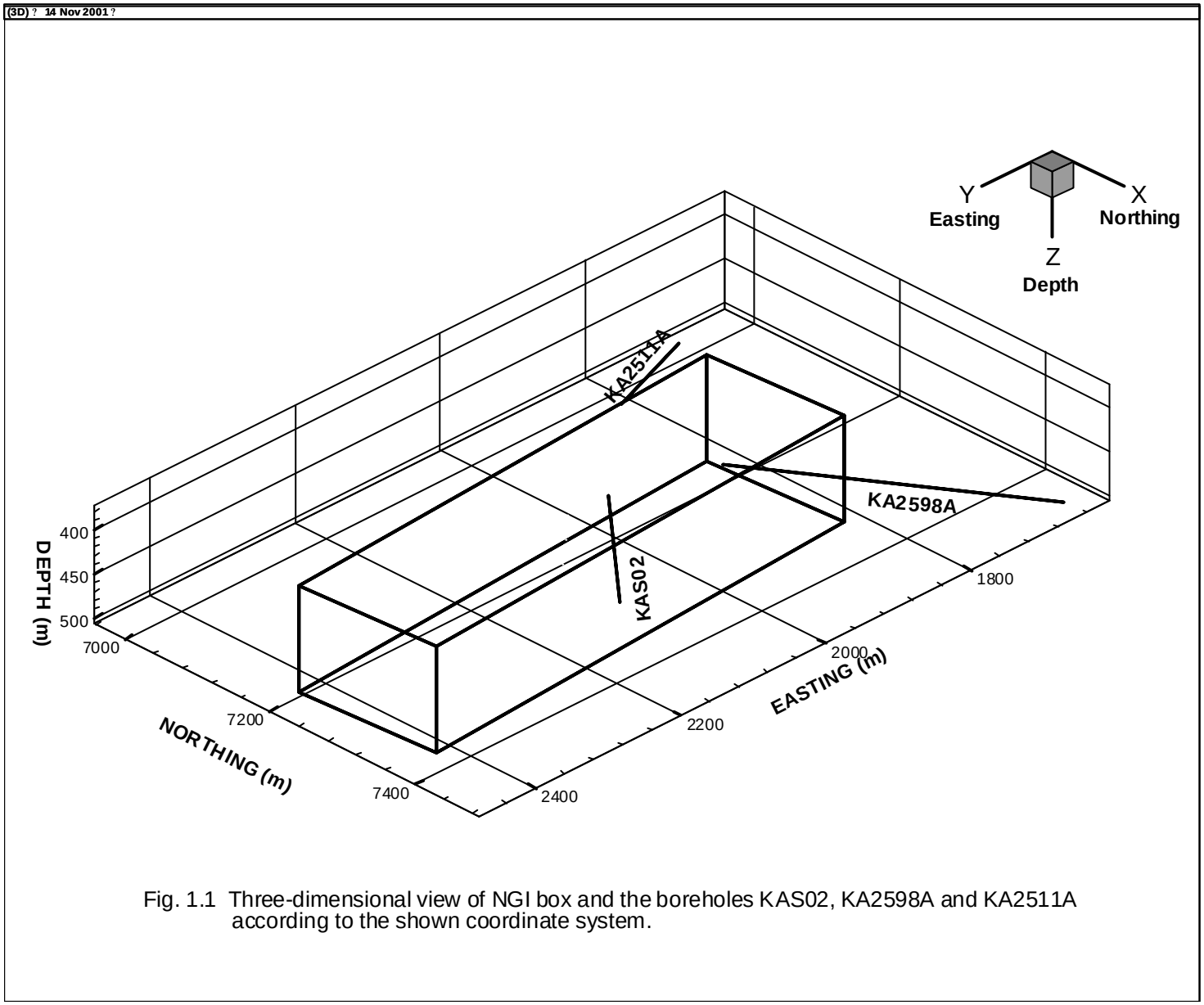

Fig. 1.1 Three-dimensional view of NGI box and the boreholes KAS02, KA2598A and KA2511A according to the shown coordinate system.

1	2	3	4	5	6	7	8	9	10	11	12	13	14	15	16	17	18	19	20
21	22	23	24	25	26	27	28	29	30	31	32	33	34	35	36	37	38	39	40
41	42	43	44	45	46	47	48	49	50	51	52	53	54	55	56	57	58	59	60
61	62	63	64	65	66	67	68	69	70	71	72	73	74	75	76	77	78	79	80
81	82	83	84	85	86	87	88	89	90	91	92	93	94	95	96	97	98	99	100
101	102	103	104	105	106	107	108	109	110	111	112	113	114	115	116	117	118	119	120

Fig. 1.2 *Block numbers for the topmost layer (380-410m) of NGI box*

Table 1.2 Co-ordinates for block centers of NGI box

Block Number	X (m)	Y (m)	Z (m)	Block Number	X (m)	Y (m)	Z (m)	Block Number	X (m)	Y (m)	Z (m)
1	7328.46	1843.98	395	43	7272.23	1907.53	395	85	7216.01	1971.09	395
2	7330.29	1873.93	395	44	7274.07	1937.48	395	86	7217.84	2001.03	395
3	7332.12	1903.87	395	45	7275.90	1967.42	395	87	7219.67	2030.97	395
4	7333.95	1933.82	395	46	7277.73	1997.37	395	88	7221.50	2060.92	395
5	7335.78	1963.76	395	47	7279.56	2027.31	395	89	7223.33	2090.86	395
6	7337.62	1993.70	395	48	7281.39	2057.26	395	90	7225.17	2120.81	395
7	7339.45	2023.65	395	49	7283.22	2087.20	395	91	7227.00	2150.75	395
8	7341.28	2053.59	395	50	7285.05	2117.14	395	92	7228.83	2180.69	395
9	7343.11	2083.54	395	51	7286.89	2147.09	395	93	7230.66	2210.64	395
10	7344.94	2113.48	395	52	7288.72	2177.03	395	94	7232.49	2240.58	395
11	7346.77	2143.42	395	53	7290.55	2206.98	395	95	7234.32	2270.53	395
12	7348.60	2173.37	395	54	7292.38	2236.92	395	96	7236.15	2300.47	395
13	7350.44	2203.31	395	55	7294.21	2266.86	395	97	7237.99	2330.41	395
14	7352.27	2233.26	395	56	7296.04	2296.81	395	98	7239.82	2360.36	395
15	7354.10	2263.20	395	57	7297.87	2326.75	395	99	7241.65	2390.30	395
16	7355.93	2293.14	395	58	7299.71	2356.70	395	100	7243.48	2420.25	395
17	7357.76	2323.09	395	59	7301.54	2386.64	395	101	7178.74	1853.14	395
18	7359.59	2353.03	395	60	7303.37	2416.58	395	102	7180.57	1883.09	395
19	7361.42	2382.98	395	61	7238.63	1849.48	395	103	7182.40	1913.03	395
20	7363.26	2412.92	395	62	7240.46	1879.42	395	104	7184.23	1942.97	395
21	7298.51	1845.82	395	63	7242.29	1909.37	395	105	7186.06	1972.92	395
22	7300.35	1875.76	395	64	7244.12	1939.31	395	106	7187.90	2002.86	395
23	7302.18	1905.70	395	65	7245.95	1969.25	395	107	7189.73	2032.81	395
24	7304.01	1935.65	395	66	7247.78	1999.20	395	108	7191.56	2062.75	395
25	7305.84	1965.59	395	67	7249.62	2029.14	395	109	7193.39	2092.69	395
26	7307.67	1995.54	395	68	7251.45	2059.09	395	110	7195.22	2122.64	395
27	7309.50	2025.48	395	69	7253.28	2089.03	395	111	7197.05	2152.58	395
28	7311.33	2055.42	395	70	7255.11	2118.97	395	112	7198.88	2182.53	395
29	7313.17	2085.37	395	71	7256.94	2148.92	395	113	7200.72	2212.47	395
30	7315.00	2115.31	395	72	7258.77	2178.86	395	114	7202.55	2242.41	395
31	7316.83	2145.26	395	73	7260.60	2208.81	395	115	7204.38	2272.36	395
32	7318.66	2175.20	395	74	7262.44	2238.75	395	116	7206.21	2302.30	395
33	7320.49	2205.14	395	75	7264.27	2268.69	395	117	7208.04	2332.25	395
34	7322.32	2235.09	395	76	7266.10	2298.64	395	118	7209.87	2362.19	395
35	7324.16	2265.03	395	77	7267.93	2328.58	395	119	7211.70	2392.13	395
36	7325.99	2294.98	395	78	7269.76	2358.53	395	120	7213.54	2422.08	395
37	7327.82	2324.92	395	79	7271.59	2388.47	395	121	7328.46	1843.98	425
38	7329.65	2354.86	395	80	7273.42	2418.42	395	122	7330.29	1873.93	425
39	7331.48	2384.81	395	81	7208.68	1851.31	395	123	7332.12	1903.87	425
40	7333.31	2414.75	395	82	7210.51	1881.25	395	124	7333.95	1933.82	425
41	7268.57	1847.65	395	83	7212.35	1911.20	395	125	7335.78	1963.76	425
42	7270.40	1877.59	395	84	7214.18	1941.14	395	126	7337.62	1993.70	425

Table 1.2 Continued

Block Number	X (m)	Y (m)	Z (m)	Block Number	X (m)	Y (m)	Z (m)	Block Number	X (m)	Y (m)	Z (m)
127	7339.45	2023.65	425	173	7290.55	2206.98	425	217	7237.99	2330.41	425
128	7341.28	2053.59	425	174	7292.38	2236.92	425	218	7239.82	2360.36	425
129	7343.11	2083.54	425	175	7294.21	2266.86	425	219	7241.65	2390.30	425
130	7344.94	2113.48	425	176	7296.04	2296.81	425	220	7243.48	2420.25	425
131	7346.77	2143.42	425	177	7297.87	2326.75	425	221	7178.74	1853.14	425
132	7348.60	2173.37	425	178	7299.71	2356.70	425	222	7180.57	1883.09	425
133	7350.44	2203.31	425	179	7301.54	2386.64	425	223	7182.40	1913.03	425
134	7352.27	2233.26	425	180	7303.37	2416.58	425	224	7184.23	1942.97	425
135	7354.10	2263.20	425	181	7238.63	1849.48	425	225	7186.06	1972.92	425
136	7355.93	2293.14	425	182	7240.46	1879.42	425	226	7187.90	2002.86	425
137	7357.76	2323.09	425	183	7242.29	1909.37	425	227	7189.73	2032.81	425
138	7359.59	2353.03	425	184	7244.12	1939.31	425	228	7191.56	2062.75	425
139	7361.42	2382.98	425	185	7245.95	1969.25	425	229	7193.39	2092.69	425
140	7363.26	2412.92	425	186	7247.78	1999.20	425	230	7195.22	2122.64	425
141	7298.51	1845.82	425	187	7249.62	2029.14	425	231	7197.05	2152.58	425
142	7300.35	1875.76	425	188	7251.45	2059.09	425	232	7198.88	2182.53	425
143	7302.18	1905.70	425	189	7253.28	2089.03	425	233	7200.72	2212.47	425
144	7304.01	1935.65	425	190	7255.11	2118.97	425	234	7202.55	2242.41	425
145	7305.84	1965.59	425	191	7256.94	2148.92	425	235	7204.38	2272.36	425
146	7307.67	1995.54	425	192	7258.77	2178.86	425	236	7206.21	2302.30	425
147	7309.50	2025.48	425	193	7260.60	2208.81	425	237	7208.04	2332.25	425
148	7311.33	2055.42	425	194	7262.44	2238.75	425	238	7209.87	2362.19	425
149	7313.17	2085.37	425	195	7264.27	2268.69	425	239	7211.70	2392.13	425
150	7315.00	2115.31	425	196	7266.10	2298.64	425	240	7213.54	2422.08	425
151	7316.83	2145.26	425	197	7267.93	2328.58	425	241	7328.46	1843.98	455
152	7318.66	2175.20	425	198	7269.76	2358.53	425	242	7330.29	1873.93	455
153	7320.49	2205.14	425	199	7271.59	2388.47	425	243	7332.12	1903.87	455
154	7322.32	2235.09	425	200	7273.42	2418.42	425	244	7333.95	1933.82	455
155	7324.16	2265.03	425	201	7208.68	1851.31	425	245	7335.78	1963.76	455
156	7325.99	2294.98	425	202	7210.51	1881.25	425	246	7337.62	1993.70	455
157	7327.82	2324.92	425	203	7212.35	1911.20	425	247	7339.45	2023.65	455
158	7329.65	2354.86	425	204	7214.18	1941.14	425	248	7341.28	2053.59	455
159	7331.48	2384.81	425	205	7216.01	1971.09	425	249	7343.11	2083.54	455
162	7270.40	1877.59	425	206	7217.84	2001.03	425	250	7344.94	2113.48	455
163	7272.23	1907.53	425	207	7219.67	2030.97	425	251	7346.77	2143.42	455
164	7274.07	1937.48	425	208	7221.50	2060.92	425	252	7348.60	2173.37	455
165	7275.90	1967.42	425	209	7223.33	2090.86	425	253	7350.44	2203.31	455
166	7277.73	1997.37	425	210	7225.17	2120.81	425	254	7352.27	2233.26	455
167	7279.56	2027.31	425	211	7227.00	2150.75	425	255	7354.10	2263.20	455
168	7281.39	2057.26	425	212	7228.83	2180.69	425	256	7355.93	2293.14	455
169	7283.22	2087.20	425	213	7230.66	2210.64	425	257	7357.76	2323.09	455
170	7285.05	2117.14	425	214	7232.49	2240.58	425	258	7359.59	2353.03	455
171	7286.89	2147.09	425	215	7234.32	2270.53	425	259	7361.42	2382.98	455
172	7288.72	2177.03	425	216	7236.15	2300.47	425	260	7363.26	2412.92	455

Table 1.2 Continued

Block Number	X (m)	Y (m)	Z (m)	Block Number	X (m)	Y (m)	Z (m)	Block Number	X (m)	Y (m)	Z (m)
261	7298.51	1845.82	455	305	7245.95	1969.25	455	349	7193.39	2092.69	455
262	7300.35	1875.76	455	306	7247.78	1999.20	455	350	7195.22	2122.64	455
263	7302.18	1905.70	455	307	7249.62	2029.14	455	351	7197.05	2152.58	455
264	7304.01	1935.65	455	308	7251.45	2059.09	455	352	7198.88	2182.53	455
265	7305.84	1965.59	455	309	7253.28	2089.03	455	353	7200.72	2212.47	455
266	7307.67	1995.54	455	310	7255.11	2118.97	455	354	7202.55	2242.41	455
267	7309.50	2025.48	455	311	7256.94	2148.92	455	355	7204.38	2272.36	455
268	7311.33	2055.42	455	312	7258.77	2178.86	455	356	7206.21	2302.30	455
269	7313.17	2085.37	455	313	7260.60	2208.81	455	357	7208.04	2332.25	455
270	7315.00	2115.31	455	314	7262.44	2238.75	455	358	7209.87	2362.19	455
271	7316.83	2145.26	455	315	7264.27	2268.69	455	359	7211.70	2392.13	455
272	7318.66	2175.20	455	316	7266.10	2298.64	455	360	7213.54	2422.08	455
273	7320.49	2205.14	455	317	7267.93	2328.58	455	361	7328.46	1843.98	485
274	7322.32	2235.09	455	318	7269.76	2358.53	455	362	7330.29	1873.93	485
275	7324.16	2265.03	455	319	7271.59	2388.47	455	363	7332.12	1903.87	485
276	7325.99	2294.98	455	320	7273.42	2418.42	455	364	7333.95	1933.82	485
277	7327.82	2324.92	455	321	7208.68	1851.31	455	365	7335.78	1963.76	485
278	7329.65	2354.86	455	322	7210.51	1881.25	455	366	7337.62	1993.70	485
279	7331.48	2384.81	455	323	7212.35	1911.20	455	367	7339.45	2023.65	485
280	7333.31	2414.75	455	324	7214.18	1941.14	455	368	7341.28	2053.59	485
281	7268.57	1847.65	455	325	7216.01	1971.09	455	369	7343.11	2083.54	485
282	7270.40	1877.59	455	326	7217.84	2001.03	455	370	7344.94	2113.48	485
283	7272.23	1907.53	455	327	7219.67	2030.97	455	371	7346.77	2143.42	485
284	7274.07	1937.48	455	328	7221.50	2060.92	455	372	7348.60	2173.37	485
285	7275.90	1967.42	455	329	7223.33	2090.86	455	373	7350.44	2203.31	485
286	7277.73	1997.37	455	330	7225.17	2120.81	455	374	7352.27	2233.26	485
287	7279.56	2027.31	455	331	7227.00	2150.75	455	375	7354.10	2263.20	485
288	7281.39	2057.26	455	332	7228.83	2180.69	455	376	7355.93	2293.14	485
289	7283.22	2087.20	455	333	7230.66	2210.64	455	377	7357.76	2323.09	485
290	7285.05	2117.14	455	334	7232.49	2240.58	455	378	7359.59	2353.03	485
291	7286.89	2147.09	455	335	7234.32	2270.53	455	379	7361.42	2382.98	485
292	7288.72	2177.03	455	336	7236.15	2300.47	455	380	7363.26	2412.92	485
293	7290.55	2206.98	455	337	7237.99	2330.41	455	381	7298.51	1845.82	485
294	7292.38	2236.92	455	338	7239.82	2360.36	455	382	7300.35	1875.76	485
295	7294.21	2266.86	455	339	7241.65	2390.30	455	383	7302.18	1905.70	485
296	7296.04	2296.81	455	340	7243.48	2420.25	455	384	7304.01	1935.65	485
297	7297.87	2326.75	455	341	7178.74	1853.14	455	385	7305.84	1965.59	485
298	7299.71	2356.70	455	342	7180.57	1883.09	455	386	7307.67	1995.54	485
299	7301.54	2386.64	455	343	7182.40	1913.03	455	387	7309.50	2025.48	485
300	7303.37	2416.58	455	344	7184.23	1942.97	455	388	7311.33	2055.42	485
301	7238.63	1849.48	455	345	7186.06	1972.92	455	389	7313.17	2085.37	485
302	7240.46	1879.42	455	346	7187.90	2002.86	455	390	7315.00	2115.31	485
303	7242.29	1909.37	455	347	7189.73	2032.81	455	391	7316.83	2145.26	485
304	7244.12	1939.31	455	348	7191.56	2062.75	455	392	7318.66	2175.20	485

Table 1.2 Continued

Block Number	X (m)	Y (m)	Z (m)	Block Number	X (m)	Y (m)	Z (m)	Block Number	X (m)	Y (m)	Z (m)
393	7320.49	2205.14	485	423	7242.29	1909.37	485	453	7230.66	2210.64	485
394	7322.32	2235.09	485	424	7244.12	1939.31	485	454	7232.49	2240.58	485
395	7324.16	2265.03	485	425	7245.95	1969.25	485	455	7234.32	2270.53	485
396	7325.99	2294.98	485	426	7247.78	1999.20	485	456	7236.15	2300.47	485
397	7327.82	2324.92	485	427	7249.62	2029.14	485	457	7237.99	2330.41	485
398	7329.65	2354.86	485	428	7251.45	2059.09	485	458	7239.82	2360.36	485
399	7331.48	2384.81	485	429	7253.28	2089.03	485	459	7241.65	2390.30	485
400	7333.31	2414.75	485	430	7255.11	2118.97	485	460	7243.48	2420.25	485
401	7268.57	1847.65	485	431	7256.94	2148.92	485	461	7178.74	1853.14	485
402	7270.40	1877.59	485	432	7258.77	2178.86	485	462	7180.57	1883.09	485
403	7272.23	1907.53	485	433	7260.60	2208.81	485	463	7182.40	1913.03	485
404	7274.07	1937.48	485	434	7262.44	2238.75	485	464	7184.23	1942.97	485
405	7275.90	1967.42	485	435	7264.27	2268.69	485	465	7186.06	1972.92	485
406	7277.73	1997.37	485	436	7266.10	2298.64	485	466	7187.90	2002.86	485
407	7279.56	2027.31	485	437	7267.93	2328.58	485	467	7189.73	2032.81	485
408	7281.39	2057.26	485	438	7269.76	2358.53	485	468	7191.56	2062.75	485
409	7283.22	2087.20	485	439	7271.59	2388.47	485	469	7193.39	2092.69	485
410	7285.05	2117.14	485	440	7273.42	2418.42	485	470	7195.22	2122.64	485
411	7286.89	2147.09	485	441	7208.68	1851.31	485	471	7197.05	2152.58	485
412	7288.72	2177.03	485	442	7210.51	1881.25	485	472	7198.88	2182.53	485
413	7290.55	2206.98	485	443	7212.35	1911.20	485	473	7200.72	2212.47	485
414	7292.38	2236.92	485	444	7214.18	1941.14	485	474	7202.55	2242.41	485
415	7294.21	2266.86	485	445	7216.01	1971.09	485	475	7204.38	2272.36	485
416	7296.04	2296.81	485	446	7217.84	2001.03	485	476	7206.21	2302.30	485
417	7297.87	2326.75	485	447	7219.67	2030.97	485	477	7208.04	2332.25	485
418	7299.71	2356.70	485	448	7221.50	2060.92	485	478	7209.87	2362.19	485
419	7301.54	2386.64	485	449	7223.33	2090.86	485	479	7211.70	2392.13	485
420	7303.37	2416.58	485	450	7225.17	2120.81	485	480	7213.54	2422.08	485
421	7238.63	1849.48	485	451	7227.00	2150.75	485				
422	7240.46	1879.42	485	452	7228.83	2180.69	485				

2 Selection of 4 cubic blocks having different lithology

Based on the data provided by SKB, lithology information is available for the boreholes KAS02, KA2598A and KA2511A. The orientation and location data for these three boreholes are given in Table 2.1. Figure 1.1 shows the location of these boreholes in three-dimensions with respect to the NGI box. Plan view of the NGI box and the boreholes are shown in Figure 2.1. From these figures, it is clear that borehole KA2511A only touches the NGI box. Therefore, the lithology information of borehole KA 2511A is not useful in selecting the 4 cubic blocks from the NGI box. However, the lithology data of the other two boreholes are useful in selecting the 4 cubic blocks. Figures 2.2 and 2.3 provide lithology data of the boreholes KAS02 and KA2598A, respectively.

In the borehole KAS02, at the depth region 470-500m the rock type is Äspö diorite. At the mid-point of this depth region (485m) the borehole KAS02 has the coordinates X= 7297.26m and Y= 2093.51m. Note that the coordinates of the center of cubic block # 409 are X= 7283.22m, Y= 2087.20m and Z= 485m (Table 1.2). Comparison of these two coordinate sets show that the borehole KAS02 goes through NGI block number 409 at a depth of 485m. Therefore, cubic block number 409 can be used to represent the fracture system in Äspö diorite rock mass.

In the borehole KAS02, the depth region 410-440m contains about a 25m thick layer of Småland granite and a 5m thick layer of Äspö diorite. Therefore, in this depth region about 84% of the rock type is Småland granite. The X and Y coordinates of the borehole KAS 02 at depth 425m (mid-point of 410-440m depth region) are given by X= 7292.97m and Y= 2097.37m. The center of cubic block number 169 has the coordinates X= 7283.22m, Y=2087.20m and Z= 425m (Table 1.2). Hence it is clear that at depth 425m the borehole KAS02 goes through the cubic block number 169 of NGI box. Therefore cubic block number 169 can be used to represent the fracture system in Småland granite.

Fine-grained granite exists in borehole KA2598A in the depth range 380-410m. The X and Y coordinates of the borehole KA2598A at depth 395m are given by X= 7336.09m and Y= 1957.76m. The center of cubic block number 5 has the coordinates X= 7335.78m, Y= 1963.76m and Z= 395m (Table 1.2). Hence it is clear that at depth 395m the borehole KA2598A goes through the cubic block number 5 of NGI box. Therefore cubic block number 5 can be used to represent the fracture system in fine-grained granite.

Out of the two given boreholes, the highest thickness for greenstone exists in the depth region of 380-410m of borehole KAS02. In addition to greenstone, in this depth region Småland granite, fine-grained granite and Äspö diorite exist. In this depth range, the composition in the borehole is approximately 49% of Småland granite, 22% of Äspö diorite, 15% greenstone and 14% of fine-grained granite. Therefore this depth region can be considered as a fully mixed lithology. The X and Y coordinates of the borehole

KAS02 at depth 395m are given by X= 7290.82m and Y= 2099.30m. The center of cubic block number 49 has the coordinates X= 7283.22m, Y= 2087.20m and Z= 395m (Table 1.2). Hence it is clear that at depth 395m the borehole KAS02 goes through the cubic block number 49 of NGI box. Therefore cubic block number 49 can be used to represent the fracture system in a mixed lithology containing the aforementioned 4 rock types.

Table 2.1 Orientation and location of the boreholes used in this study

Borehole number	Trend (deg.)	Downward plunge (deg.)	Location		
			Northing (m)	Easting (m)	Elevation (m.a.s.l.) (m)
KAS02	318.04	84.50	7261.986	2125.224	7.680
KA2598A	292.60	32.15	7303.926	2035.028	-342.394
KA2511A	234.73	33.36	7210.358	2018.039	-337.479

3 Available fracture data for the project

For the project, raw fracture data were mainly available from the three boreholes KAS02, KA2598A and KA2511A. These data provided fracture orientation and spacing information. However, the number of **quality** orientation data available for different lithologies were quite limited to perform **reliable** analysis for fracture set delineation and estimation of orientation distributions for fracture sets. **No raw data were provided on fracture trace length**. However, some summarized information about fracture size is available in the report by Hermanson et al. (1998?). In overall, fracture data available for the project were quite limited **with respect to both quality and quantity** to build **reliable**, **comprehensive** fracture network models for the selected 4 blocks.

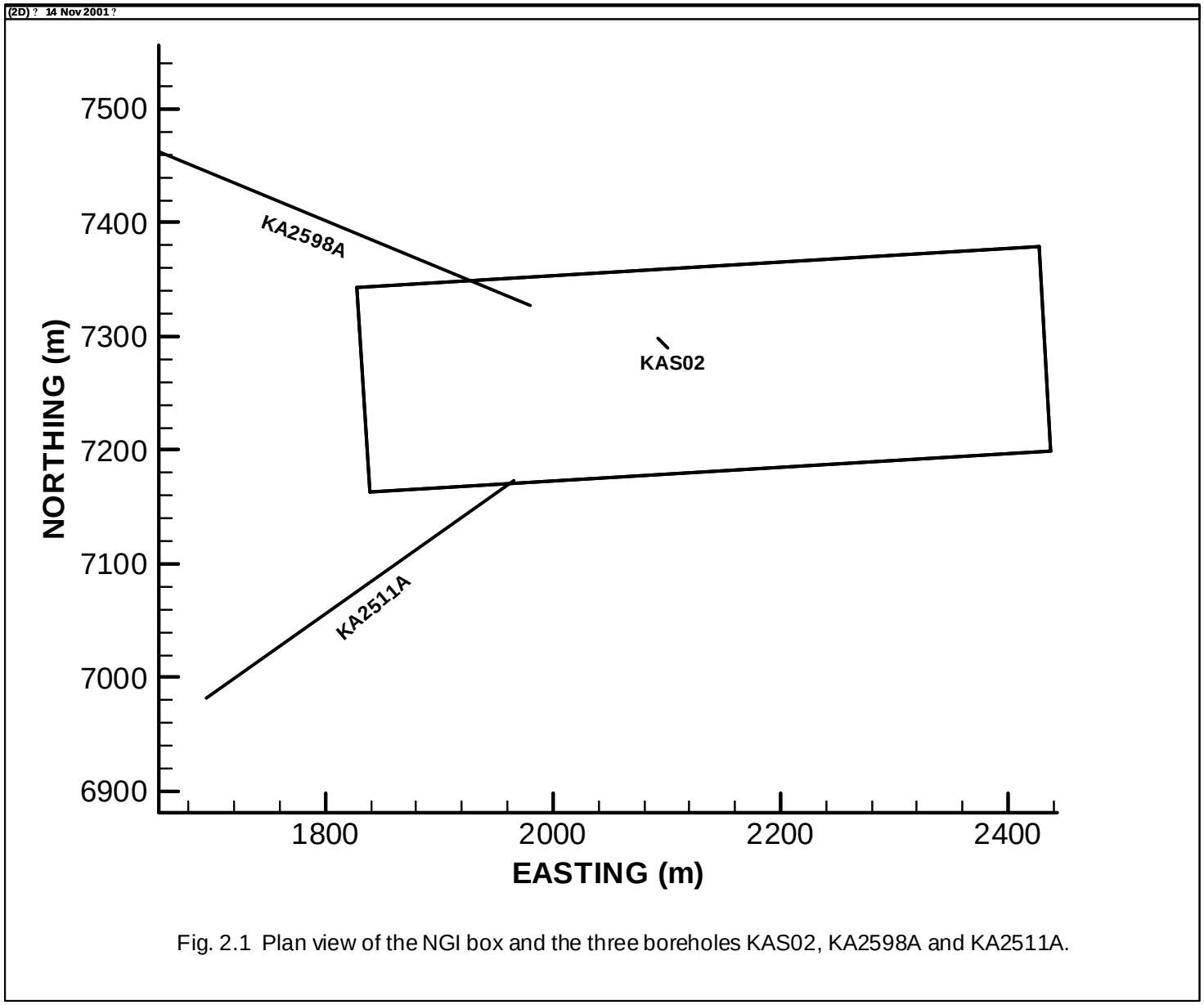

Fig. 2.1 Plan view of the NGI box and the three boreholes KAS02, KA2598A and KA2511A.

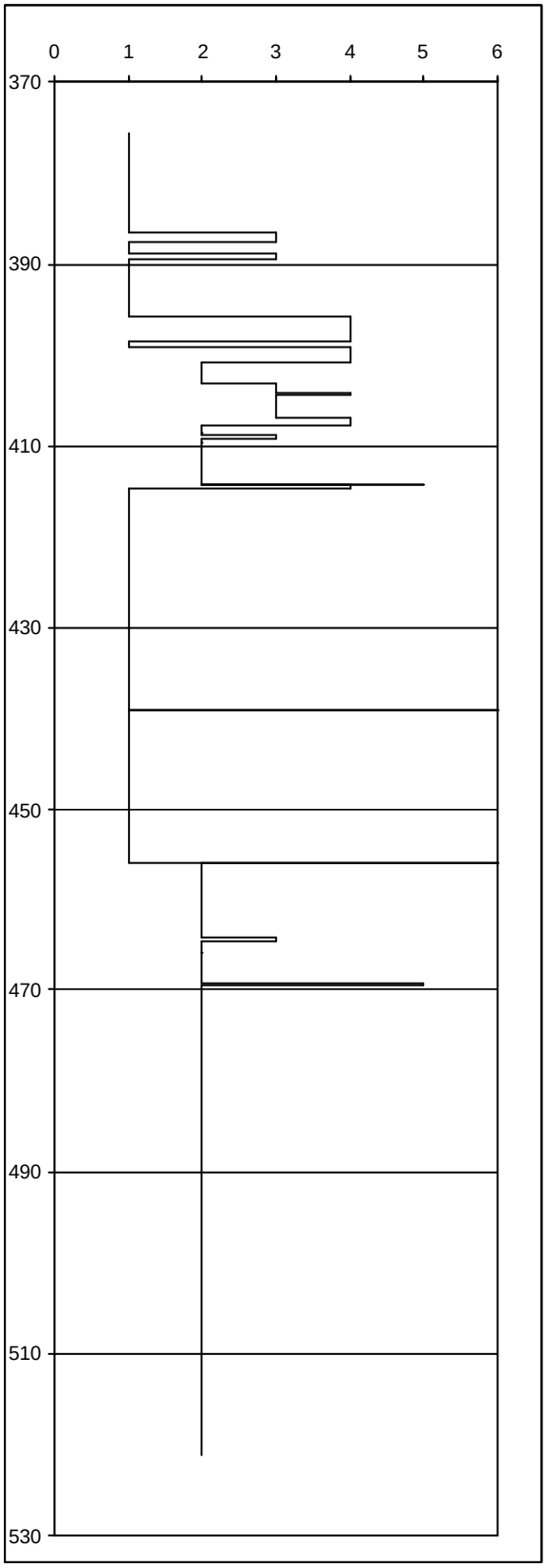

Lithology	Code	
Smaland Granite	PSE	1
Aspo Diorite	PSF	2
Fine-Grained Granite	HSC	3
Greenstone	VB	4
Pegmatite	HSB	5
Mylonite	MTA	6

Fig. 2.2 *Lithology log of borehole KAS02*

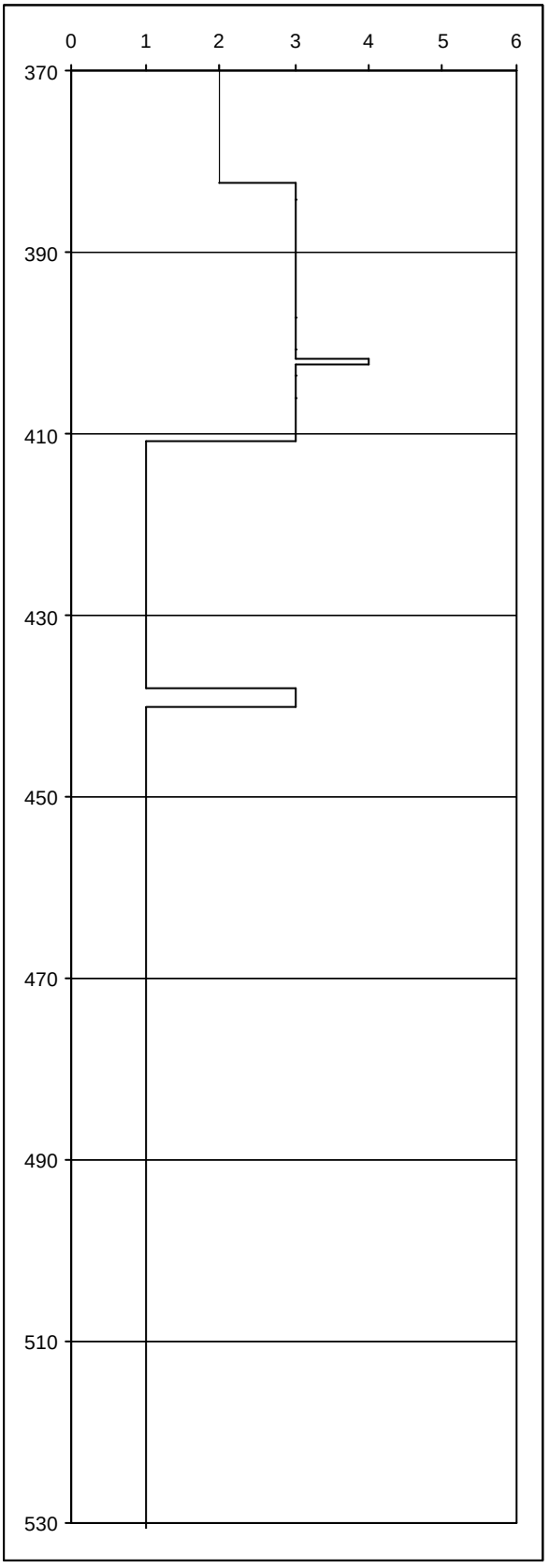

Lithology	Code	
Smaland Granite	PSE	1
Aspo Diorite	PSF	2
Fine-Grained Granite	HSC	3
Greenstone	VB	4
Pegmatite	HSB	5
Mylonite	MTA	6

Fig. 2.3 *Lithology log of borehole KA2598A*

4 Stochastic 3-D fracture network model for Äspö diorite rock mass (NGI block number 409)

4.1 Number of Fracture Sets and Correction for Orientation Bias

NGI block number 409 is located in the depth region of 470-500m of borehole KAS02. However, around this depth region Äspö diorite exists in the depth region 457.4-536.0. In order to enlarge the data base for Äspö diorite, orientation data were obtained from the depth region 457.4-536.0m of borehole KAS02. The fracture data were analyzed using the computer program CLUSDEL-BINGHAM of FRACNTWK software package (Kulatilake, 1998), according to the clustering algorithm of Shanley and Mahtab (1976) and Mahtab and Yegulalp (1984) to find the dense points and the resulting fracture sets. Even though this methodology suggests a procedure for finding the optimum number of fracture sets using three objective functions, for the analyzed data, it was not possible to find a unique number for the optimum number of fracture sets only from the results of this procedure. A number of fracture sets between three and four was found to be suitable according to the results obtained from the applied method. Therefore, the quality of the separation between the fracture sets was considered in addition to the values obtained for objective functions to make a decision on the optimum number of fracture sets. The final results obtained for fracture set delineation are shown in Figure 4.1. All three fracture sets show high variability. This high variability is partly reflected by the low number of data available for orientation analyses. Number of orientation data belonging to each fracture set and the mean directions obtained for the fracture sets are shown in Table 4.1.

The procedures available in the literature for correcting orientation bias (Kulatilake and Wu, 1984a; Wathugala et. al. 1990; Kulatilake 1998) was applied to study the effect of orientation sampling bias on orientation distribution of fracture sets using the computer program OBIAS1D of FRACNTWK software package (Kulatilake, 1998). The expression for the correction has been derived by looking into the probability of intersection between a borehole and each fracture in the fracture set. The expression incorporates the effect of the angle between the borehole direction and each fracture plane belonging to the fracture set, borehole length, borehole diameter and size of each fracture. Note that the capabilities of this correction is far superior to the traditional Terzaghi's (1965) correction that incorporates only the angle between the borehole direction and each fracture plane belonging to the fracture set. The obtained results are shown in Figures 4.2 through 4.4. All three fracture sets intersect with the same borehole. Due to lack of fracture size data, the same probability distribution is used to model fracture size of the 3 fracture sets (see section 4.3). Therefore, comparisons between the 3 fracture sets depend only on the relative orientation distribution between the borehole direction and the directions of fractures of each fracture set. Note that both the borehole and fracture set 1 are almost vertical. Fracture set 3 is sub-horizontal and the angle between fracture set 2 and the borehole direction is about 30 degrees. Due to the aforementioned facts, out of the three fracture sets, fracture set 1 has the lowest chance of intersection with the borehole. However, out of the three fracture sets this fracture set has the lowest orientation variability (see Table 4.2 and section 4.2). It seems that for fracture set 1, the low

(Sketch) ? 14 Nov 2001 ?

Fig. 4.1 Fracture set delineation results on an upper hemispherical polar equal area projection for Aspo diorite (NGI box # 409)

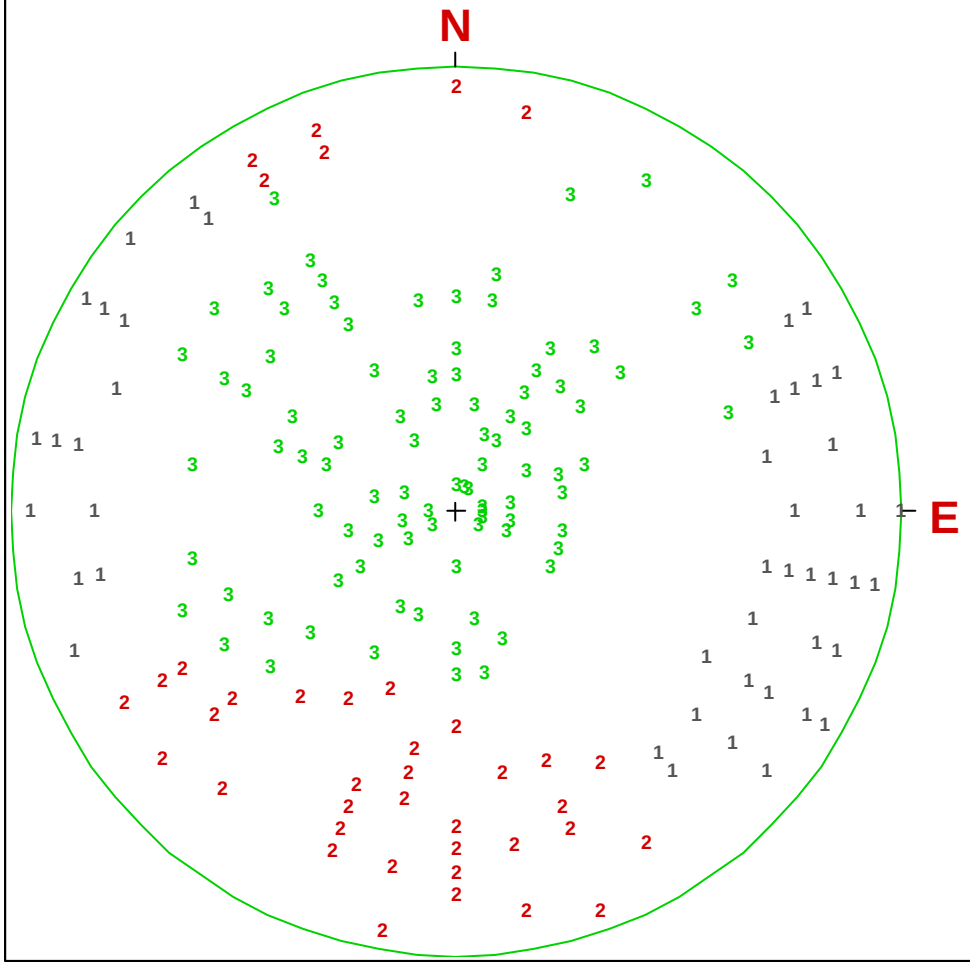

210 POLES

SMALL CIRCLE RADIUS VALUE =
14.25 DEGREES

OBJECTIVE FUNCTION VALUES
F2 = 1.05
F3 = .55
F4 = .53

SYMBOL	FRACTURE SET #	# OF DATA
1	1	50
2	2	52
3	3	108

Table 4.1 Delineated fracture sets and goodness-of-fit results of Bingham distribution for orientation data of Äspö diorite

	Fracture		Mu 3		Mu 2		Mu 1		Chi-square Test			
Nobs.	Set	Npts.	Trend (°)	Plunge (°)	Trend (°)	Plunge (°)	Trend (°)	Plunge (°)	D.F.	chi	95chi	P
210	1	50	101.51	8.70	191.99	3.14	301.85	80.75	2	10.02	5.94	0.007
	2	52	187.11	26.42	292.47	28.07	81.33	49.64	2	6.66	5.94	0.038
	3	108	331.79	77.31	61.93	0.03	151.94	12.69	14	17.68	23.67	0.228

Note:

Nobs.=Number of fractures observed on the borehole

Npts.=Number of fractures belonging to the fracture set

Mu3=Mean normal vector direction (upward) of fracture set

Trend of Mu3=Dip direction of fracture set

Plunge of Mu3=90°-Dip angle of fracture set

Mu2=Vector normal to minor axis plane of Bingham distribution

Mu1=Vector normal to major axis plane of Bingham distribution

DF= Degrees of freedom for Chi-square test for Bingham distribution

Chi=Calculated Chi-square value

95Chi=Table Chi-square value at 5% significance level

P=Maximum significance level at which Bingham distribution can be used to represent the statistical distribution of orientation of fracture set

(a minimum of 0.05 is required to represent orientation data by a Bingham distribution)

(3D) ? 16 Nov 2001 ? NGI BOX #409 (Aspo Diorite)

Fig. 4.2a Observed relative frequency of orientation for fracture set 1 of Aspo diorite (NGI box #409).

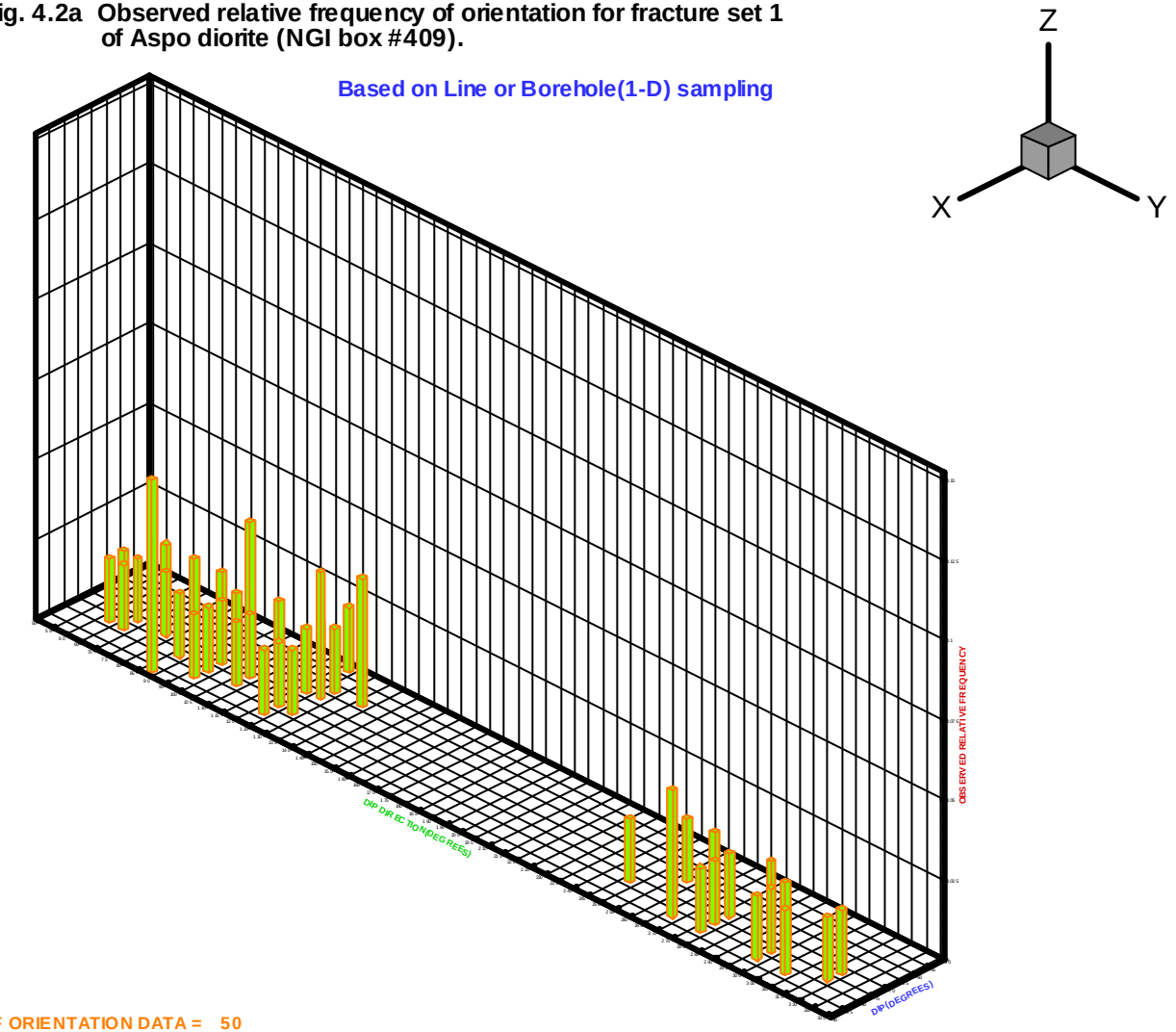

NUMBER OF ORIENTATION DATA = 50
LENGTH OF BOREHOLE = 78.60
TREND OF BOREHOLE = 318.00 (DEG.)
PLUNGE OF BOREHOLE = 85.00 (DEG.)
DIAMETER OF FRACTURE PLANES FROM 5.26 TO 5.26
DIAMETER OF BOREHOLE = .10

A COLUMN REPRESENTS 10 DEGREES(DIP) X 10 DEGREES(DIP DIRE.)
THE MAXIMUM VALUE FOR OBSERVED RELATIVE FREQUENCY = .0600
IT IS LOCATED FROM 85.00 TO 90.00 FOR DIP(DEG.)
AND 85.00 TO 90.00 FOR DIP DIRECTION(DEG.)
THE UNIT FOR LENGTH: Meter

(3D) ? 16 Nov 2001 ? NGI BOX #409 (Aspo Diorite)

Fig. 4.2b Corrected relative frequency of orientation for fracture set 1 of Aspo diorite (NGI box #409).

Based on Line or Borehole(1-D) sampling

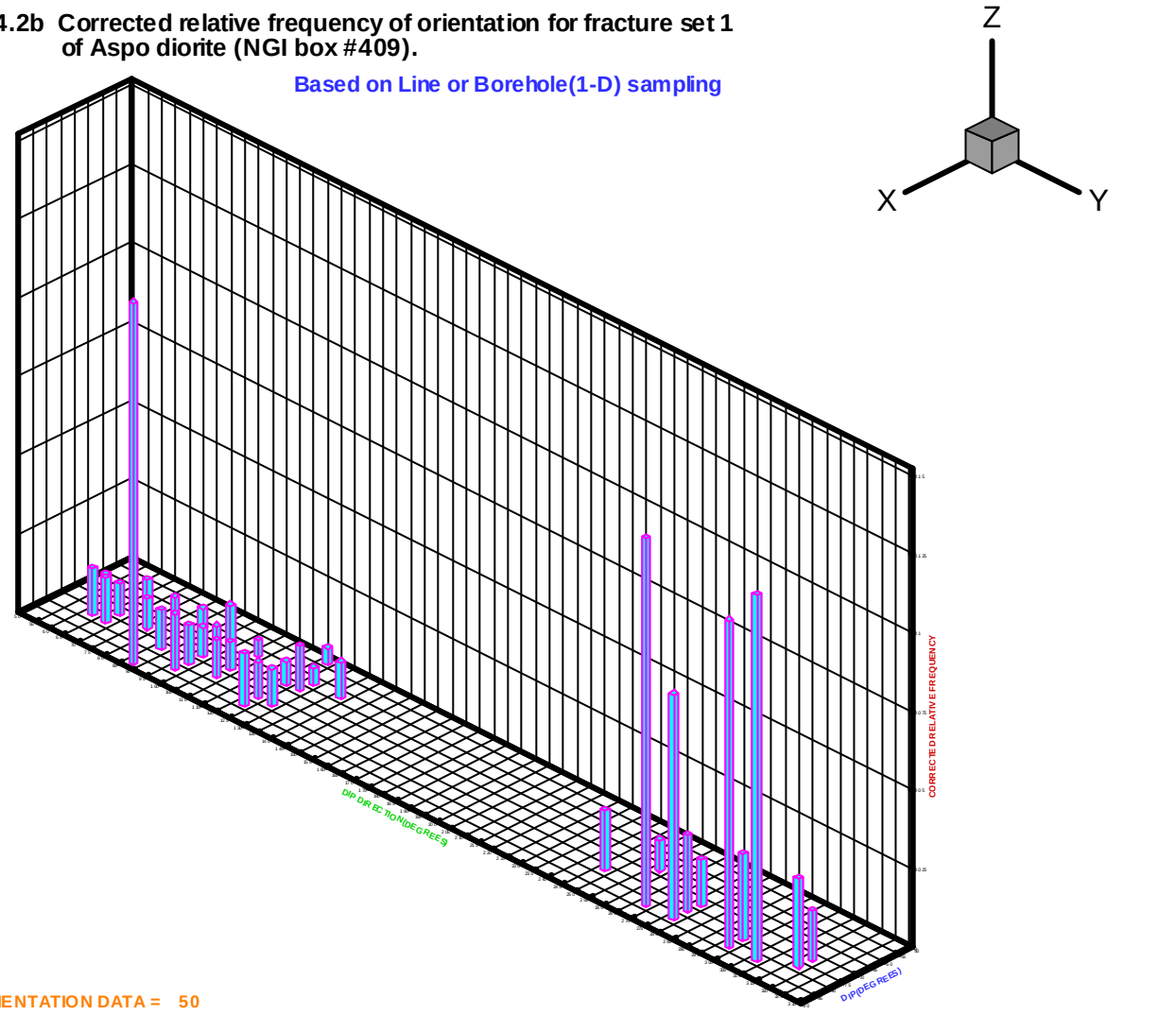

NUMBER OF ORIENTATION DATA = 50
LENGTH OF BOREHOLE = 78.60
TREND OF BOREHOLE = 318.00 (DEG.)
PLUNGE OF BOREHOLE = 85.00 (DEG.)
DIAMETER OF FRACTURE PLANES FROM 5.26 TO 5.26
DIAMETER OF BOREHOLE = .10

A COLUMN REPRESENTS 10 DEGREES(DIP) X 10 DEGREES(DIP DIRE.)
THE MAXIMUM VALUE FOR CORRECTED RELATIVE FREQUENCY = .1170
IT IS LOCATED FROM 80.00 TO 85.00 FOR DIP(DEG.)
AND 265.00 TO 270.00 FOR DIP DIRECTION(DEG.)
THE UNIT FOR LENGTH: Meter

(3D) ? 14 Nov 2001 ? NGI BOX #409 (Aspo Diorite)

Fig. 4.3a Observed relative frequency of orientation for fracture set 2 of Aspo diorite (NGI box #409).

Based on Line or Borehole(1-D) sampling

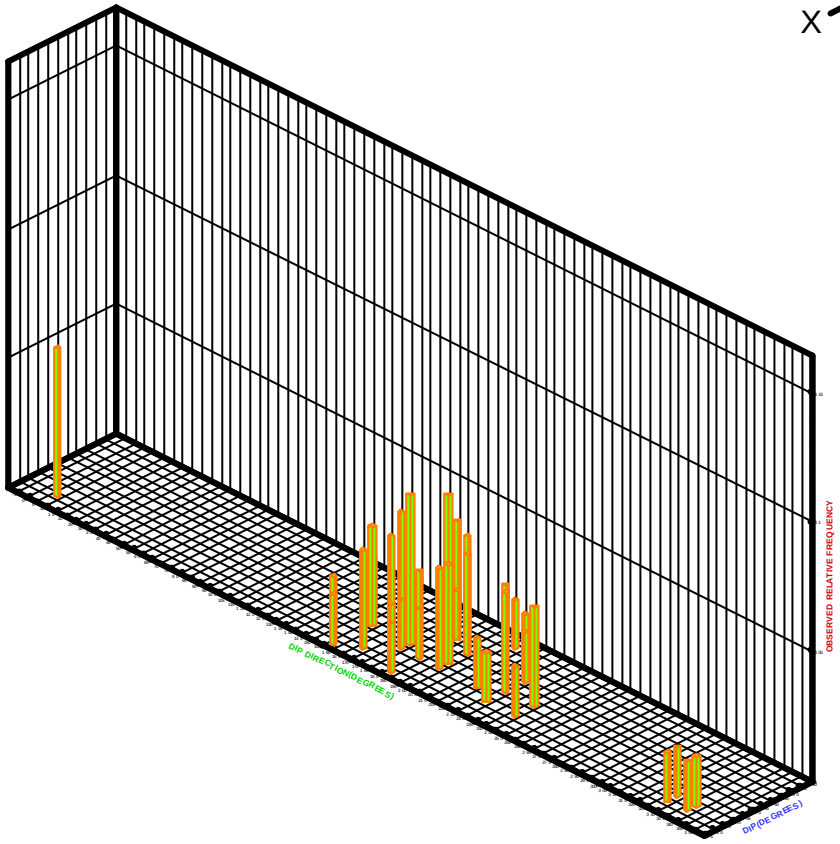

NUMBER OF ORIENTATION DATA = 52
LENGTH OF BOREHOLE = 78.60
TREND OF BOREHOLE = 318.00 (DEG.)
PLUNGE OF BOREHOLE = 85.00 (DEG.)
DIAMETER OF FRACTURE PLANES FROM 5.26 TO 5.26
DIAMETER OF BOREHOLE = .10

A COLUMN REPRESENTS 10 DEGREES(DIP) X 10 DEGREES(DIP DIRE.)
THE MAXIMUM VALUE FOR OBSERVED RELATIVE FREQUENCY = .0577
IT IS LOCATED FROM 50.00 TO 55.00 FOR DIP(DEG.)
AND 185.00 TO 190.00 FOR DIP DIRECTION(DEG.)
THE UNIT FOR LENGTH: Meter

(3D) ? 14 Nov 2001 ? NGI BOX #409 (Aspo Diorite)

Fig. 4.3b Corrected relative frequency of orientation for fracture set 2 of Aspo diorite (NGI box #409).

Based on Line or Borehole(1-D) sampling

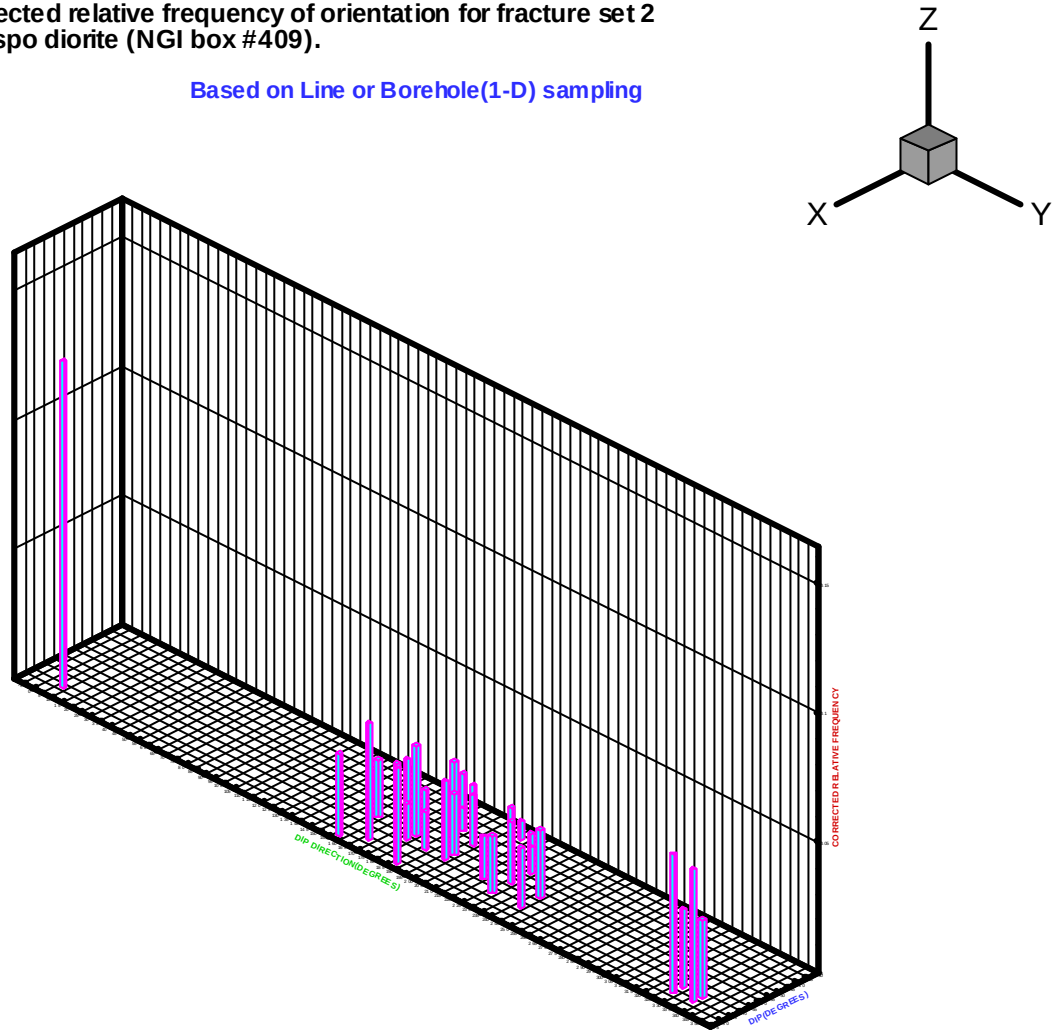

NUMBER OF ORIENTATION DATA = 52
LENGTH OF BOREHOLE = 78.60
TREND OF BOREHOLE = 318.00 (DEG.)
PLUNGE OF BOREHOLE = 85.00 (DEG.)
DIAMETER OF FRACTURE PLANES FROM 5.26 TO 5.26
DIAMETER OF BOREHOLE = .10

A COLUMN REPRESENTS 10 DEGREES(DIP) X 10 DEGREES(DIP DIRE.)
THE MAXIMUM VALUE FOR CORRECTED RELATIVE FREQUENCY = .1266
IT IS LOCATED FROM 75.00 TO 80.00 FOR DIP(DEG.)
AND 5.00 TO 10.00 FOR DIP DIRECTION(DEG.)
THE UNIT FOR LENGTH: Meter

(3D) ? 14 Nov 2001 ? NGI BOX #409 (Aspo Diorite)

Fig. 4.4a Observed relative frequency of orientation for fracture set 3 of Aspo diorite (NGI box #409).

Based on Line or Borehole(1-D) sampling

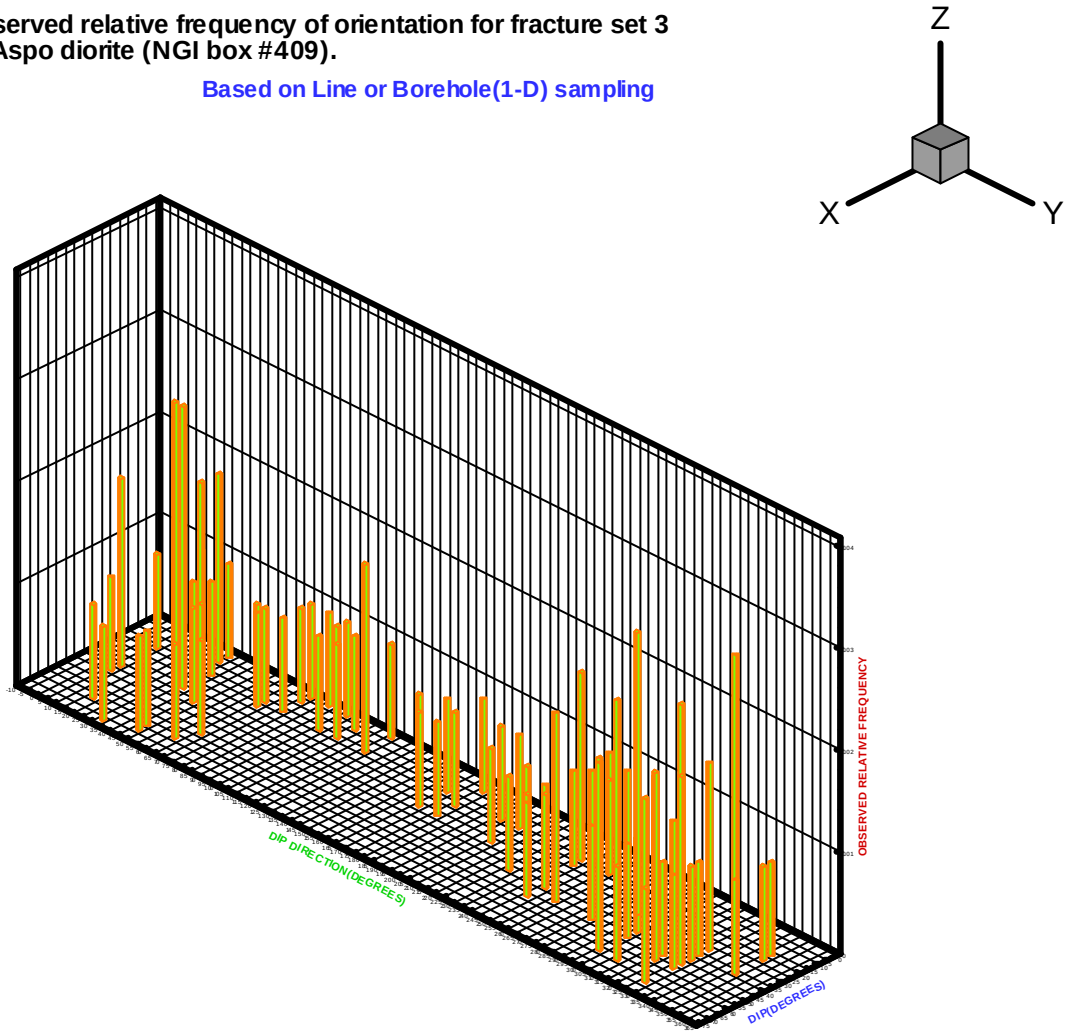

NUMBER OF ORIENTATION DATA = 108
LENGTH OF BOREHOLE = 78.60
TREND OF BOREHOLE = 318.00 (DEG.)
PLUNGE OF BOREHOLE = 85.00 (DEG.)
DIAMETER OF FRACTURE PLANES FROM 5.26 TO 5.26
DIAMETER OF BOREHOLE = .10

A COLUMN REPRESENTS 10 DEGREES(DIP) X 10 DEGREES(DIP DIRE.)
THE MAXIMUM VALUE FOR OBSERVED RELATIVE FREQUENCY = .0278
IT IS LOCATED FROM 15.00 TO 20.00 FOR DIP(DEG.)
AND 325.00 TO 330.00 FOR DIP DIRECTION(DEG.)
THE UNIT FOR LENGTH: Meter

(3D) ? 14 Nov 2001 ? NGI BOX #409 (Aspo Diorite)

Fig. 4.4b Corrected relative frequency of orientation for fracture set 3 of Aspo diorite (NGI box #409).

Based on Line or Borehole(1-D) sampling

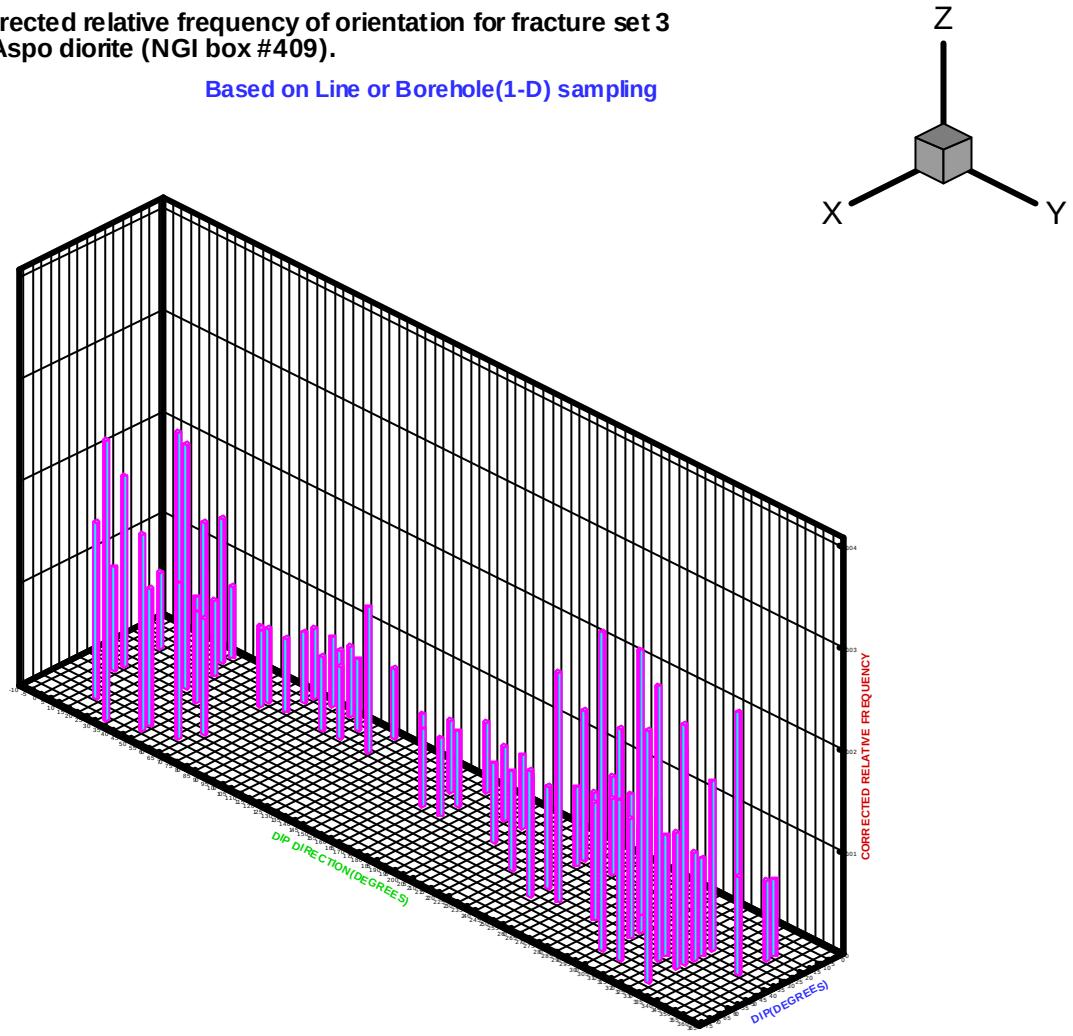

NUMBER OF ORIENTATION DATA = 108
LENGTH OF BOREHOLE = 78.60
TREND OF BOREHOLE = 318.00 (DEG.)
PLUNGE OF BOREHOLE = 85.00 (DEG.)
DIAMETER OF FRACTURE PLANES FROM 5.26 TO 5.26
DIAMETER OF BOREHOLE = .10

A COLUMN REPRESENTS 10 DEGREES(DIP) X 10 DEGREES(DIP DIRE.)
THE MAXIMUM VALUE FOR CORRECTED RELATIVE FREQUENCY = .0314
IT IS LOCATED FROM 60.00 TO 65.00 FOR DIP(DEG.)
AND 295.00 TO 300.00 FOR DIP DIRECTION(DEG.)
THE UNIT FOR LENGTH: Meter

probability of intersection is playing a dominant role compared to the low variability of the fracture set. Therefore, fracture set 1has shown the highest effect with respect to the orientation bias correction (compare a and b plots of Figs. 4.2 through 4.4). Because fracture set 3 is sub-horizontal it intersects the borehole very well. However, fracture set 3 has the highest orientation variability (see Table 4.2 and section 4.2). For fracture set 3, high probability of intersection is playing a dominant role compared to the high variability of the fracture set. Therefore, fracture set 3 shows the lowest effect on orientation sampling bias (compare a and b plots of Figs. 4.2 through 4.4) out of the three fracture sets. Fracture set 2 intersects the borehole better than fracture set 1, but less than fracture set 3. The orientation variability of this fracture set is in-between the variability of fracture sets 1 and 3 (see Table 4.2 and section 4.2). The combined influence of the two factors has produced an orientation bias effect for fracture set 2 that is higher than that of fracture set 3 and lower than that of fracture set 1 (compare a and b plots of Figs. 4.2 through 4.4).

4.2 Orientation Distribution for Each Fracture Set

Goodness-of-fit of hemispherical normal distribution (Kulatilake, 1985, Kulatilake et al. 1990a) was performed for both the raw and corrected orientation data of each fracture set using the computer program HEMISPHN of FRACNTWK software package (Kulatilake, 1998). For all three fracture sets the mean normal vector direction and the distribution of the orientation have changed to some extent due to the orientation bias correction (compare plots a and b of Figs. 4.5 through 4.7 and Table 4.2). This indicates the importance of applying the orientation sampling bias correction in modeling joint orientation distribution. The summary results (Table 4.2) indicate that hemispherical normal distribution (in the rock mechanics literature some researchers call this as the Fisher distribution) is not suitable to represent the statistical distribution of orientation of all 3 fracture sets. Note that the variability of a fracture set increases with increasing spherical variance and decreasing k.

Goodness-of-fit of Bingham distribution (Bingham, 1964) was performed for the orientation data of each fracture set using the computer program CLUSDEL-BINGHAM of FRACNTWK software package (Kulatilake, 1998). The results (Table 4.1) show that the Bingham distribution is suitable to represent the statistical distribution of orientation data only for fracture set 3.

The available theoretical probability distributions (hemispherical normal and Bingham distributions) were found to be insufficient to represent the statistical distribution of orientation for two of the three fracture sets. A number of previous studies conducted by the authors have shown clearly that the available theoretical probability distributions (hemispherical normal and Bingham distributions) are insufficient to represent the statistical distribution of orientation data for many field sites (Kulatilake et al., 1990b; 1993; 1996; 1998; Um et al., 2000). For a fracture set that cannot be represented by a theoretical orientation probability distribution, the empirical orientation distribution obtained from the corrected relative frequency data can be used for generation of orientation values (Kulatilake et al., 1990b).

(2D) ? 14 Nov 2001 ? Upper-Hemispherical Stereographic Projection

Fig. 4.5a Results of hemispherical normal distribution fit for observed orientation data of fracture set 1 of Aspo diorite (NGI box #409).

Probability(Confidence) Contours for the Hemispherical Normal Distribution of Fracture Normals

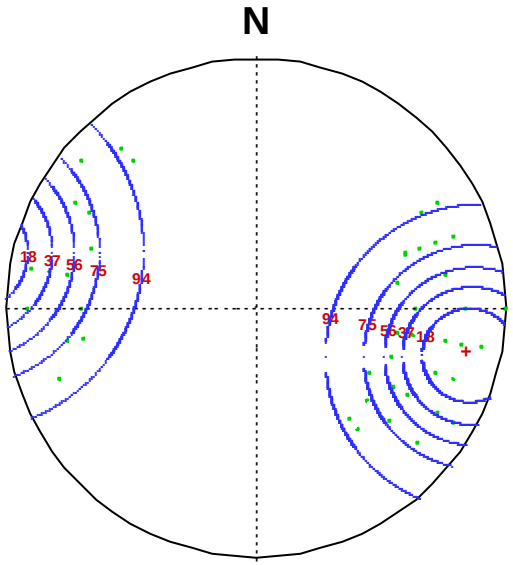

The number given for the contour is the percent(%) confidence

Maximum significance level at which the hemispherical normal distribution is suitable to represent the statistical distribution of joint orientation data : .009

Number of Joint Data = 50

Average L = -.1993
Average M = -.9682
Average N = .1510

Magnitude of Mean Vector = .8916
Mean Plunge(up) = 8.6841 (deg.)
Mean Trend = 101.6310 (deg.)
K Value of the Distribution = 9.0409
Spherical Variance = .1084

The small . indicate the joint normal vectors
The small + indicates the mean normal vector to the joint set

Upper-Hemispherical Stereographic Projection

(2D) ? 14 Nov 2001 ?HEMISPHERICAL NORMAL DISTRIBUTION GOODNESS-OF-FIT RESULTS

Fig. 4.5b Results of hemispherical normal distribution fit for orientation data of fracture set 1 of Aspo diorite (NGI box #409) corrected for sampling bias.

Probability(Confidence) Contours for the
Hemispherical Normal Distribution of Fracture Normals

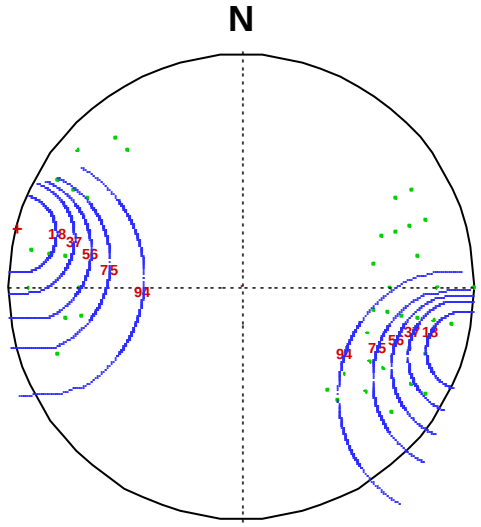

The number given for the contour is the percent(%) confidence

Maximum significance level at which the hemispherical normal distribution is suitable to represent the statistical distribution of joint orientation data : < 0.005

Number of Joint Data = 50

Average L = -.2513
Average M = -.9679
Average N = -.0028

Magnitude of Mean Vector = .9173
Mean Plunge(up) = .1600 (deg.)
Mean Trend = 284.5547 (deg.)
K Value of the Distribution = 11.8569
Spherical Variance = .0827

The small + indicates the mean normal vector to the joint set
The small . indicate the joint normal vectors

Upper-Hemispherical Stereographic Projection

(2D) ? 14 Nov 2001 ? HEMISPHERICAL NORMAL DISTRIBUTION GOODNESS-OF-FIT RESULTS

Probability(Confidence) Contours for the
Hemispherical Normal Distribution of Fracture Normals

Fig. 4.6b Results of hemispherical normal distribution fit for orientation data of fracture set 2 of Aspo diorite (NGI box #409) corrected for sampling bias.

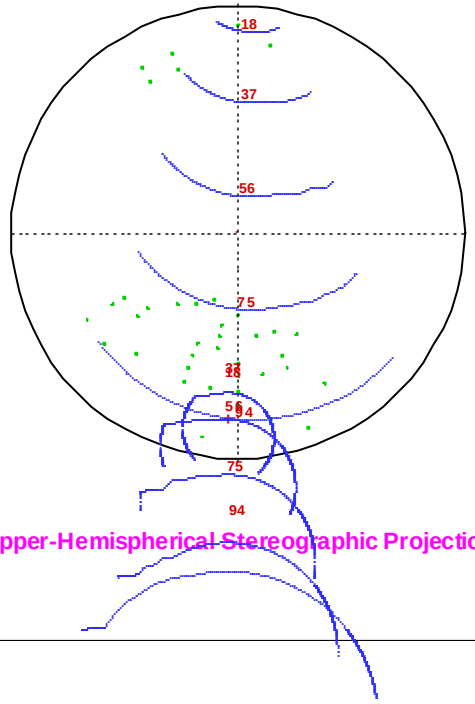

Upper-Hemispherical Stereographic Projection

Maximum significance level at which the hemispherical normal distribution is suitable to represent the statistical distribution of joint orientation data : < 0.005

Number of Joint Data = 52

Average L = .9805
Average M = -.0471
Average N = -.1910

Magnitude of Mean Vector = .8688
Mean Plunge(up) = 11.0130 (deg.)
Mean Trend = 182.7482 (deg.)
K Value of the Distribution = 7.4734
Spherical Variance = .1312

The small + indicates the mean normal vector to the joint set

The small . indicate the joint normal vectors

Fig. 4.6b Results of hemispherical normal distribution fit for orientation data of fracture set 2 of Aspodibonite (NGI box #409) corrected for sampling bias.

Probability of Fracture Set 2 of Aspodibonite

Hemispherical Normal Distribution of Fracture Normals

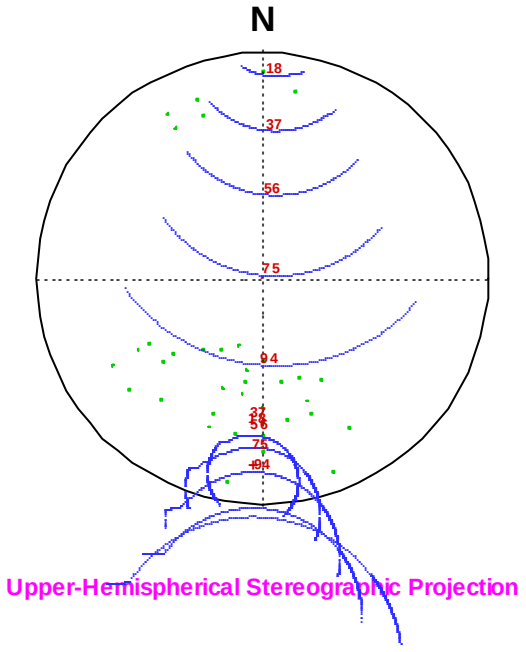

The number given for the contour is the percent(%) confidence

Maximum significance level at which the hemispherical normal distribution is suitable to represent the statistical distribution of joint orientation data : < 0.005

Number of Joint Data = 52

Average L = .9805
Average M = -.0471
Average N = -.1910

Magnitude of Mean Vector = .8688
Mean Plunge(up) = 11.0130 (deg.)
Mean Trend = 182.7482 (deg.)
K Value of the Distribution = 7.4734
Spherical Variance = .1312

The small + indicates the mean normal vector to the joint set

The small . indicate the joint normal vectors

(2D) ? 14 Nov 2001 ? Upper-Hemispherical Stereographic Projection

Fig. 4.7a Results of hemispherical normal distribution fit for observed orientation data of fracture set 3 of Aspo diorite (NGI box #409).

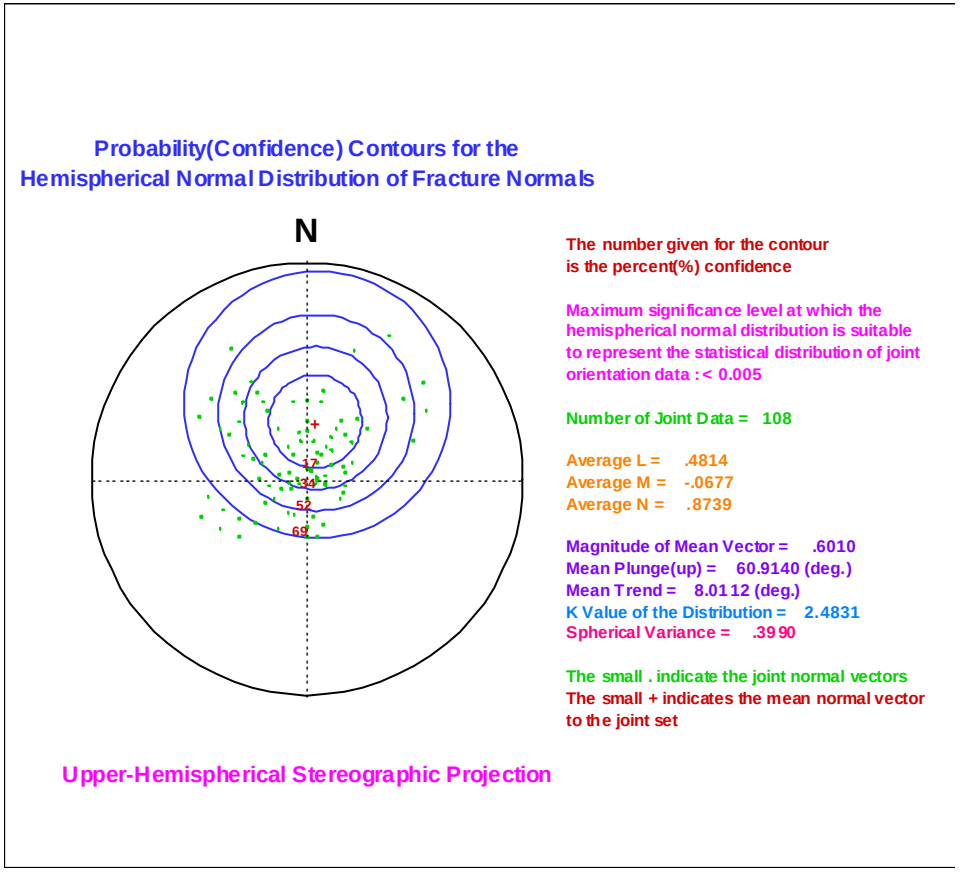

(2D) ? 14 Nov 2001 ? HEMISPHERICAL NORMAL DISTRIBUTION GOODNESS-OF-FIT RESULTS

Fig. 4.7b Results of hemispherical normal distribution fit for orientation data of fracture set 3 of Aspo diorite (NGI box #409) corrected for sampling bias.

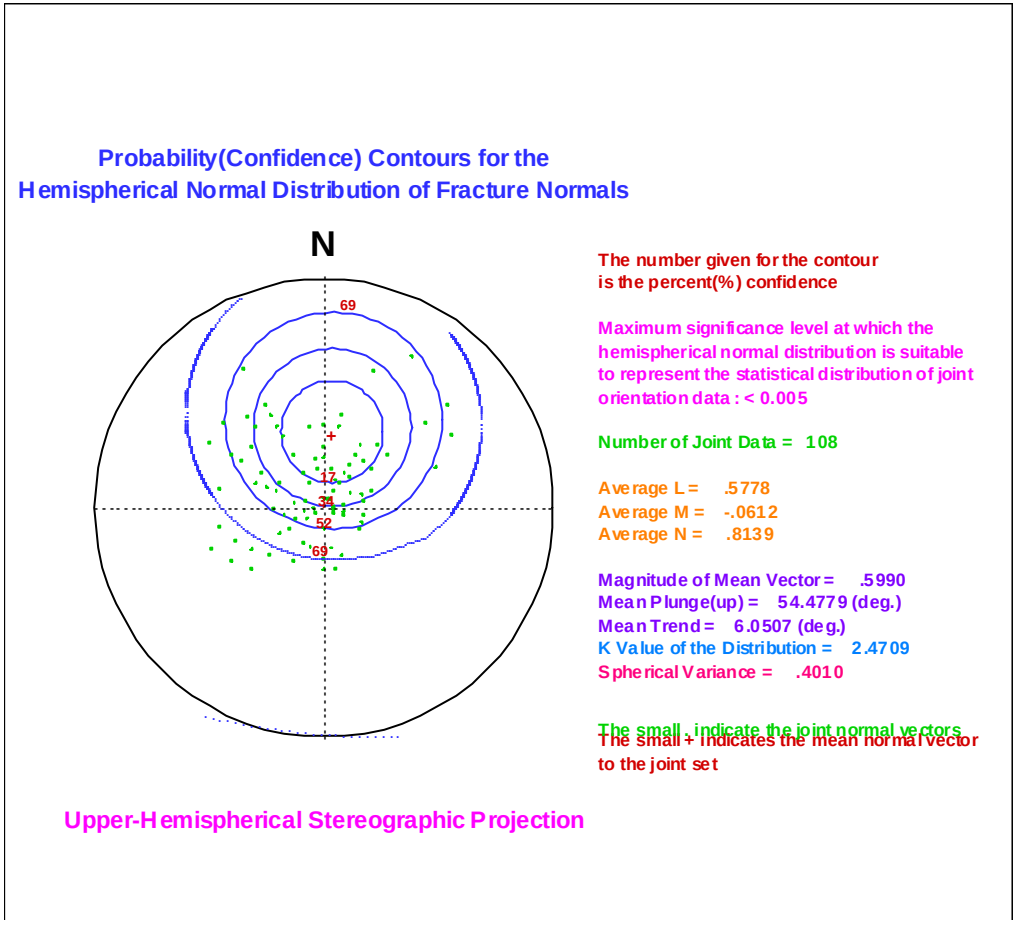

Table 4.2 Goodness-of-fit results of hemispherical normal distribution for orientation data of Äspö diorite

(a) Raw orientation data

Nobs.	Fracture set #	Npts.	Upward mean normal vector		K	Sp. Var.	P
			Trend (°)	Plunge (°)			
210	1	50	101.63	8.68	9.04	0.1084	0.009
	2	52	187.41	25.45	7.92	0.1238	0.047
	3	108	8.01	60.91	2.48	0.3990	<0.005

(b) Data corrected for sampling bias

Nobs.	Fracture set #	Npts.	Upward mean normal vector		K	Sp. Var.	P
			Trend (°)	Plunge (°)			
210	1	50	284.55	0.16	11.86	0.0827	<0.005
	2	52	182.74	11.01	7.47	0.1312	<0.005
	3	108	6.05	54.48	2.47	0.4010	<0.005

Nobs.=Number of fractures observed on the borehole
Npts.=Number of fractures belonging to the fracture set
K=A parameter in the hemispherical normal distribution
Sp. Var.=Spherical variance
P=Maximum significance level at which the hemispherical normal distribution is suitable to represent the statistical distribution of fracture orientation data
(a minimum of 0.05 is required to represent orientation data by a hemispherical normal distribution)

4.3 Trace Length and Size Distributions for Each Fracture Set

As mentioned before, no fracture trace data were provided for this project to model fracture trace length distribution and size distribution in 3-D. However, some summarized results about fracture trace and size are available in the report by Hermanson et al. (1998?). It is important to point out that the procedures KULATILAKE & ASSOCIATES use in estimating fracture size (Kulatilake and Wu, 1984b; 1986) are different to the procedures used by Hermanson et al. (1998). Therefore, the model given for fracture size in the report by Hermanson et al. (1998) is not used in this project. However, the information available in Hermanson et al. (1998) was used to get some approximate estimates for mean and standard deviation of fracture size. Previous projects on fracture modeling conducted by the authors (Kulatilake et al., 1990a; 1993; 1996; 1998; Um et al., 2000) have shown that a gamma distribution is the best to represent fracture trace length distribution in 2-D and equivalent fracture diameter distribution in 3-D. Therefore, a gamma distribution was selected to represent fracture trace length distribution in 2-D. Due to lack of reliable data on fracture traces, the same gamma distribution (mean=5m and coefficient of variation=0.5) was used to represent the fracture trace length distribution in 2-D for all 3 fracture sets.

For the Äspö diorite rock mass (NGI box # 409), the discontinuity size in 3-D for each of the fracture sets can be estimated by assuming an equivalent circular disk shape for the 3-D discontinuities. A procedure is available in the literature to compute fracture diameter distribution in 3-D from fracture trace length distribution on infinite 2-D exposure (Kulatilake and Wu, 1986). This procedure was used to estimate the fracture size distribution for the 3 fracture sets of Äspö diorite using the computer program JTSIZE3D of FRACNTWK software package (Kulatilake, 1998). For all three fracture sets, the gamma distribution with mean = 5.26m and standard deviation = 2.25m was found to be suitable to represent fracture diameter distributions.

4.4 Spacing Distribution and 1-D Fracture frequency for Each Fracture Set

Fracture spacing data were obtained from the depth region 457.4-536.0m of borehole KAS02. Goodness-of-fit tests were performed using GDFT computer program of FRACNTWK software to find the suitable probability distributions as well as the best probability distribution to represent the statistical distribution of spacing for each fracture set. The results (Table 4.3) indicate that all three probability distributions lognormal, gamma and exponential are highly suitable to represent the statistical distribution of spacing for any of the 3 fracture sets. The lognormal distribution was found to be the best distribution for 2 fracture sets. The gamma distribution turned out to be the 2nd best distribution for all 3 fracture sets. The exponential distribution was found to be the best distribution for 1 fracture set. As an example, Figure 4.8 shows detailed results obtained for the goodness of fit tests performed for fracture set 3.
The estimation of mean spacing and linear frequency (1/spacing) are based on the measurements carried out on a finite length of the borehole. However, unbiased estimates of these parameters should be based on infinite length. A correction was applied for this

Table 4.3 Goodness-of-fit test results for spacing of the three fracture sets of Äspö diorite (NGI box # 409)

Fracture set #	No. of data	Mean (m)	Var (m^2)	Probability Distribution	K-S_{stat} Value	df	P-value	Best Distribution Rank
1	49	1.5904	5.7369	Exponential	0.0936	7	>0.2	3
				Gamma	0.0931	7	>0.2	2
				LogNormal	0.0356	7	>0.2	1
2	46	1.6174	3.0515	Exponential	0.1046	7	>0.2	3
				Gamma	0.0808	7	>0.2	2
				LogNormal	0.0627	7	>0.2	1
3	112	0.6946	0.9258	Exponential	0.0231	8	>0.2	1
				Gamma	0.0303	8	>0.2	2
				LogNormal	0.0345	8	>0.2	3

Note: A minimum P value of 0.05 is required to accept the tried probability distribution to represent the spacing distribution of the fracture set.

Table 4.4 Mean spacings and linear frequencies along the borehole KAS02 and mean normal vector directions for fracture sets of Äspö diorite (NGI box #409)

Fracture set #	Orientation of fracture set		Dir. of borehole		Obs. mean spacing along borehole (m)	Length of borehole (m)	Corr. mean spacing along borehole (m)	1-D fracture frequency along borehole (# per m)	Angle between borehole & MNV (deg.)	1-D fracture frequency along MNV (# per m)
	Dip dir. (degs.)	Dip (degs.)	Trend (degs.)	Plunge (degs.)						
1	102	81	318	85	1.59	78.60	1.59	0.63	*70 (76.9)	1.84
2	187	64	318	85	1.62	78.60	1.62	0.62	60.06	1.23
3	332	13	318	85	0.69	78.60	0.69	1.44	18.08	1.51

MNV = Mean Normal Vector of fracture set

* = Actual angle is 76.9°; however the angle was limited to 70° to calculate the 1-D fracture frequency along MNV direction

(XY) ? 14 Nov 2001 ? Histogram and the Goodness-of-Fit Test Results

Fig. 4.8a Histogram for spacing and the goodness-of-fit test results of fracture set 3 of Aspo diorite (NGI box #409).

Number of data in the sample = 112
Total number of intervals = 7
The range for SPACING : FROM .0000E+00 TO .7070E+01
Interval size for first cell = .1019E+01; Others = .1008E+01

The tested probability distribution : EXPONENTIAL

Maximum significance level at which the tested distribution
is suitable to represent the statistical distribution of the data :
For CHI-SQUARE TEST: INSUFFICIENT DATA
For K--S TEST: >0.2

Calculated mean = .6946E+00
Calculated standard deviation = .9622E+00

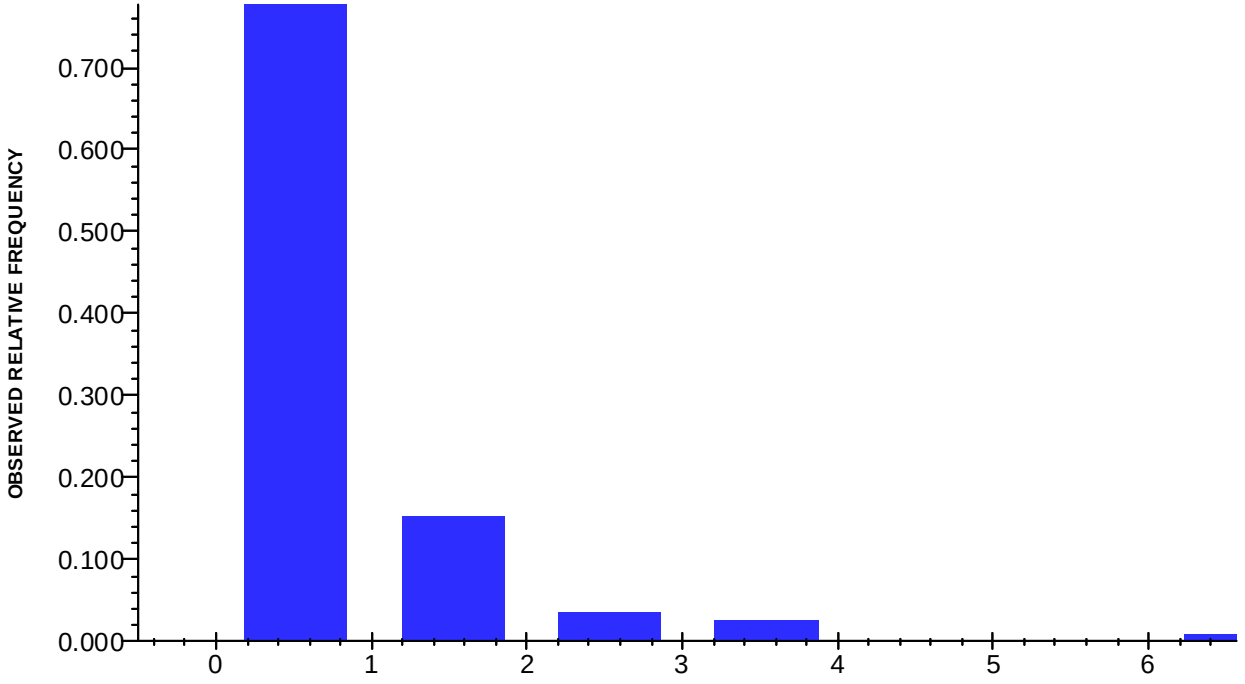

Interval Size for First Cell = .1019E+01
FROM .0000E+00 TO .1019E+01

(XY) ? 14 Nov 2001 ? CUMULATIVE FREQUENCY(PROBABILITY) DISTRIBUTIONS

Fig. 4.8b Observed and theoretical cumulative distributions for spacing of fracture set 3 of Aspo diorite (NGI box #409).

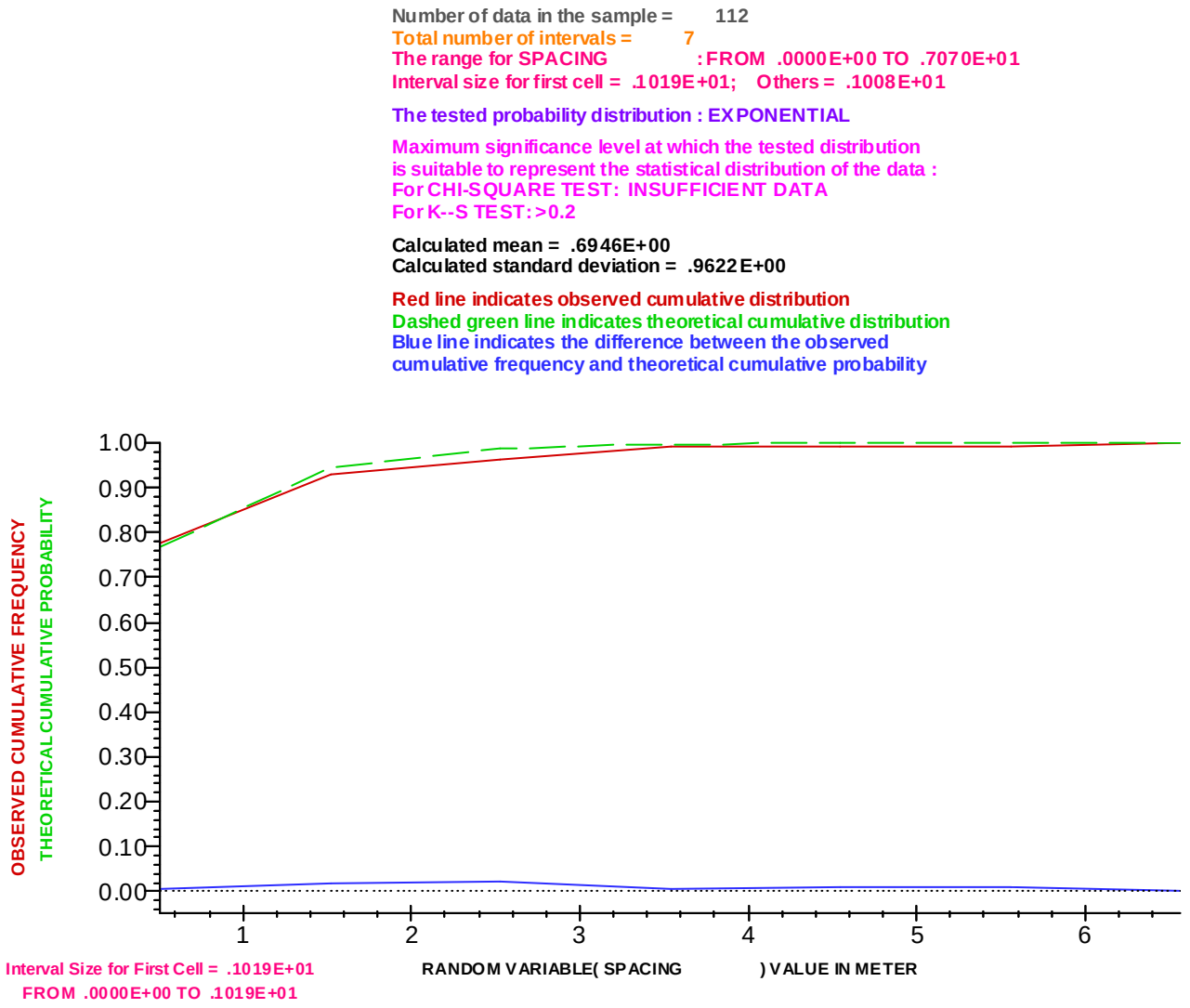

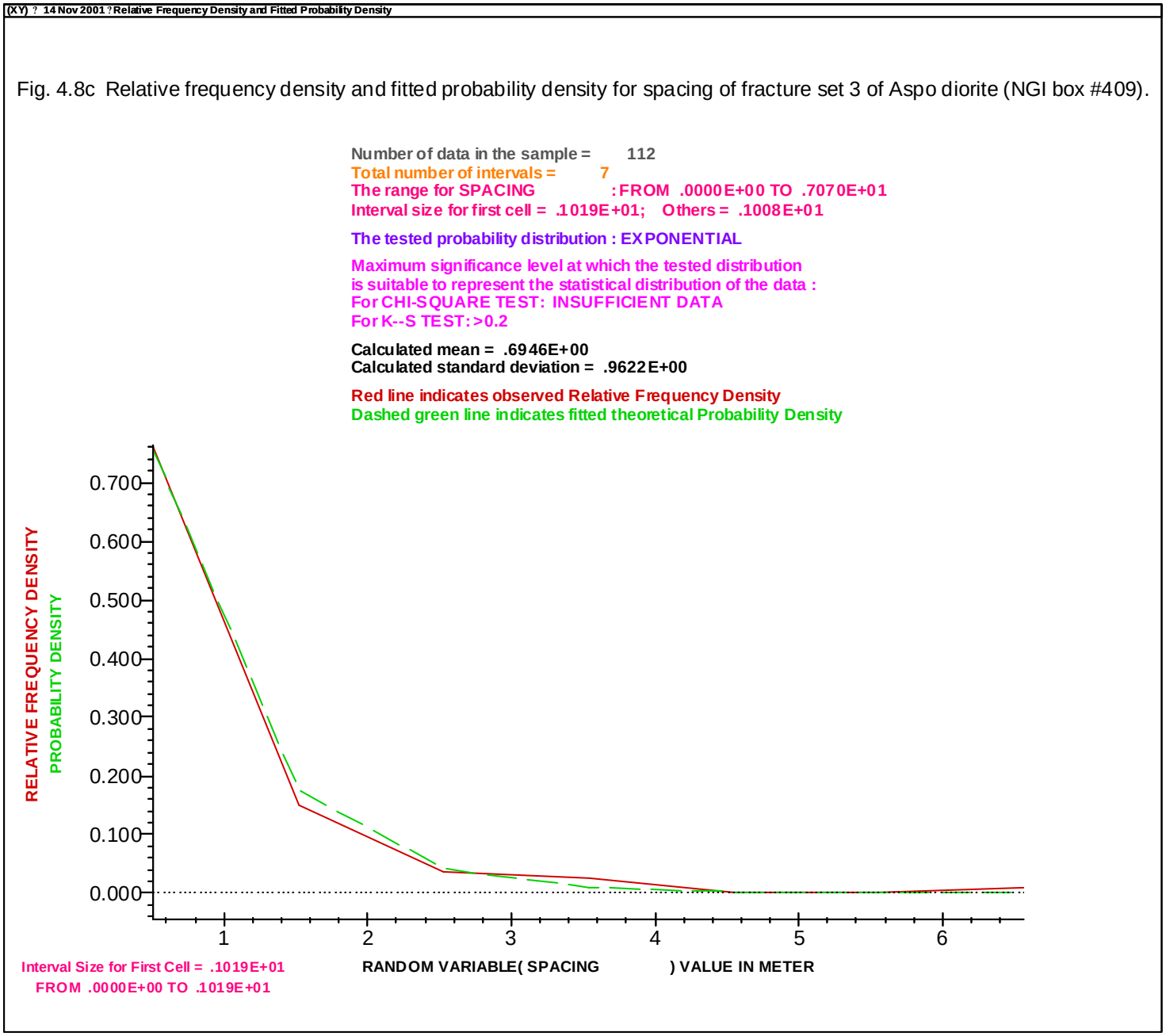

Fig. 4.8c Relative frequency density and fitted probability density for spacing of fracture set 3 of Aspo diorite (NGI box #409).

sampling bias on spacing to obtain corrected mean spacing along the borehole according to the procedure given in Kulatilake (1988) using the computer program COR1DFM1 of FRACNTWK software package (Kulatilake, 1998). For each fracture set, the spacing distribution, including the observed mean spacing and the standard deviation of spacing, is available along the borehole direction (see Table 4.3). Assuming the exponential distribution for spacing, the mean spacing corrected for spacing sampling bias was calculated for each fracture set by using the observed mean spacing and the length of the borehole. For all 3 fracture sets, the length of the borehole was found to be more than 9 times of the observed mean spacing. Therefore, no difference was found between the observed and corrected mean spacing for any of the fracture sets. After the aforementioned calculations, for each fracture set, the corrected mean spacing is available along the borehole direction (see Table 4.4). From the fracture set delineation analysis, the mean normal vector direction is known, for each fracture set (see Table 4.4). This information was used to calculate the mean 1-D fracture frequency along the mean normal vector direction for each fracture set according to the procedure given in Kulatilake (1988) using the computer program COR1DFM1 of FRACNTWK software package (Kulatilake, 1998). All the results are given in Table 4.4. Note that for fracture set 1, the angle between the borehole direction and the mean normal vector direction of the fracture set is 76.9 degrees (Table 4.4). Based on this value, the 1-D fracture frequency along the mean normal vector direction is estimated to be 2.77 per m. When the angle increases beyond 70 degrees, the reliability of the 1-D fracture frequency estimation decreases. Therefore in this study, when the angle is greater than 70 degrees, the 1-D fracture frequency along the mean normal vector direction is estimated using the angle of 70 degrees.

4.5 1-D Fracture frequency in any Direction in 3-D

The 1-D fracture frequencies obtained along the mean normal vector directions of the 3 fracture sets were then used to estimate the 1-D fracture frequency in all the directions in 3-D by using the computer program FREQ1DALLDIR of FRACNTWK software package (Kulatilake, 1998). Figure 4.9 shows the obtained results. This figure also pin points the directions and magnitudes for the minimum and maximum fracture frequencies for the Äspö diorite rock mass.

4.6 Mean Estimates for Block Size, Number of Blocks per Unit Volume and Number of Fractures per Unit Volume

The spacing distributions obtained along the mean normal vector directions for the 3 fracture sets were used along with the orientation distributions of the fracture sets in generating rock blocks in 3-D using the Monte-Carlo simulation procedure. This was performed using the computer program FREQ3DMVDJS in the software package FRACNTWK (Kulatilake, 1998). Orientations for the fracture sets were generated according to the obtained empirical orientation distributions (Kulatilake et al., 1990b). When spacing values are generated from a certain distribution, irrespective of the distribution, a certain proportion of small values are produced. Because the block volume is proportional to the third power of spacing, even moderate spacing values can produce

(2D) ? 14 Nov 2001 ?

Fig. 4.9 1-D fracture frequency distribution in 3-D on an equal-angle equatorial net on the upper hemispherical for Aspo diorite rock mass (NGI box #409).

LENGTH UNIT: Meter

Minimum Fracture Frequency:		Maximum Fracture Frequency:	
Magnitude(#/Length Unit):	1.1720	Magnitude(#/Length Unit):	2.9759
Trend(Deg.):	193.0000	Trend(Deg.):	128.0100
Plunge(Deg.):	9.6100	Plunge(Deg.):	50.5700

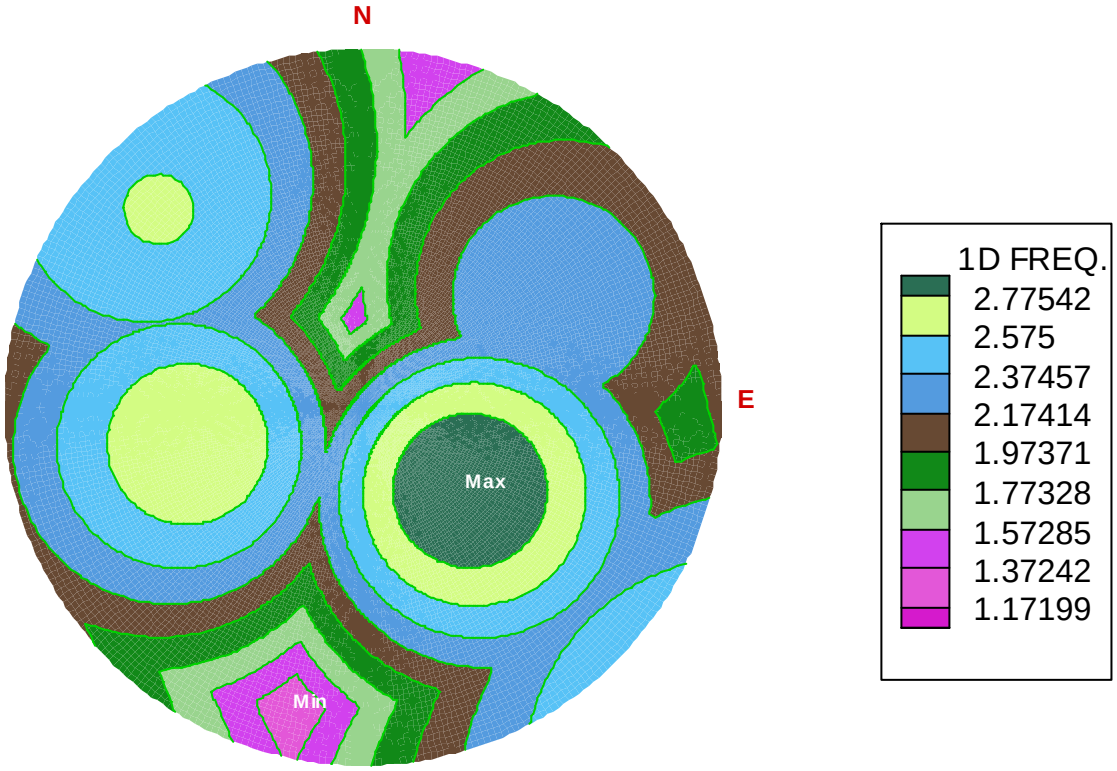

extremely small block volume values. These extremely small block volumes can produce extremely large values for the parameter number of blocks per unit volume because this parameter is inversely proportional to the block volume. These extremely high values can totally distort the estimation obtained for mean of the parameter number of blocks per unit volume. By the same token, extremely high spacing values generated through probability distributions, can give rise to large block volumes and small values for the parameter number of blocks per unit volume. These extreme values can also distort the estimation obtained for the mean. Therefore, it is reasonable to calculate the mean by removing these low and high extreme values from the distributions. Such estimations are termed as trimmed values. Trimming can be done at different percentage levels. The obtained results for the distribution of volume of equivalent matrix block at a trimming level of 30% are shown in Figure 4.10 along with the trimmed mean value. Similar results for the number of matrix blocks per unit volume are shown in Figure 4.11.

Volumetric fracture frequency for a fracture set (number of fracture centers per unit volume), λ_v, can be related to linear fracture frequency, λ_l, fracture diameter, D, and fracture orientation using the following equation (Kulatilake et al., 1990b):

$$(l_v)_i = \frac{4(l_l)_i}{pE(D^2)E(|n_i|)} \tag{1a}$$

$$E(|n_i|) = E(|\mathbf{n}\cdot\mathbf{i}|) \tag{1b}$$

where

$(l_v)_i$ = volumetric fracture frequency of ith fracture set
$(l_l)_i$ = linear frequency of ith fracture set along the mean normal vector direction
$E(D^2)$ = expected value of squared diameter
$E(|n_i|)$ = expected value of $|n_i|$
n = unit normal vector of a fracture in the fracture set
i = unit vector along the mean normal vector (MNV) of fracture set i.

All the estimated l_v values for 3 fracture sets using the computer program 3DINTF1D of FRACNTWK software package (Kulatilake, 1998) are given in Table 4.5. All three fracture sets produced high variability with respect to the orientation distribution (see Figure 4.1 and Table 4.2). This high variability partly resulted from low number of data used in the orientation analysis. When the orientation variability of a fracture set becomes very high, the value of $E(|n_i|)$ becomes very low. These very low $E(|n_i|)$ values results in unrealistic $(l_v)_i$ values. $E(|n_i|)$ varies between 0 and 1 with 1 resulting for no variability and 0 resulting for infinite variability. Due to the aforementioned reasons, with respect to the orientation variability of the 3 fracture sets, significant uncertainty exists of the values obtained. Therefore, lowest $E(|n_i|)$ was set to 0.6 to avoid obtaining unrealistic $(l_v)_i$ values.

(XY) ? 14 Nov 2001 ?

Fig. 4.10 Probability distribution of volume of equivalent matrix block for Aspo diorite rock mass (NGI box #409). (Unit of length: meter)

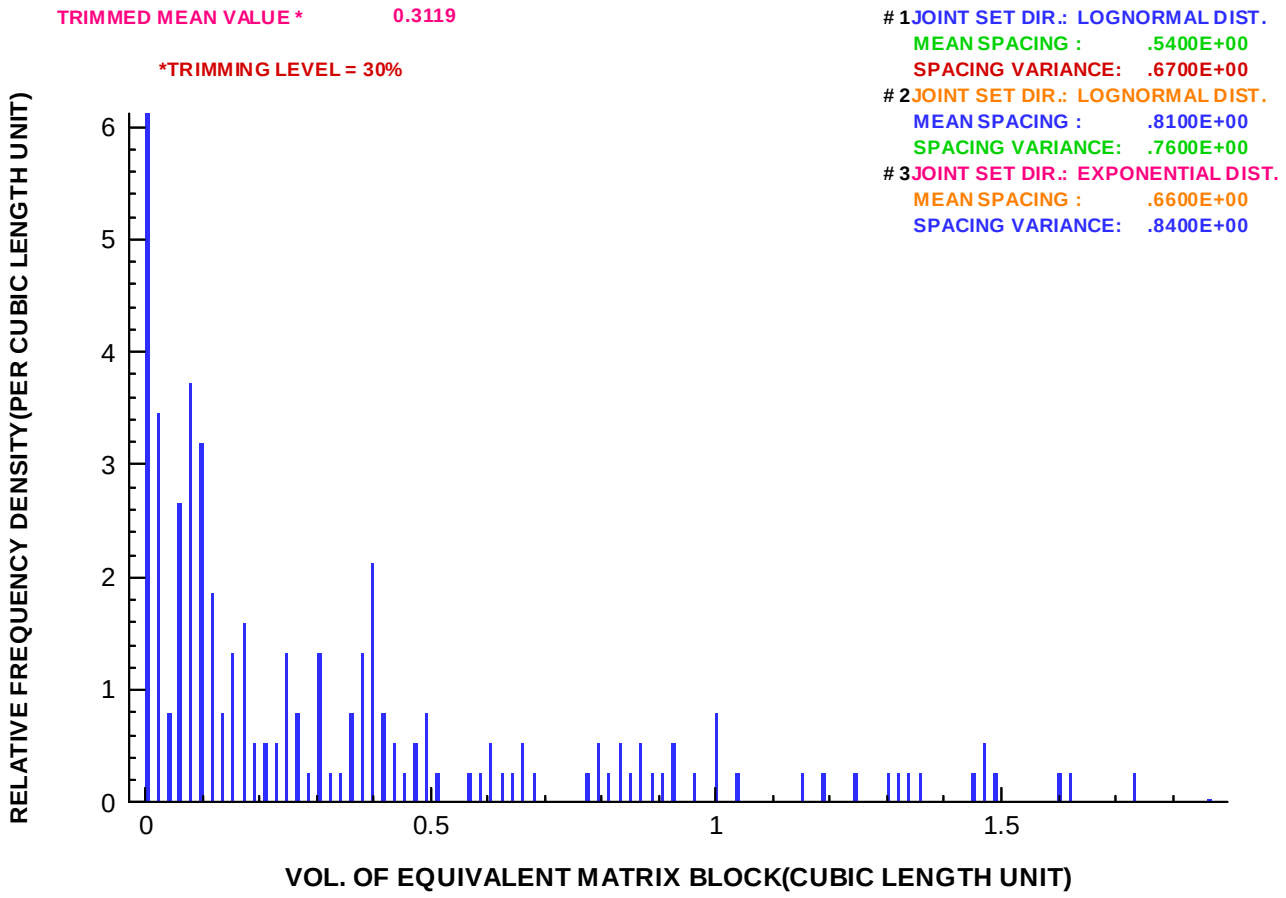

(XY) ? 14 Nov 2001 ?

Fig. 4.11 Probability distribution of number of blocks per unit volume for Aspo diorite rock mass (NGI box #409). (Unit: #/cubic meter)

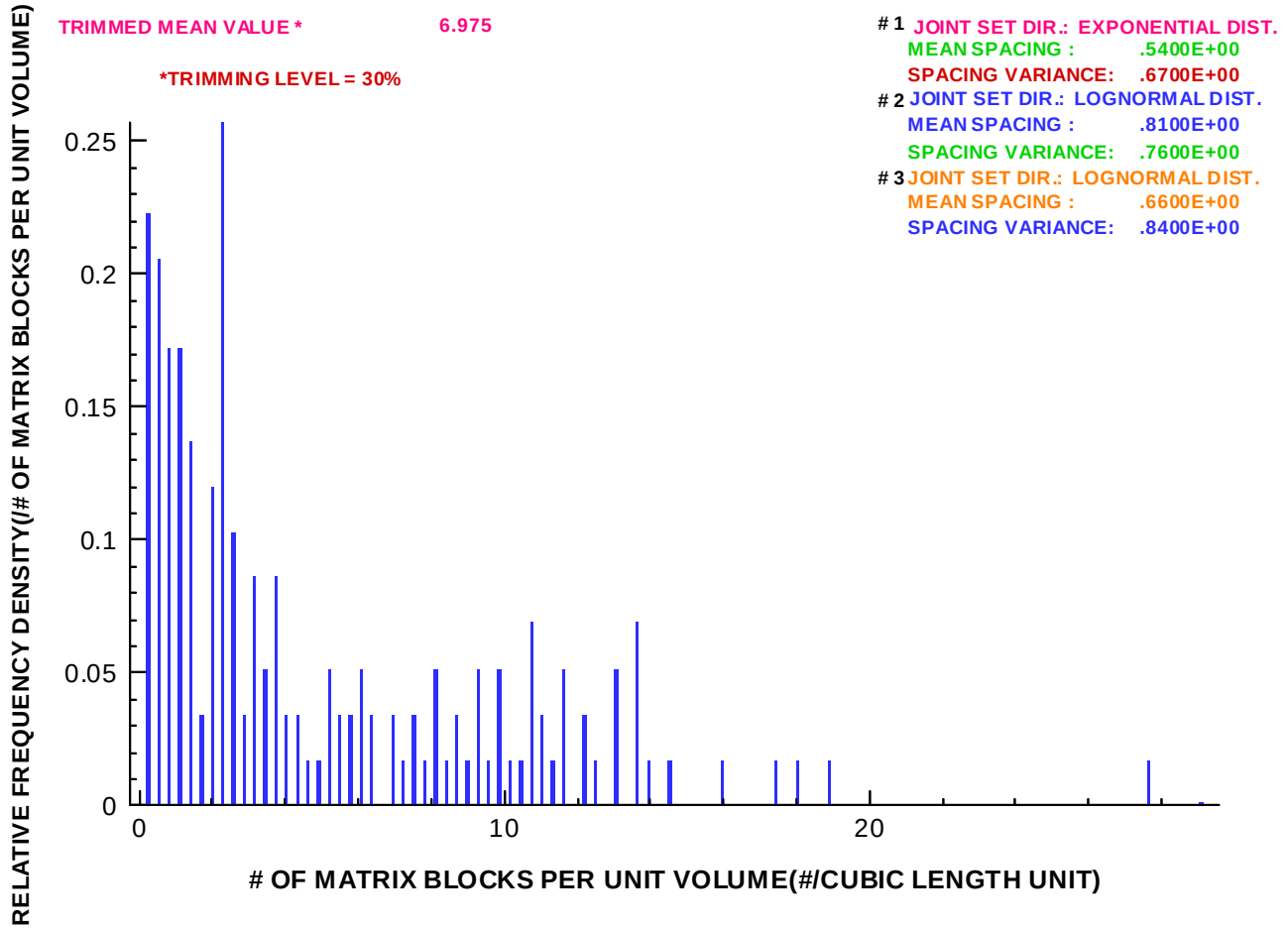

Table 4.5 Volumetric fracture frequency results for Äspö diorite (NGI box #409) fracture sets

Fracture set #	1D-Intensity (#/m)	E(n·i)	$E(D^2)$ (m^2)	3D-Intensity ($\#/m^3$)
1	1.84	0.60	32.75	0.1192
2	1.23	0.60	32.75	0.0797
3	1.51	0.60	32.75	0.0978

Note: Lowest E(n·i) is limited to 0.6

4.7 Fracture System Generation in 3-D and Validation

To describe the fracture geometry pattern in 3-D, it is necessary to specify the number of fracture sets, and the statistical distributions for the following fracture geometry parameters for each fracture set: (1) number of fractures per unit volume; (2) orientation; (3) diameter; and (4) location of fracture centers. Mean 3-D fracture intensity for each fracture set was estimated in section 4.6. Because the exponential distribution was found to be a suitable distribution to represent the fracture spacing for each fracture set, according to the statistical theory, the Poisson distribution can be used to model the 3-D fracture intensity distribution for each fracture set with the calculated mean 3-D fracture intensity value given in Table 4.5. The empirical distribution obtained for the orientation was used to model the orientation distribution for each fracture set. For each fracture set, the diameter was represented by the selected gamma distribution mentioned in section 4.3. Because the exponential distribution was found to be a suitable distribution to represent the fracture spacing for each fracture set, according to the statistical theory, the location of fracture centers in 3-D can be modeled using a uniform distribution. These statistical models were used to generate the fracture system in 3-D for a cubic block of size 30m (having two vertical sides parallel to north-south) for the Äspö diorite rock mass (NGI box # 409) using the computer program GENERATE in the software package FRACNTWK (Kulatilake, 1998). Figure 4.12 shows the fracture traces obtained from the fracture generation on a horizontal square window of 15m placed at the mid-level of the 30m cube. Out of the three fracture sets, the first two fracture sets are sub vertical and fracture set 3 is sub horizontal (see Figure 4.1). Therefore, fracture sets 1 and 2 should intersect the horizontal window better than fracture set 3. According to Table 4.2b, the mean strike values of fracture sets 1 and 2 are S 15° W and S 87° E, respectively. Strike directions around these two strikes can be seen very well in Figure 4.12. Although the mean strike for fracture set 3 is N 84° W, because it is a sub horizontal fracture set, strikes of the fractures coming from this set can cover a wide range (see Figure 4.1). These variable strike directions are also can be seen in Figure 4.12. Figure 4.13 shows the fracture traces obtained from the fracture generation on a vertical square window of size 15m having the strike direction same as the trend direction of borehole KAS02 (318°) and placed at the middle of the 30m cube. Note that fracture set 1 is almost vertical and the mean strike is S 15° W. Therefore, fracture set 1 should intersect the chosen vertical window well and produce sub-vertical traces. Such traces can be seen very well on Figure 4.13. Fracture set 2 strikes S 87° E and dips 79° S. Therefore, fracture set 2 should intersect the chosen vertical window well and produce traces having moderately high

apparent dip angles. Figure 4.13 shows such traces very well. Fracture set 3 is sub horizontal. Therefore, fracture set 3 should make sub-horizontal fracture traces on the chosen vertical window. Figure 4.13 shows sub-horizontal fracture traces very well. Figure 4.13 also shows that the traces appear on the figure come from 3 fracture sets. A 10m length of KAS02 borehole is simulated on Figure 4.13. The 1-D fracture frequency on this simulated borehole is about 3.2 fractures per m. This number compares reasonably well with the observed 1-D fracture frequency of 2.7 fractures per m on actual KAS02 borehole (see Table 4.4). Fracture traces simulated on a 40m square vertical window produced a mean trace length value of 4.28m and a coefficient of variation of 0.5. When the vertical window size was increased to 55m square, the mean trace length value increased to 4.75m keeping the value of coefficient of variation almost the same. This shows clearly that the mean trace length increases with window size. Note that for infinite size window, a mean trace length of 5m along with a coefficient of variation of 0.5 was used in modeling the fracture size. These numbers validate the used fracture size model. The above findings show that the fracture geometry features of the generated fracture system agree well with the fracture data used to model the 3-D stochastic fracture system.

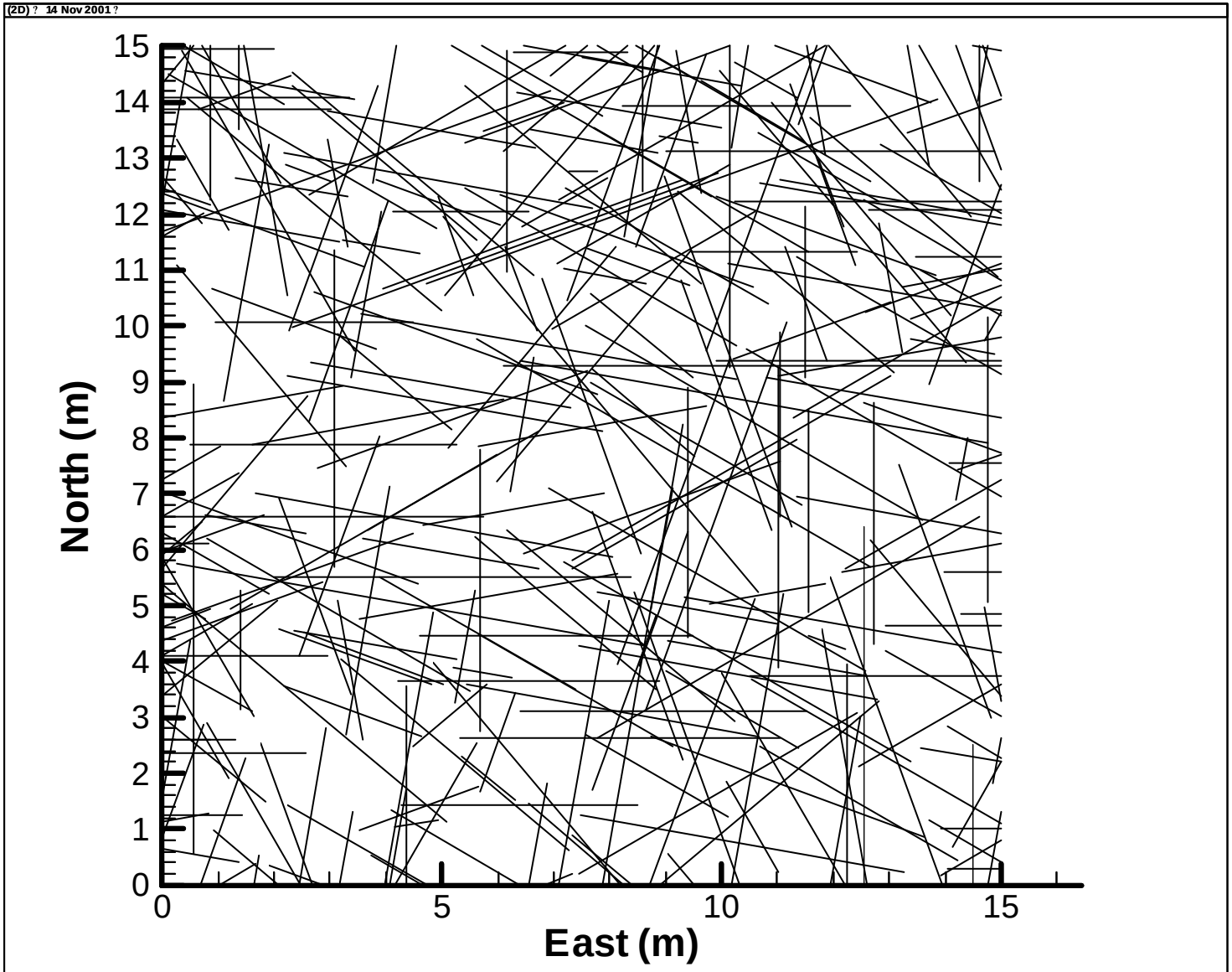

Fig. 4.12 Fracture traces obtained from fracture generation on a horizontal square window of size 15 m placed at the mid level of cube of 30m of Aspo diorite rock mass (NGI box #409).

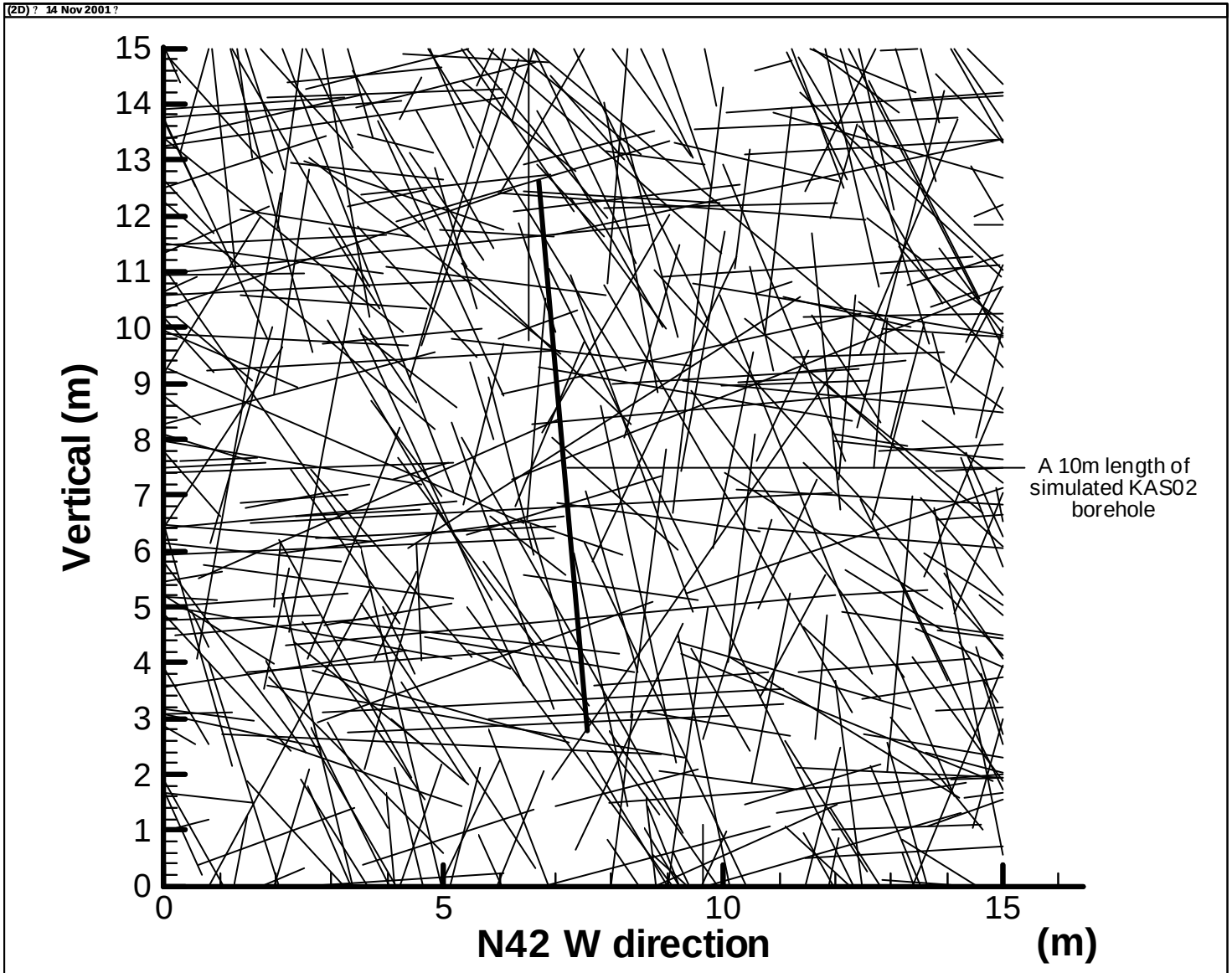

Fig. 4.13 Fracture traces obtained from fracture generation on a vertical square window of size 15 m having strike same as the trend direction of borehole KAS02 placed at the middle of 30m cube of Aspo diorite rock mass (NGI box #409).

5 Stochastic 3-D fracture network model for Småland granite rock mass (NGI block number 169)

5.1 Number of Fracture Sets and Correction for Orientation Bias

NGI block number 169 is located in the depth region 410-440m of borehole KAS02. The number of fractures that exist in Småland granite in this region only is quite limited. However, Småland granite exist in the following depth regions in KAS02 borehole: (a) 375.5-386.3m, (b) 392.4-395.7m and (c) 415.1-455.9m. These three regions are quite close to the region 410-440m. Therefore, to enlarge the Småland granite fracture data base, orientation data were obtained from all the aforementioned three depth regions of borehole KAS02. The fracture data were analyzed in a similar manner to the analysis conducted for Äspö diorite using the computer program CLUSDEL-BINGHAM. The final results obtained for fracture set delineation are shown in Figure 5.1. All four fracture sets show high variability. This high variability is partly reflected by the low number of data available for orientation analyses. Number of orientation data belonging to each fracture set and the mean directions obtained for the fracture sets are shown in Table 5.1.

The computer program OBIAS1D was applied to study the effect of orientation sampling bias on orientation distribution of each of the 4 fracture sets. The obtained results are shown in Figures 5.2 through 5.5. All four fracture sets intersect with the same borehole KAS02. Due to lack of fracture size data, the same probability distribution is used to model fracture size of the 4 fracture sets (see section 5.3). Therefore, comparisons between the 4 fracture sets depend only on the relative orientation distribution between the borehole direction and the directions of fractures of each fracture set. Because borehole KAS02 is almost vertical, according to the obtained mean orientations of fracture sets (Table 5.1), the intersection probabilities between the borehole and the fracture sets in the order of lowest to highest would be for fracture set 2, 1, 3 and 4. With respect to the orientation variability, in the increasing order the 4 fracture sets can be arranged as fracture set 4, 1, 2 and 3 (see Figure 5.1, Table 5.2 and section 5.2). Therefore, fracture sets 3 and 2 have shown the highest effect and fracture set 4 has shown the lowest effect with respect to the orientation bias correction (compare a and b plots of Figs. 5.2 through 5.5).

(Sketch) ? 15 Nov 2001 ?

Fig. 5.1 Fracture set delineation results on an upper hemispherical polar equal area projection for Smaland Granite (NGI box # 169)

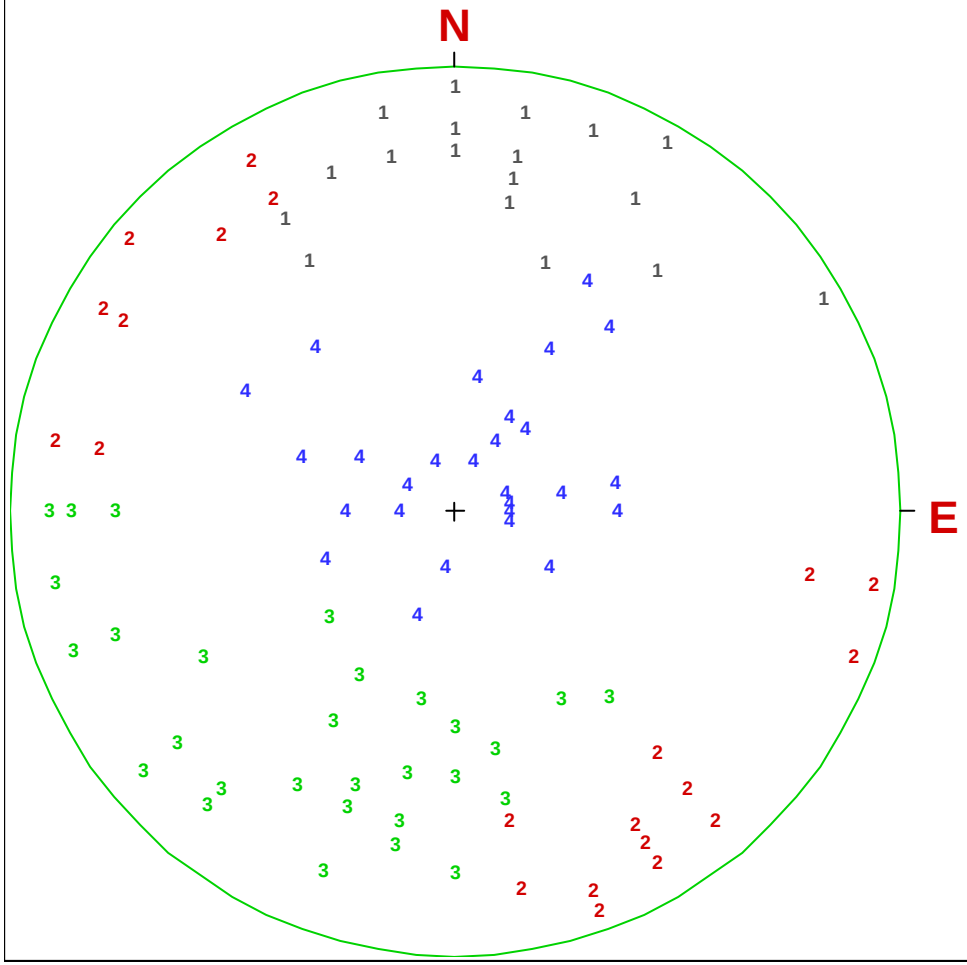

108 POLES

SMALL CIRCLE RADIUS VALUE =
16.19 DEGREES

OBJECTIVE FUNCTION VALUES
F2 = .35
F3 = .37
F4 = 1.06

SYMBOL	FRACTURE SET #	# OF DATA
1	1	21
2	2	26
3	3	33
4	4	28

Table 5.1 Delineated fracture sets and goodness-of-fit results of Bingham distribution for orientation data of Småland granite

Nobs.	Fracture Set	Npts.	Mu 3		Mu 2		Mu 1		Chi-square Test			
			Trend (°)	Plunge (°)	Trend (°)	Plunge (°)	Trend (°)	Plunge (°)	D.F.	chi	95chi	P
108	1	21	10.69	18.79	277.12	10.37	159.88	68.35	-	-	-	-
	2	26	141.35	4.90	233.43	23.03	40.04	66.40	-	-	-	-
	3	33	209.22	35.38	107.08	16.49	358.54	49.84	-	-	-	-
	4	28	12.01	81.24	258.80	3.48	168.31	8.03	-	-	-	-

Note:

Nobs.=Number of fractures observed on the borehole

Npts.=Number of fractures belonging to the fracture set

Mu3=Mean normal vector direction (upward) of fracture set

Trend of Mu3=Dip direction of fracture set

Plunge of Mu3=90°-Dip angle of fracture set

Mu2=Vector normal to minor axis plane of Bingham distribution

Mu1=Vector normal to major axis plane of Bingham distribution

DF= Degrees of freedom for Chi-square test for Bingham distribution

Chi=Calculated Chi-square value

95Chi=Table Chi-square value at 5% significance level

P=Maximum significance level at which Bingham distribution can be used to represent the statistical distribution of orientation of fracture set

(a minimum of 0.05 is required to represent orientation data by a Bingham distribution)

(3D) ? 16 Nov 2001 ? NGI BOX #169 (Smaland Granite)

Fig. 5.2a Observed relative frequency of orientation for fracture set 1 of Smaland granite (NGI box #169).

Based on Line or Borehole(1-D) sampling

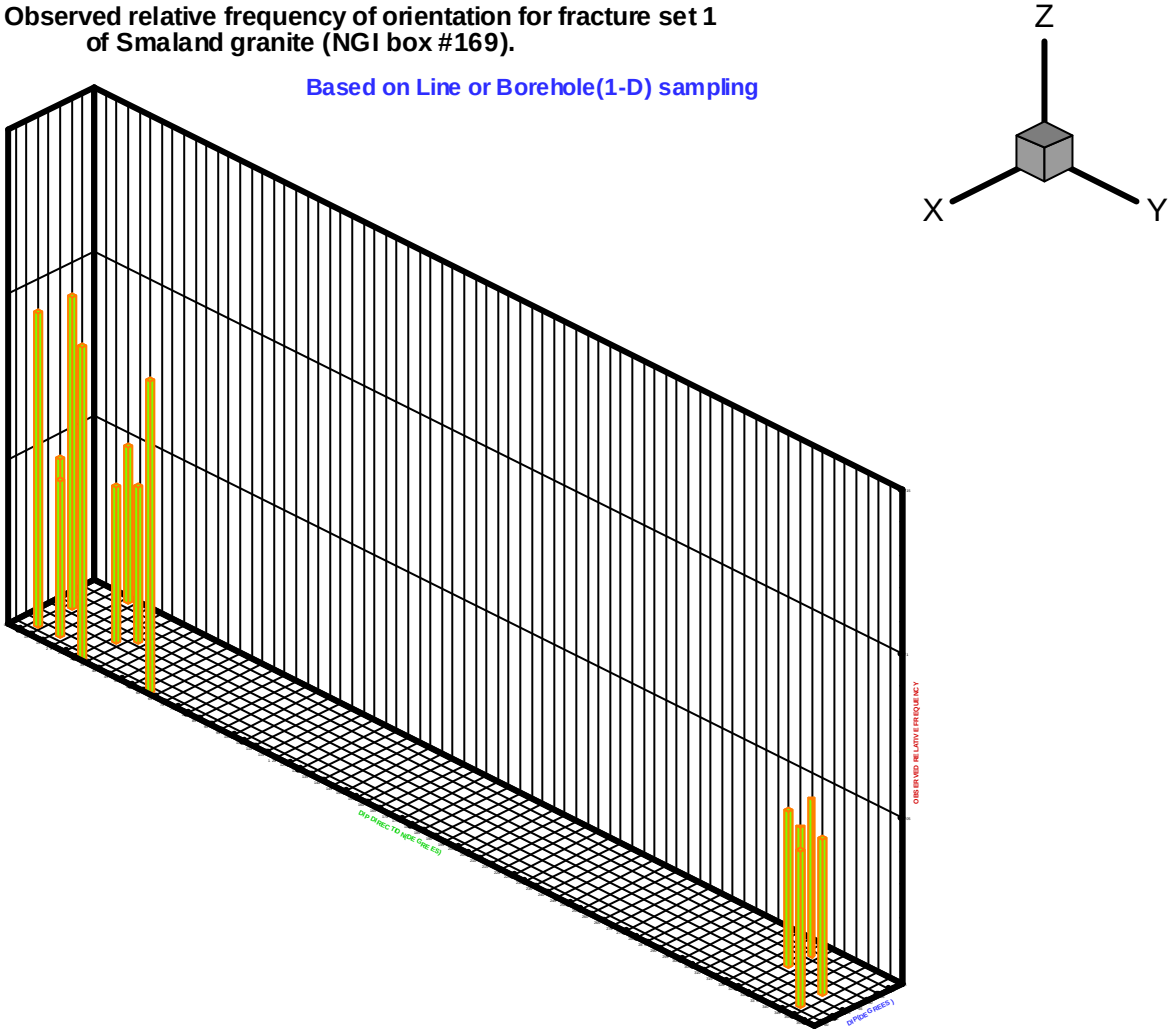

NUMBER OF ORIENTATION DATA = 21
LENGTH OF BOREHOLE = 54.84
TREND OF BOREHOLE = 318.00 (DEG.)
PLUNGE OF BOREHOLE = 85.00 (DEG.)
DIAMETER OF FRACTURE PLANES FROM 5.26 TO 5.26
DIAMETER OF BOREHOLE = .10

A COLUMN REPRESENTS 10 DEGREES(DIP) X 10 DEGREES(DIP DIRE.)
THE MAXIMUM VALUE FOR OBSERVED RELATIVE FREQUENCY = .0952
IT IS LOCATED FROM 60.00 TO 65.00 FOR DIP(DEG.)
AND 5.00 TO 10.00 FOR DIP DIRECTION(DEG.)
THE UNIT FOR LENGTH: Meter

(3D) ? 16 Nov 2001 ? NGI BOX #169 (Smaland Granite)

Fig. 5.2b Corrected relative frequency of orientation for fracture set 1 of Smaland granite (NGI box #169).

Based on Line or Borehole(1-D) sampling

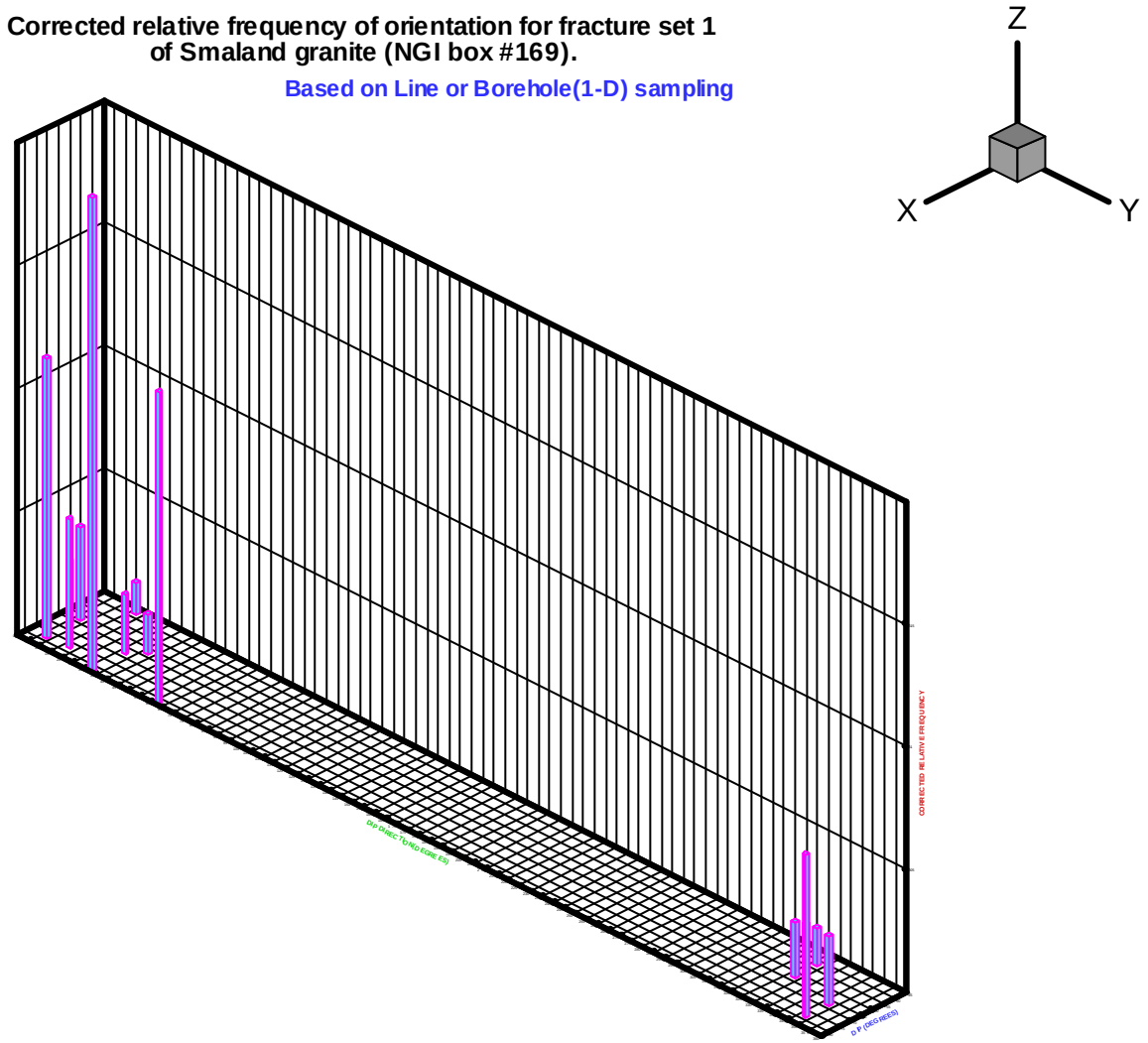

NUMBER OF ORIENTATION DATA = 21
LENGTH OF BOREHOLE = 54.84
TREND OF BOREHOLE = 318.00 (DEG.)
PLUNGE OF BOREHOLE = 85.00 (DEG.)
DIAMETER OF FRACTURE PLANES FROM 5.26 TO 5.26
DIAMETER OF BOREHOLE = .10

A COLUMN REPRESENTS 10 DEGREES(DIP) X 10 DEGREES(DIP DIRE.)
THE MAXIMUM VALUE FOR CORRECTED RELATIVE FREQUENCY = .1925
IT IS LOCATED FROM 80.00 TO 85.00 FOR DIP(DEG.)
AND 30.00 TO 35.00 FOR DIP DIRECTION(DEG.)
THE UNIT FOR LENGTH: Meter

Fig. 5.3a Observed relative frequency of orientation for fracture set 2 of Smaland granite (NGI box #169).

Based on Line or Borehole(1-D) sampling

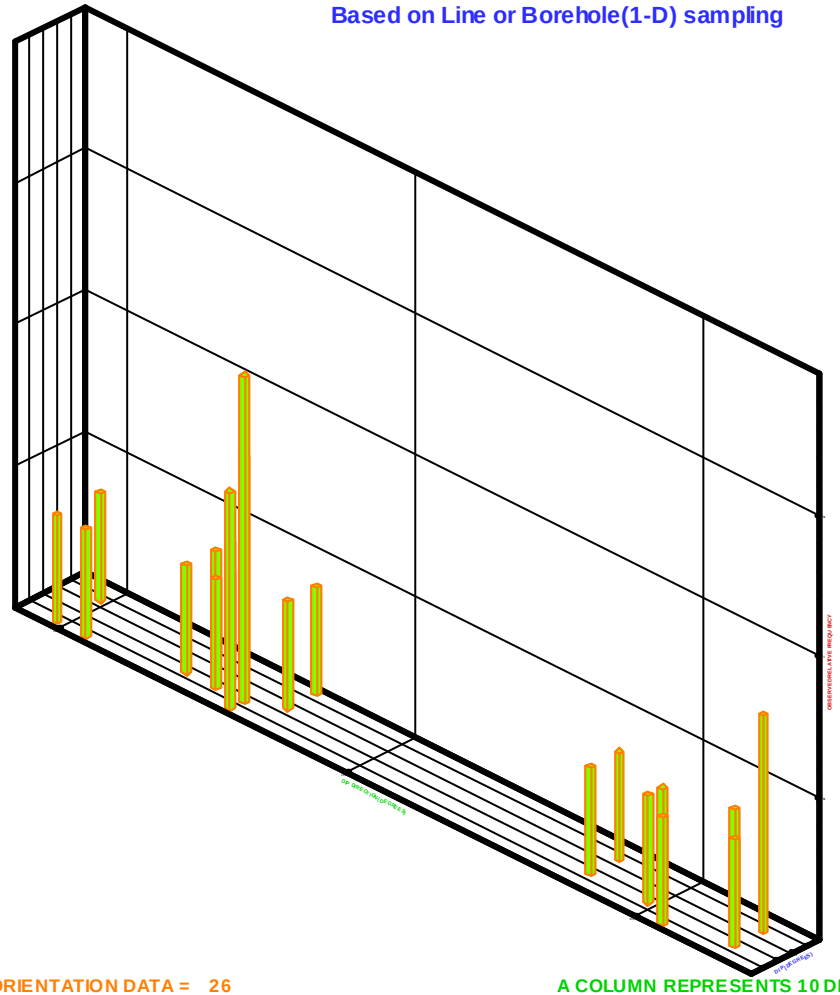

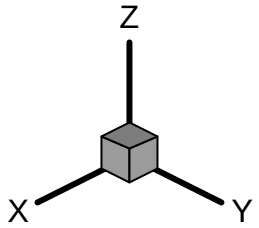

NUMBER OF ORIENTATION DATA = 26
LENGTH OF BOREHOLE = 54.84
TREND OF BOREHOLE = 318.00 (DEG.)
PLUNGE OF BOREHOLE = 85.00 (DEG.)
DIAMETER OF FRACTURE PLANES FROM 5.26 TO 5.26
DIAMETER OF BOREHOLE= .10

A COLUMN REPRESENTS 10 DEGREES(DIP) X 10 DEGREES(DIP DIRE.)
THE MAXIMUM VALUE FOR OBSERVED RELATIVE FREQUENCY = .1154
IT IS LOCATED FROM 75.00 TO 80.00 FOR DIP(DEG.)
AND 155.00 TO 160.00 FOR DIP DIRECTION(DEG.)
THE UNIT FOR LENGTH: Meter

(3D) ? 16 Nov 2001 ? NGI BOX #169 (Smaland Granite)

Fig. 5.3b Corrected relative frequency of orientation for fracture set 2 of Smaland granite (NGI box #169).

Based on Line or Borehole(1-D) sampling

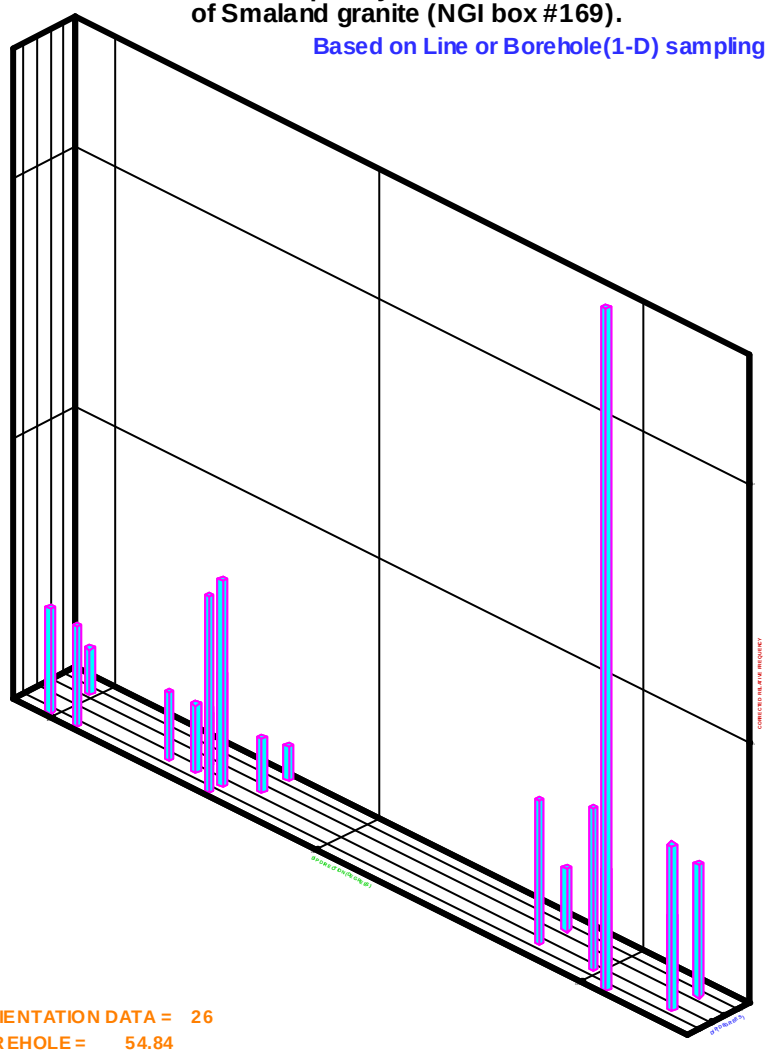

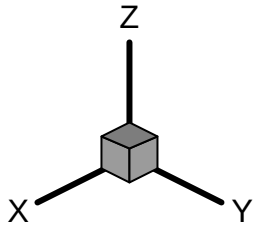

NUMBER OF ORIENTATION DATA = 26
LENGTH OF BOREHOLE = 54.84
TREND OF BOREHOLE = 318.00 (DEG.)
PLUNGE OF BOREHOLE = 85.00 (DEG.)
DIAMETER OF FRACTURE PLANES FROM 5.26 TO 5.26
DIAMETER OF BOREHOLE = .10

A COLUMN REPRESENTS 10 DEGREES(DIP) X 10 DEGREES(DIP DIRE.)
THE MAXIMUM VALUE FOR CORRECTED RELATIVE FREQUENCY = .2633
IT IS LOCATED FROM 80.00 TO 85.00 FOR DIP(DEG.)
AND 305.00 TO 310.00 FOR DIP DIRECTION(DEG.)
THE UNIT FOR LENGTH: Meter

Fig. 5.4a Observed relative frequency of orientation for fracture set 3 of Smaland granite (NGI box #169).

Based on Line or Borehole(1-D) sampling

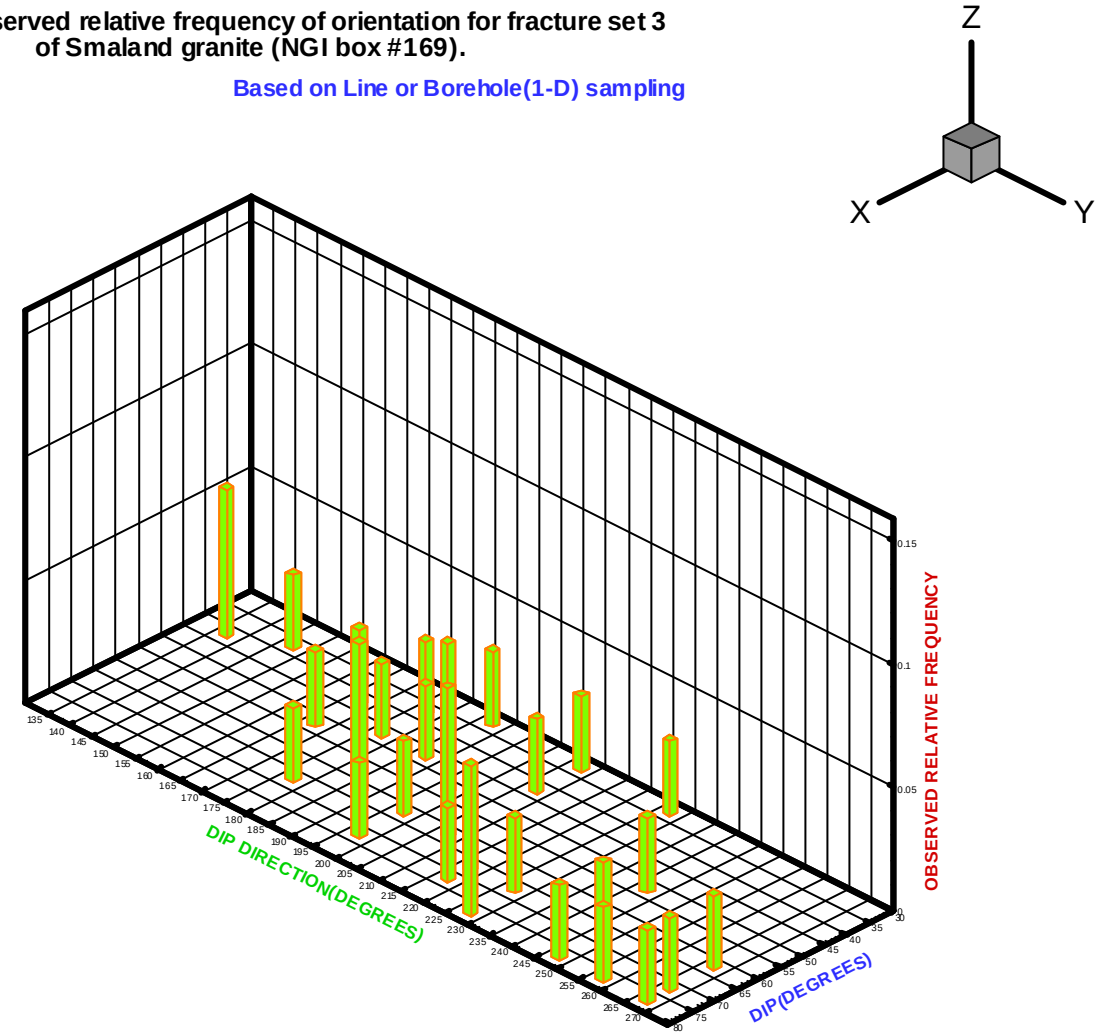

NUMBER OF ORIENTATION DATA = 33
LENGTH OF BOREHOLE = 54.84
TREND OF BOREHOLE = 318.00 (DEG.)
PLUNGE OF BOREHOLE = 85.00 (DEG.)
DIAMETER OF FRACTURE PLANES FROM 5.26 TO 5.26
DIAMETER OF BOREHOLE = .10

A COLUMN REPRESENTS 10 DEGREES(DIP) X 10 DEGREES(DIP DIRE.)
THE MAXIMUM VALUE FOR OBSERVED RELATIVE FREQUENCY = .0606
IT IS LOCATED FROM 40.00 TO 45.00 FOR DIP(DEG.)
AND 135.00 TO 140.00 FOR DIP DIRECTION(DEG.)
THE UNIT FOR LENGTH: Meter

(3D) ? 15 Nov 2001 ? NGI BOX #169 (Smaland Granite)

Fig. 5.4b Corrected relative frequency of orientation for fracture set 3 of Smaland granite (NGI box #169).

Based on Line or Borehole(1-D) sampling

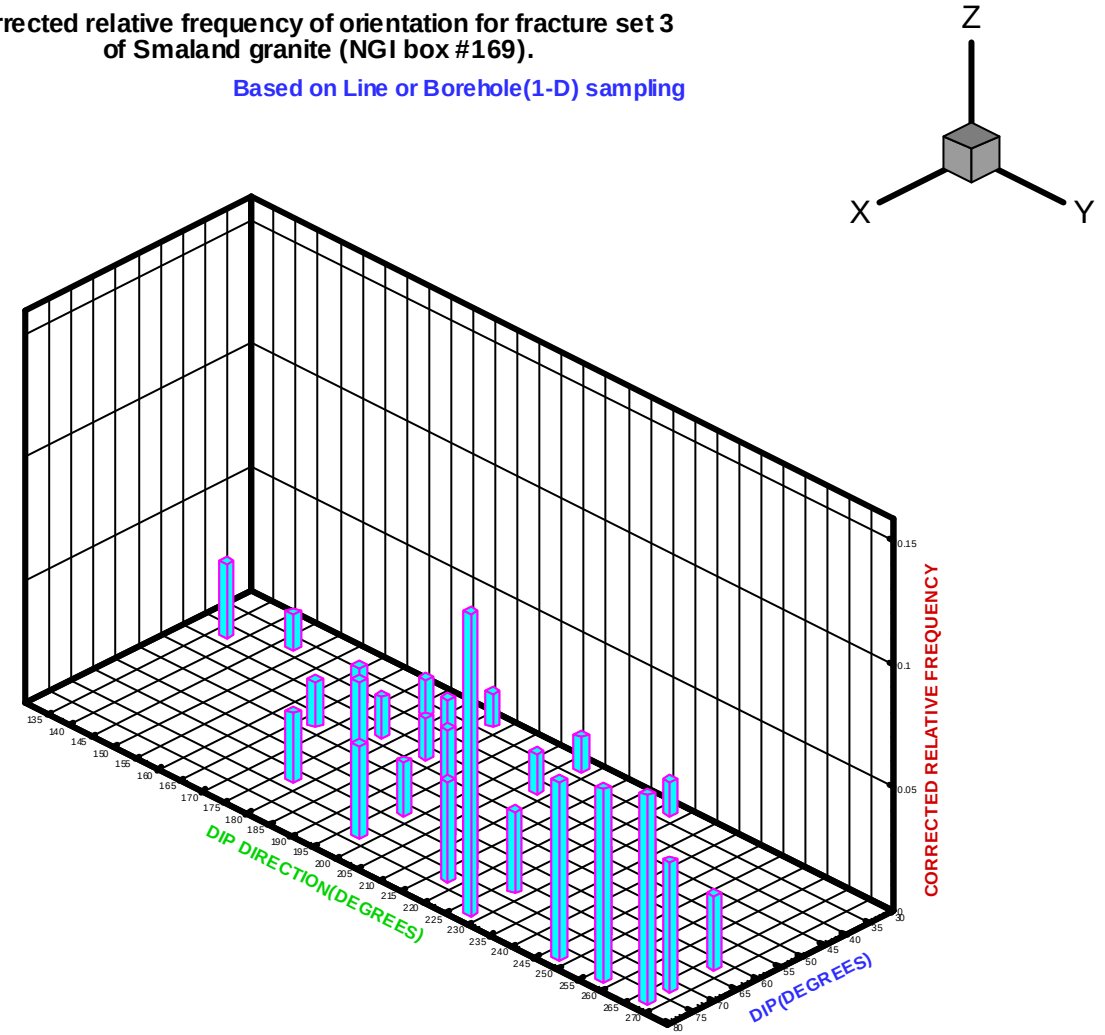

NUMBER OF ORIENTATION DATA = 33
LENGTH OF BOREHOLE = 54.84
TREND OF BOREHOLE = 318.00 (DEG.)
PLUNGE OF BOREHOLE = 85.00 (DEG.)
DIAMETER OF FRACTURE PLANES FROM 5.26 TO 5.26
DIAMETER OF BOREHOLE = .10

A COLUMN REPRESENTS 10 DEGREES(DIP) X 10 DEGREES(DIP DIRE.)
THE MAXIMUM VALUE FOR CORRECTED RELATIVE FREQUENCY = .1226
IT IS LOCATED FROM 75.00 TO 80.00 FOR DIP(DEG.)
AND 225.00 TO 230.00 FOR DIP DIRECTION(DEG.)
THE UNIT FOR LENGTH: Meter

(3D) ? 15 Nov 2001 ? NGI BOX #169 (Smaland Granite)

Fig. 5.5a Observed relative frequency of orientation for fracture set 4 of Smaland granite (NGI box #169).

Based on Line or Borehole(1-D) sampling

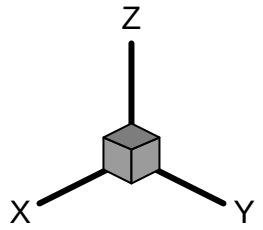

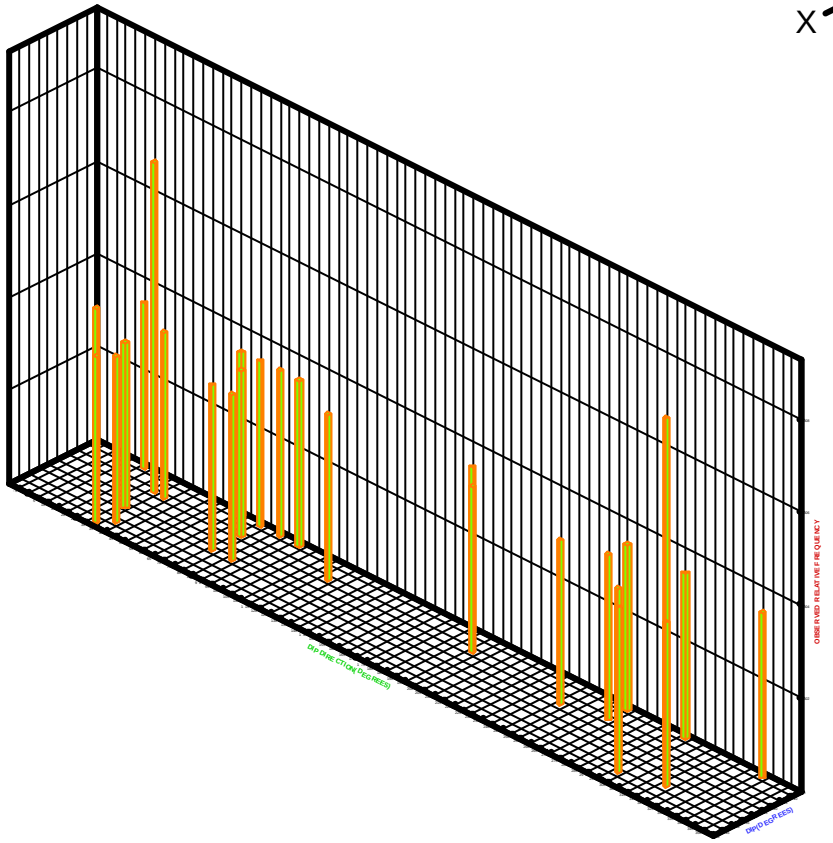

NUMBER OF ORIENTATION DATA = 28
LENGTH OF BOREHOLE = 54.84
TREND OF BOREHOLE = 318.00 (DEG.)
PLUNGE OF BOREHOLE = 85.00 (DEG.)
DIAMETER OF FRACTURE PLANES FROM 5.26 TO 5.26
DIAMETER OF BOREHOLE = .10

A COLUMN REPRESENTS 10 DEGREES(DIP) X 10 DEGREES(DIP DIRE.)
THE MAXIMUM VALUE FOR OBSERVED RELATIVE FREQUENCY = .0714
IT IS LOCATED FROM 15.00 TO 20.00 FOR DIP(DEG.)
AND 30.00 TO 35.00 FOR DIP DIRECTION(DEG.)
THE UNIT FOR LENGTH: Meter

(3D) ? 15 Nov 2001 ? NGI BOX #169 (Smaland Granite)

Fig. 5.5b Corrected relative frequency of orientation for fracture set 4 of Smaland granite (NGI box #169).

Based on Line or Borehole(1-D) sampling

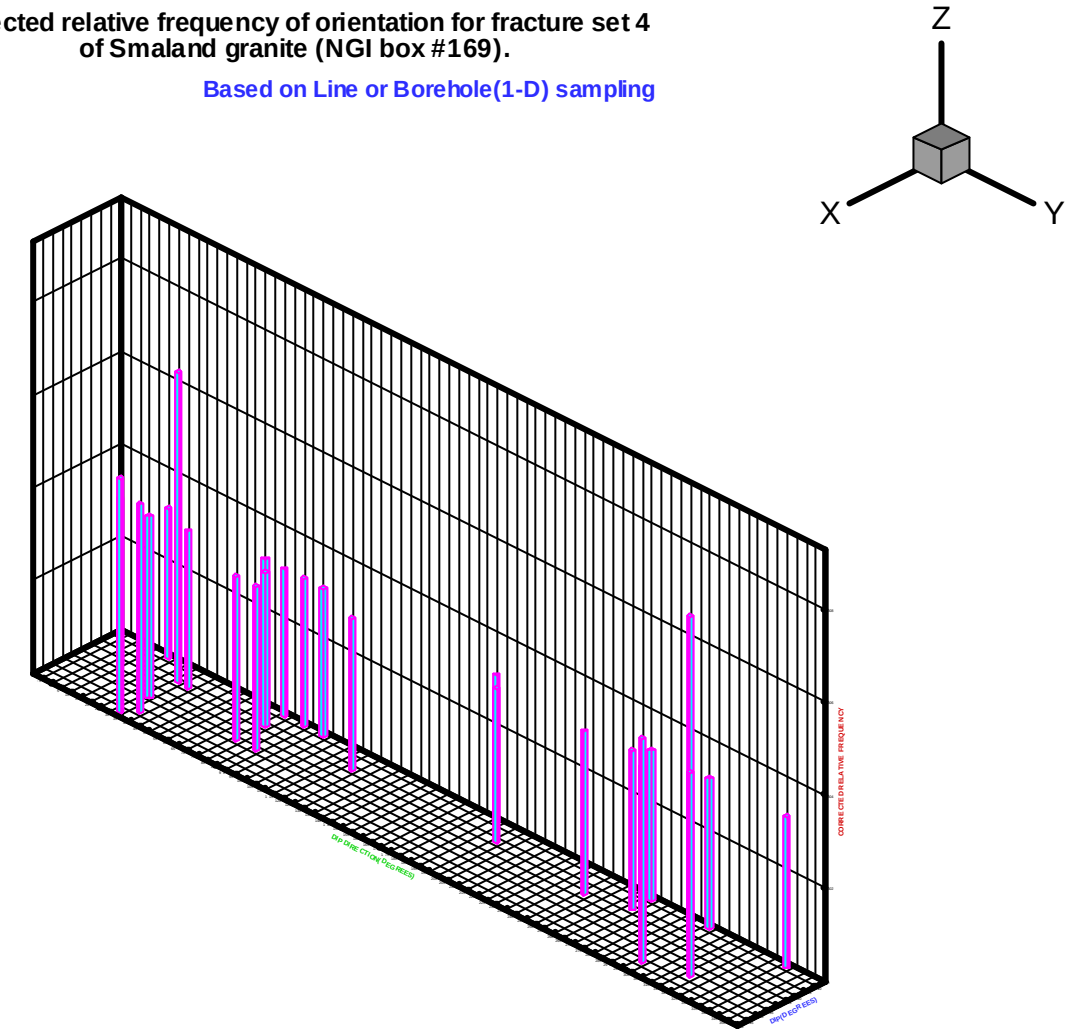

NUMBER OF ORIENTATION DATA = 28
LENGTH OF BOREHOLE = 54.84
TREND OF BOREHOLE = 318.00 (DEG.)
PLUNGE OF BOREHOLE = 85.00 (DEG.)
DIAMETER OF FRACTURE PLANES FROM 5.26 TO 5.26
DIAMETER OF BOREHOLE = .10

A COLUMN REPRESENTS 10 DEGREES(DIP) X 10 DEGREES(DIP DIRE.)
THE MAXIMUM VALUE FOR CORRECTED RELATIVE FREQUENCY = .0694
IT IS LOCATED FROM 15.00 TO 20.00 FOR DIP(DEG.)
AND 295.00 TO 300.00 FOR DIP DIRECTION(DEG.)
THE UNIT FOR LENGTH: Meter

5.2 Orientation Distribution for Each Fracture Set

Goodness-of-fit of hemispherical normal distribution was performed for both the raw and corrected orientation data of each fracture set using the computer program HEMISPHN. For fracture sets 3, 2 and 1 the mean normal vector direction and the distribution of the orientation have changed to some extent due to the orientation bias correction (compare plots a and b of Figs. 5.6 through 5.9). This indicates the importance of applying the orientation sampling bias correction in modeling joint orientation distribution. The summary results (Table 5.2) indicate that hemispherical normal distribution is not suitable to represent the statistical distribution of orientation of all 4 fracture sets. According to the spherical variance and *k* values in Table 5.2, in the increasing order of orientation variability the fracture sets can be arranged as fracture sets 4, 1, 2 and 3.

Goodness-of-fit of Bingham distribution was performed for the orientation data of each fracture set using the computer program CLUSDEL-BINGHAM. The results (Table 5.1) provide mean normal vectors for the fracture sets. However, the results show that the number of data for each fracture set is too small to perform Chi-square goodness-of-fit test for Bingham distribution.

Aforementioned results show that the available theoretical probability distributions (hemispherical normal and Bingham distributions) cannot be used to represent the statistical distribution of orientation of all four fracture sets. Therefore, the empirical orientation distribution obtained from the corrected relative frequency data is used to generate orientation values for each of the four fracture sets.

5.3 Trace Length and Size Distributions for Each Fracture Set

As mentioned before, no fracture trace data were provided for this project to model fracture trace length distribution and size distribution in 3-D. Due to lack of reliable data on fracture traces, the same gamma distribution (mean=5m and coefficient of variation=0.5) used for Äspö diorite is also used to represent the fracture trace length distribution in 2-D for all 4 fracture sets. As for Äspö diorite, the equivalent fracture diameter in 3-D for all four fracture sets is represented by the gamma distribution with mean = 5.26m and standard deviation = 2.25m.

Fig. 5.6a Results of hemispherical normal distribution fit for observed orientation data of fracture set 1 of Smaland granite (NGI box #169).

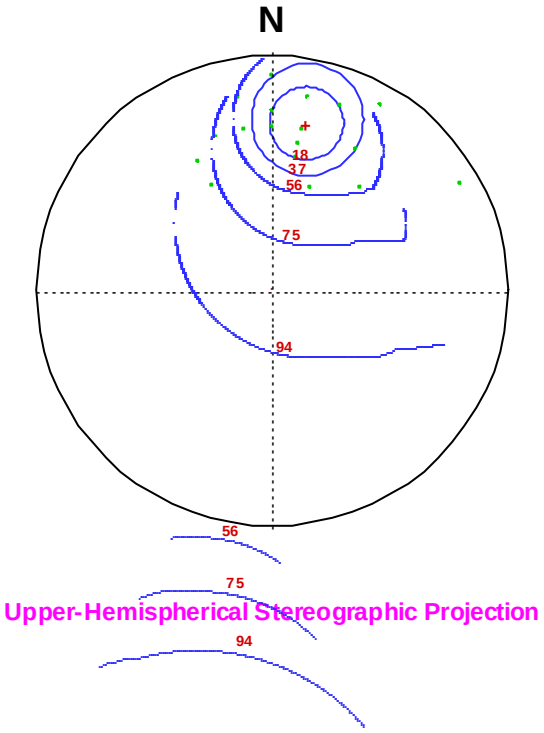

The number given for the contour is the percent(%) confidence

Maximum significance level at which the hemispherical normal distribution is suitable to represent the statistical distribution of joint orientation data : .039

Number of Joint Data = 21

Average L = .9266
Average M = -.1914
Average N = .3238

Magnitude of Mean Vector = .9060
Mean Plunge(up) = 18.8934 (deg.)
Mean Trend = 11.6715 (deg.)
K Value of the Distribution = 10.1334
Spherical Variance = .0940

The small + indicates the mean normal vector to the joint set

The small . indicate the joint normal vectors

(2D)? 15 Nov 2001 ?HEMISPHERICAL NORMAL DISTRIBUTION GOODNESS-OF-FIT RESULTS

Fig. 5.6b Results of hemispherical normal distribution fit for orientation data of fracture set 1 of Smaland granite (NGI box #169) corrected for sampling bias.

Probability(%Confidence) Contours for the
Hemispherical Normal Distribution of Fracture Normals

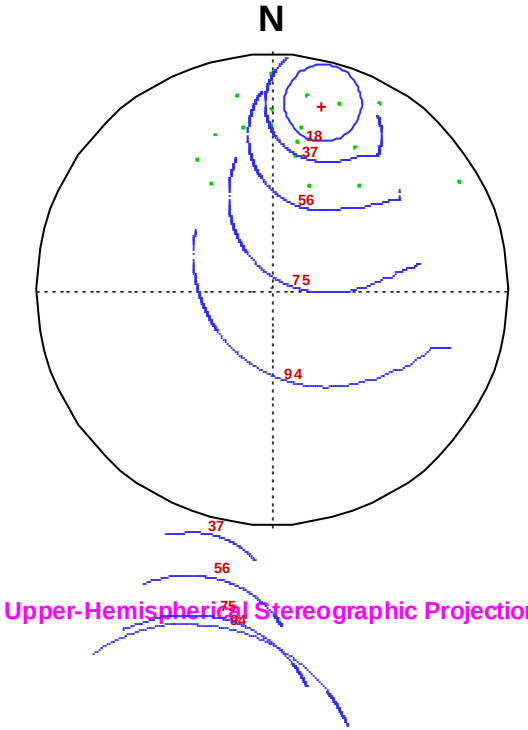

Upper-Hemispherical Stereographic Projection

The number given for the contour
is the percent(%) confidence

Maximum significance level at which the
hemispherical normal distribution is suitable
to represent the statistical distribution of joint
orientation data : < 0.005

Number of Joint Data = 21

Average L = .9433
Average M = -.2574
Average N = .2097

Magnitude of Mean Vector = .9133
Mean Plunge(up) = 12.1065 (deg.)
Mean Trend = 15.2642 (deg.)
K Value of the Distribution = 10.9910
Spherical Variance = .0867

The small + indicates the mean normal vector
to the joint set

The small . indicate the joint normal vectors

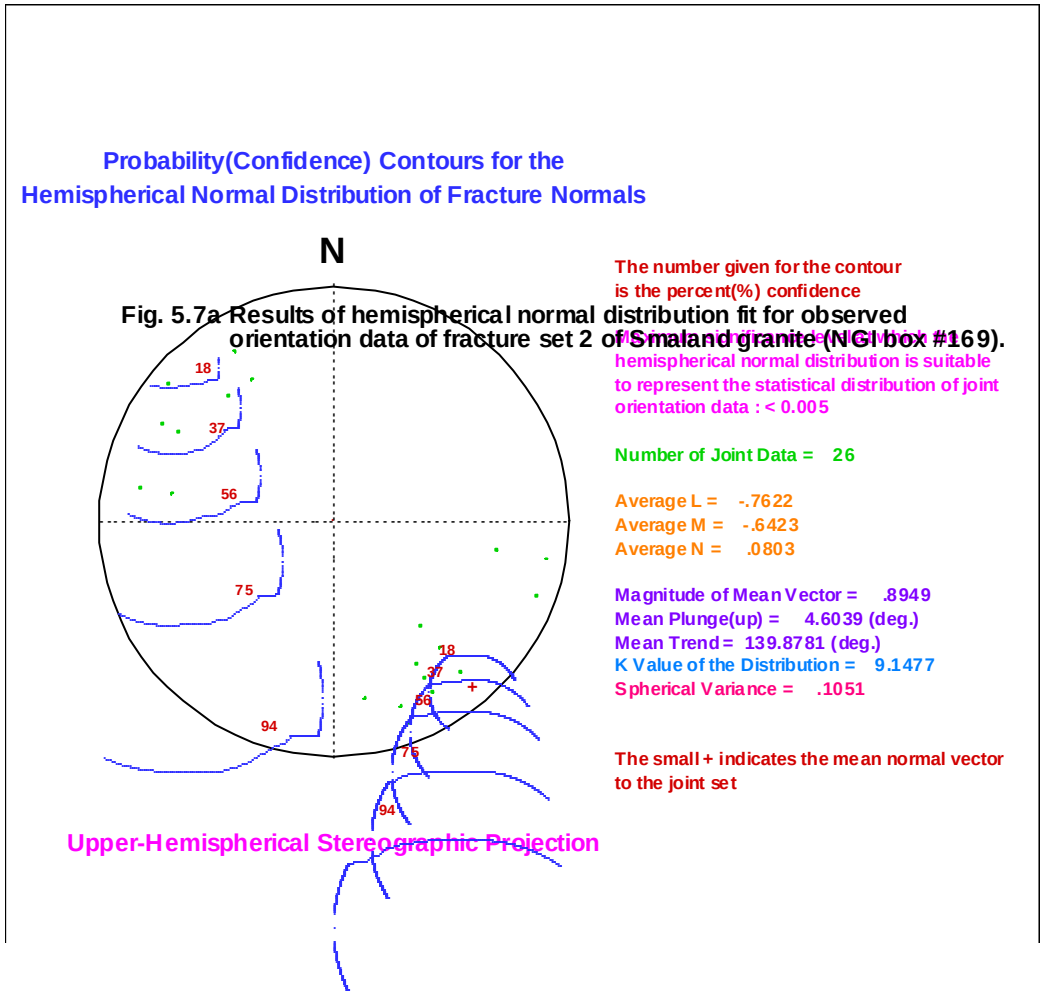

Fig. 5.7a Results of hemispherical normal distribution fit for observed orientation data of fracture set 2 of Smaland granite (NGI box #169).

(2D)? 15 Nov 2001 ?HEMISPHERICAL NORMAL DISTRIBUTION GOODNESS-OF-FIT RESULTS

Fig. 5.7b Results of hemispherical normal distribution fit for orientation data of fracture set 2 of Smaland granite (NGI box #169) corrected for sampling bias.

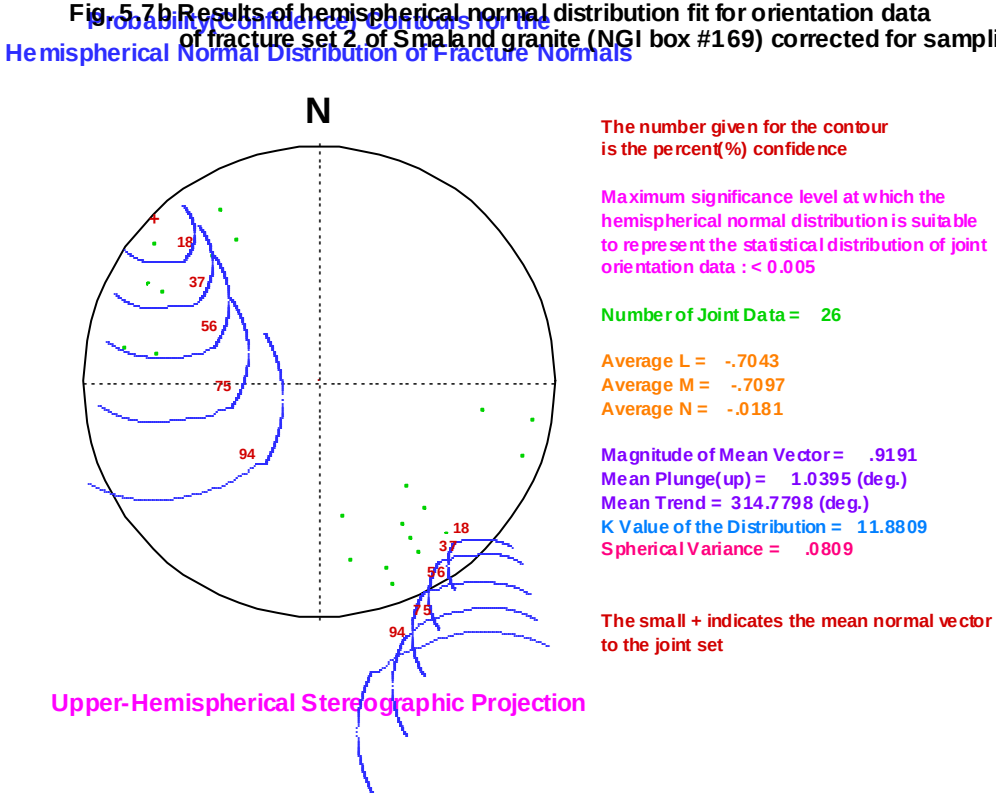

The number given for the contour is the percent(%) confidence

Maximum significance level at which the hemispherical normal distribution is suitable to represent the statistical distribution of joint orientation data : < 0.005

Number of Joint Data = 26

Average L = -.7043
Average M = -.7097
Average N = -.0181

Magnitude of Mean Vector = .9191
Mean Plunge(up) = 1.0395 (deg.)
Mean Trend = 314.7798 (deg.)
K Value of the Distribution = 11.8809
Spherical Variance = .0809

The small + indicates the mean normal vector to the joint set

The small . indicate the joint normal vectors

Fig. 5.8a Results of hemispherical normal distribution fit for observed orientation data of fracture set 3 of Smaland granite (NGI box #169).

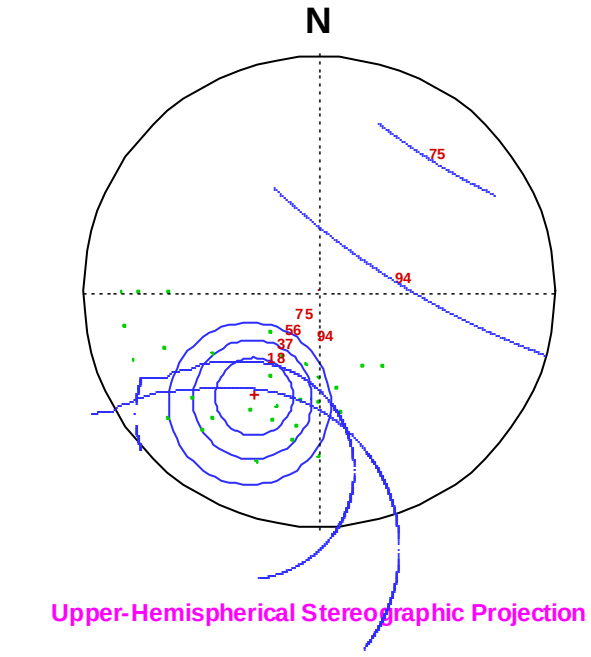

The number given for the contour is the percent(%) confidence

Maximum significance level at which the hemispherical normal distribution is suitable to represent the statistical distribution of joint orientation data : < 0.005

Number of Joint Data = 33

Average L = -.6912
Average M = .4265
Average N = .5834

Magnitude of Mean Vector = .8468
Mean Plunge(up) = 35.6876 (deg.)
Mean Trend = 211.6773 (deg.)
K Value of the Distribution = 6.3316
Spherical Variance = .1532

The small + indicates the mean normal vector to the joint set

The small . indicate the joint normal vectors

Fig. 5.8b Results of hemispherical normal distribution fit for orientation data of fracture set 3 of Smaland granite (NGI box #169) corrected for sampling bias.

Probability(Confidence) Contours for the Hemispherical Normal Distribution of Fracture Normals

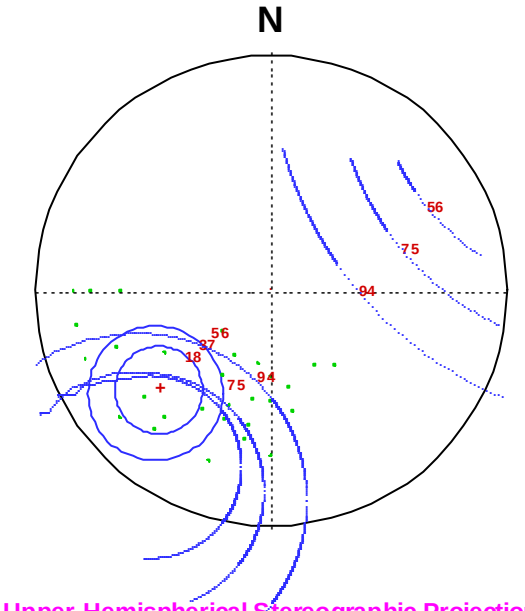

Upper-Hemispherical Stereographic Projection

The number given for the contour is the percent(%) confidence

Maximum significance level at which the hemispherical normal distribution is suitable to represent the statistical distribution of joint orientation data : < 0.005

Number of Joint Data = 33

Average L = -.5964
Average M = .6695
Average N = .4428

Magnitude of Mean Vector = .8399
Mean Plunge(up) = 26.2814 (deg.)
Mean Trend = 228.3060 (deg.)
K Value of the Distribution = 6.0587
Spherical Variance = .1601

The small + indicates the mean normal vector to the joint set

The small . indicate the joint normal vectors

(2D)? 15 Nov 2001 ?Upper-Hemispherical Stereographic Projection

Fig. 5.9a Results of hemispherical normal distribution fit for observed orientation data of fracture set 4 of Smaland granite (NGI box #169).

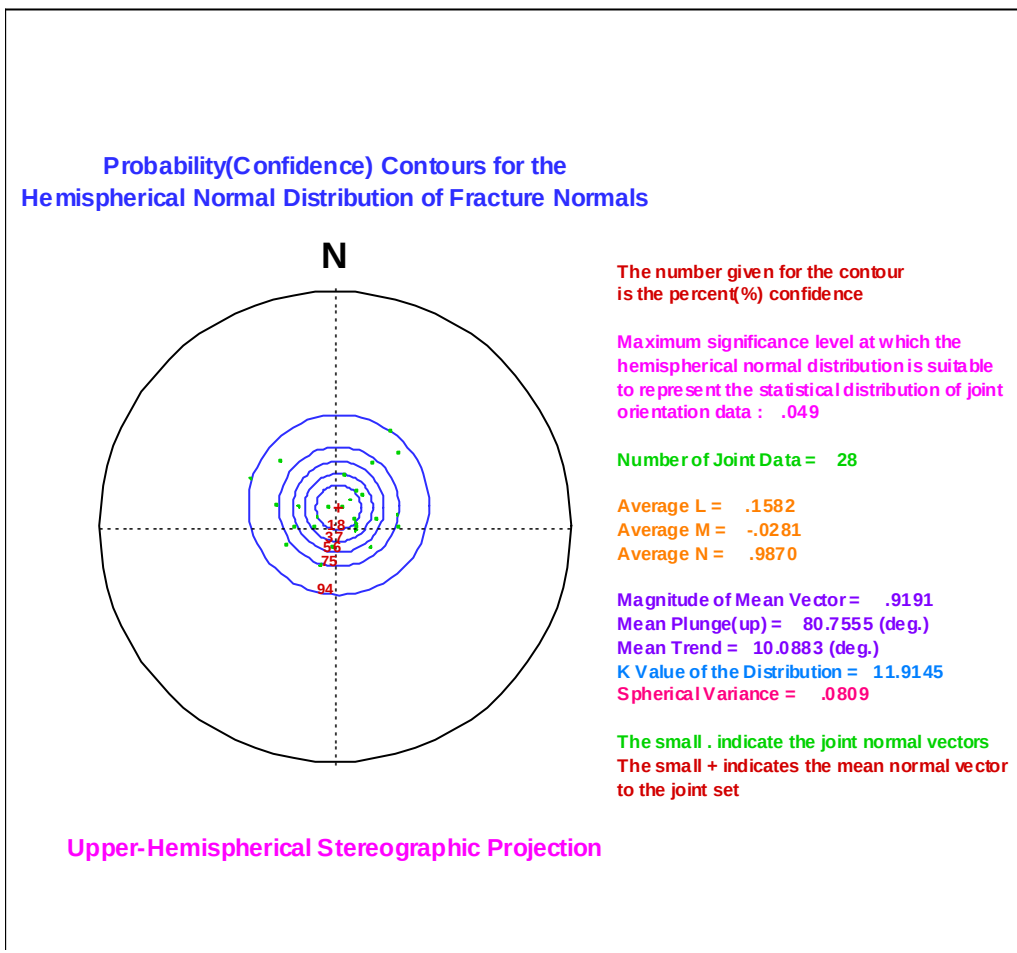

(2D)? 15 Nov 2001 ?HEMISPHERICAL NORMAL DISTRIBUTION GOODNESS-OF-FIT RESULTS

Fig. 5.9b Results of hemispherical normal distribution fit for orientation data of fracture set 4 of Smaland granite (NGI box #169) corrected for sampling bias.

Probability(Confidence) Contours for the
Hemispherical Normal Distribution of Fracture Normals

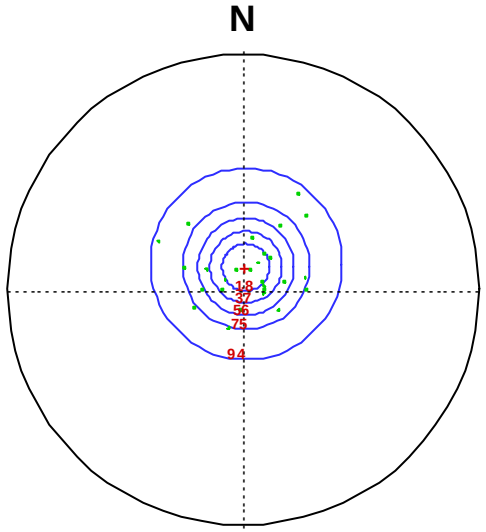

The number given for the contour
is the percent(%) confidence

Maximum significance level at which the hemispherical normal distribution is suitable to represent the statistical distribution of joint orientation data : .036

Number of Joint Data = 28

Average L = .1859
Average M = -.0232
Average N = .9823

Magnitude of Mean Vector = .9103
Mean Plunge(up) = 79.2039 (deg.)
Mean Trend = 7.1176 (deg.)
K Value of the Distribution = 10.7525
Spherical Variance = .0897

The small . indicate the joint normal vectors
The small + indicates the mean normal vector to the joint set

Upper-Hemispherical Stereographic Projection

Table 5.2 Goodness-of-fit results of hemispherical normal distribution for orientation data of Småland granite

(a) Raw orientation data

Nobs.	Fracture set #	Npts.	Upward mean normal vector		K	Sp. Var.	P
			Trend (°)	Plunge (°)			
108	1	21	11.67	18.89	10.13	0.0940	0.039
	2	26	139.88	4.60	9.15	0.1051	<0.005
	3	33	211.68	35.69	6.33	0.1532	<0.005
	4	28	10.09	80.76	11.91	0.0809	0.049

(b) Data corrected for sampling bias

Nobs.	Fracture set #	Npts.	Upward mean normal vector		K	Sp. Var.	P
			Trend (°)	Plunge (°)			
108	1	21	15.26	12.12	10.99	0.0869	<0.005
	2	26	314.78	1.04	11.88	0.0809	<0.005
	3	33	228.30	26.28	6.06	0.1601	<0.005
	4	28	7.12	79.20	10.75	0.0897	0.036

Nobs.=Number of fractures observed on the borehole
Npts.=Number of fractures belonging to the fracture set
K=A parameter in the hemispherical normal distribution
Sp. Var.=Spherical variance
P=Maximum significance level at which the hemispherical normal distribution is suitable to represent the statistical distribution of fracture orientation data
(a minimum of 0.05 is required to represent orientation data by a hemispherical normal distribution)

5.4 Spacing Distribution and 1-D Fracture frequency for Each Fracture Set

Fracture spacing data were obtained from the same depth regions of borehole KAS02 as mentioned in section 5.1. Goodness-of-fit tests were performed using GDFT computer program to find the suitable probability distributions as well as the best probability distribution to represent the statistical distribution of spacing for each fracture set. The results (Table 5.3) indicate that all three probability distributions lognormal, gamma and exponential are highly suitable to represent the statistical distribution of spacing for any of the 4 fracture sets. The gamma distribution was found to be the best distribution for 2 fracture sets and 2nd best distribution for the other two fracture sets. The exponential distribution turned out to be the best distribution for 1 fracture set and 2nd best distribution for 2 fracture sets. The lognormal distribution was found to be the best distribution for 1 fracture set.

The estimation of mean spacing and 1-D fracture frequency along the borehole direction and mean normal vector direction of each fracture set were conducted in the same way it was done for Äspö diorite rock mass using the computer program COR1DFM1 The obtained results are given in Table 5.4. Note that for fracture sets 1 and 2, the angle between the borehole direction and the mean normal vector direction of the fracture set is greater than 70 degrees (Table 5.4). Because of the reasons mentioned in section 4.4, for these two fracture sets the 1-D fracture frequency along the mean normal vector direction is estimated by limiting the aforementioned angle to 70 degrees.

Table 5.3 Goodness-of-fit test results for spacing of the four fracture sets of Småland granite (NGI box # 169)

Fracture set #	No. of data	Mean (m)	Var (m^2)	Probability Distribution	K-S_{stat} Value	df	P-value	Best Distribution Rank
1	20	2.8540	10.9042	Exponential	0.1486	6	>0.2	1
				Gamma	0.1492	6	>0.2	2
				LogNormal	0.1638	6	>0.2	3
2	24	1.9338	3.9166	Exponential	0.0797	6	>0.2	3
				Gamma	0.0773	6	>0.2	2
				LogNormal	0.0727	6	>0.2	1
3	31	1.6913	3.2072	Exponential	0.0621	6	>0.2	2
				Gamma	0.0580	6	>0.2	1
				LogNormal	0.0858	6	>0.2	3
4	25	2.0800	5.8419	Exponential	0.1088	6	>0.2	2
				Gamma	0.0944	6	>0.2	1
				LogNormal	0.1170	6	>0.2	3

Table 5.4 Mean spacings and linear frequencies along the borehole KAS02 and mean normal vector directions for fracture sets of Småland granite (NGI box #169)

Fracture set #	Orientation of fracture set		Dir. of borehole		Obs. mean spacing along borehole (m)	Length of borehole (m)	Corr. mean spacing along borehole (m)	1-D fracture frequency along borehole (# per m)	Angle between borehole & MNV (deg.)	1-D fracture frequency along MNV (# per m)
	Dip dir. (degs.)	Dip (degs.)	Trend (degs.)	Plunge (degs.)						
1	011	71	318	85	2.85	54.84	2.85	0.35	*70 (74.60)	1.02
2	141	85	318	85	1.93	54.84	1.93	0.52	*70 (79.61)	1.52
3	209	55	318	85	1.69	54.84	1.69	0.59	53.02	0.98
4	012	09	318	85	2.08	54.84	2.08	0.48	12.79	0.49

MNV = Mean Normal Vector of fracture set

* = Actual angle is greater than 70°; however the angle was limited to 70° to calculate the 1-D fracture frequency along MNV direction

5.5 1-D Fracture frequency in any Direction in 3-D

The 1-D fracture frequencies obtained along the mean normal vector directions of fracture sets were then used to estimate the 1-D fracture frequency in all the directions in 3-D by using the computer program FREQ1DALLDIR. Figure 5.10 shows the obtained results. This figure also pin points the directions and magnitudes for the minimum and maximum fracture frequencies for the Småland granite rock mass.

5.6 Mean Estimates for Block Size, Number of Blocks per Unit Volume and Number of Fractures per Unit Volume

The spacing distributions obtained along the mean normal vector directions for the 4 fracture sets were used along with the orientation distributions of the fracture sets in generating rock blocks in 3-D using the Monte-Carlo simulation procedure. This was performed using the computer program FREQ3DMVDJS. Orientations for the fracture sets were generated according to the obtained empirical orientation distributions. The obtained results for the distribution of volume of equivalent matrix block at a trimming level of 30% are shown in Figure 5.11 along with the trimmed mean value. Similar results for the number of matrix blocks per unit volume are shown in Figure 5.12.

Volumetric fracture frequencies for the 4 fracture sets were estimated in a similar manner to it was conducted for the Äspö diorite rock mass using the computer program 3DINTF1D. Obtained results are given in Table 5.5.

5.7 Fracture System Generation in 3-D and Validation

Three-dimensional fracture system for a 30m cube of Småland Granite rock mass (NGI block # 169) was generated similar to the way it was generated for Äspö diorite rock mass using the computer program GENERATE. Figure 5.13 shows the fracture traces obtained from the fracture generation on a horizontal square window of 15m placed at the mid-level of the 30m cube. Out of the four fracture sets, the first three fracture sets are sub-vertical and fracture set 4 is sub-horizontal (see Figure 5.1). Therefore, fracture sets 1, 2 and 3 should intersect the horizontal window better than fracture set 4. According to Table 5.2b, the mean strike values of the fracture sets 1, 2 and 3 are N 75° W, S 45° W, and S 42° E, respectively. Strike directions around these three mean strikes can be seen very well in Figure 5.13. Even though the mean strike for fracture set 4 is N 83° W, because it is a sub horizontal fracture set, strikes of the fractures coming from this set can cover a wide range. Such fracture traces can be seen on Figure 5.13. Figure 5.14 shows the fracture traces obtained from the fracture generation on a vertical square window of size 15m having the strike direction same as the trend direction of borehole KAS02 (318°) and placed at the middle of the 30m cube. Fracture set 1 strikes N 75° W and dips 78° NE. Therefore, fracture set 1 should intersect the chosen vertical window fairly well and produce traces having high apparent dips. Such traces can be seen very well on Figure 5.14. Fracture set 2 is almost vertical with a mean strike of S 45° W. Therefore, fracture set 2 should intersect the chosen vertical window well and produce traces around the vertical. Figure 5.14 shows such traces very well. Fracture set 3 strikes S 42° E and

(2D) ? 15 Nov 2001 ?

Fig. 5.10 1-D fracture frequency distribution in 3-D on an equal-angle equatorial net on the upper hemispherical for Smaland granite rock mass (NGI box #169).

Length Unit: Meter

Minimum Fracture Frequency:		Maximum Fracture Frequency:	
Magnitude(#/Length Unit):	1.1667	Magnitude(#/Length Unit):	2.9266
Trend(Deg.):	44.6700	Trend(Deg.):	352.9100
Plunge(Deg.):	53.6200	Plunge(Deg.):	2.2700

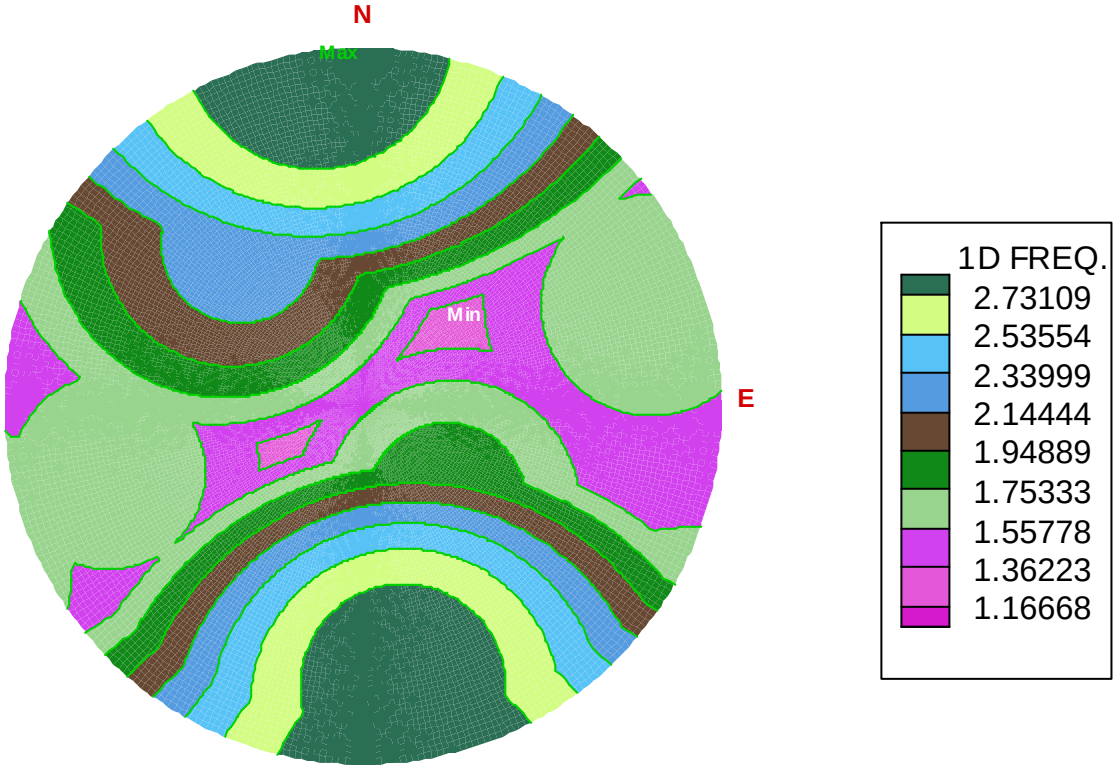

(XY) ? 15 Nov 2001 ?

Fig. 5.11 Probability distribution of volume of equivalent matrix block for Smaland granite rock mass (NGI box #169). (Unit of length: meter)

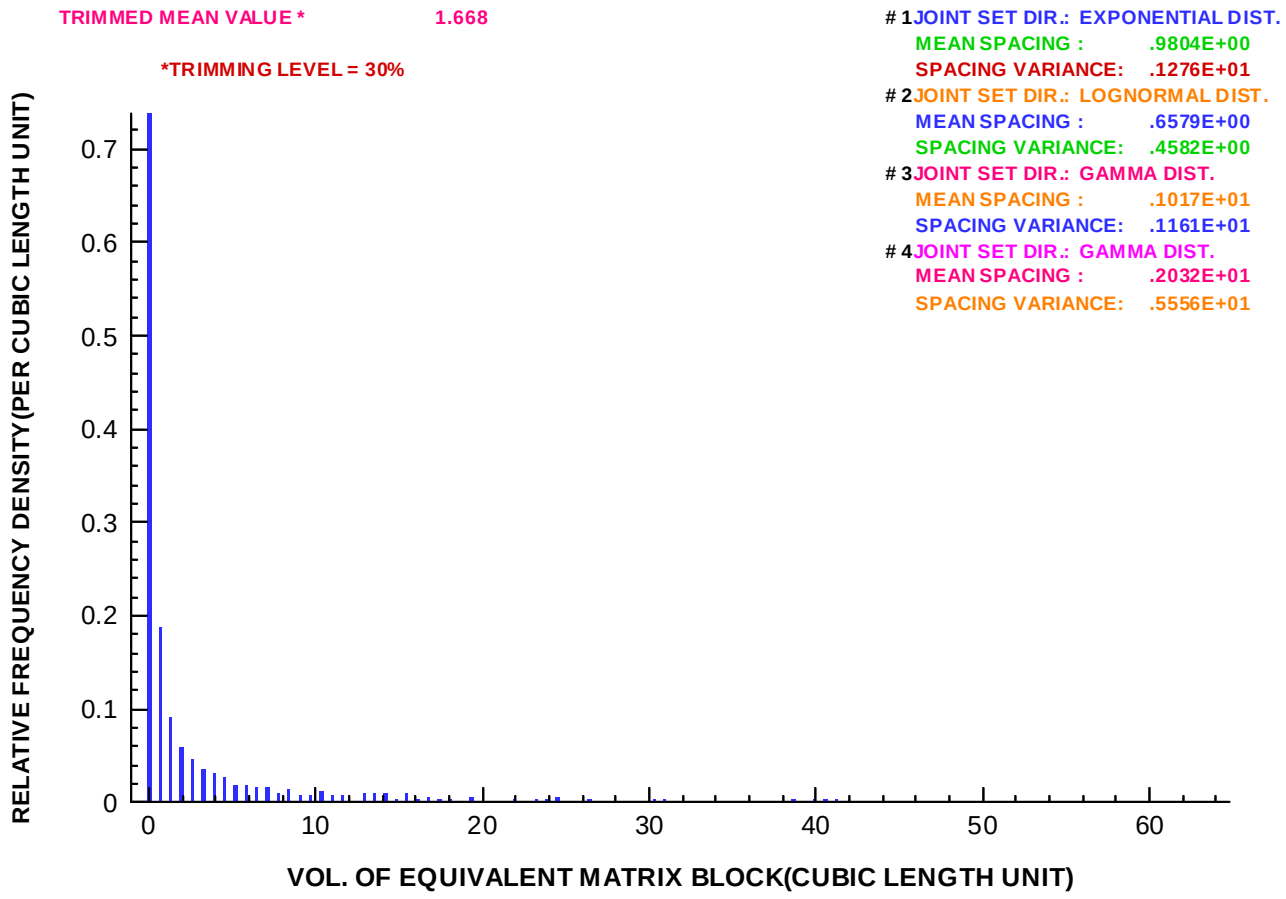

(XY) ? 15 Nov 2001 ?

Fig. 5.12 Probability distribution of number of blocks per unit volume for Smaland granite rock mass (NGI box #169). (Unit: #/cubic meter)

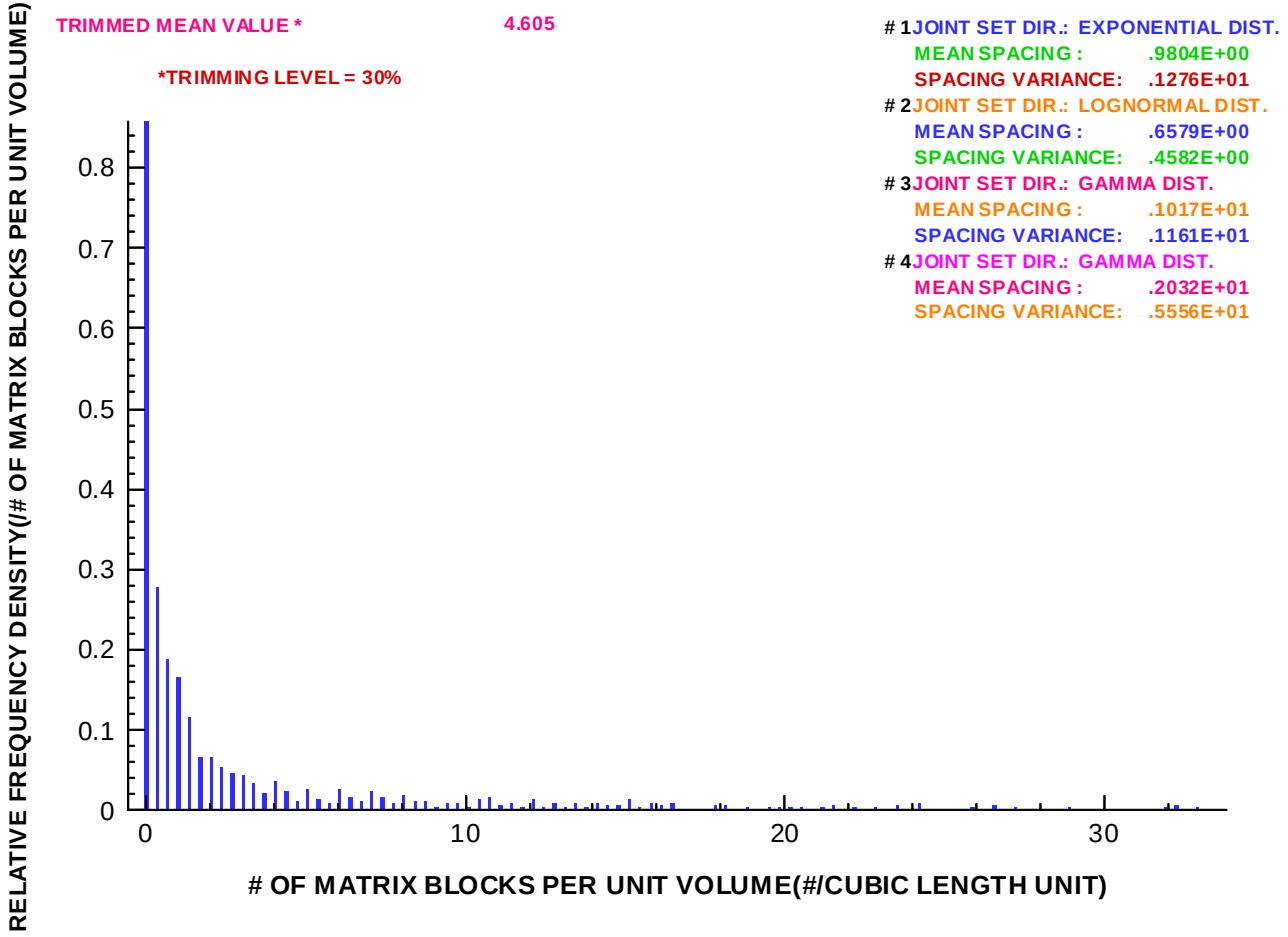

Table 5.5 Volumetric fracture frequency results for Småland granite (NGI box #169) fracture sets

Fracture set #	1D-Intensity (#/m)	E(n·i)	$E(D^2)$ (m^2)	3D-Intensity ($\#/m^3$)
1	1.02	0.6000	32.75004	0.0661
2	1.52	0.8258	32.75004	0.0716
3	0.98	0.6000	32.75004	0.0637
4	0.49	0.6000	32.75004	0.0319

Note: Lowest E(n·i) is limited to 0.6

dips 64° SW. When individual fractures of this set strike exactly parallel to the vertical window, the fracture traces will be horizontal. On the other hand, when the two strikes are not the same, fracture set 3 will make traces having apparent dips between 0° and 60° on the vertical window. Fracture set 4 is sub-horizontal. Therefore, fracture set 4 should make sub-horizontal fracture traces on the chosen vertical window. Figure 5.14 shows sub-horizontal fracture traces very well. Figure 5.14 also shows that the traces appear on the figure come from 4 fracture sets. A 10m length of KAS02 borehole is simulated on Figure 5.14. The 1-D fracture frequency on this simulated borehole is about 2.0 fractures per m. This number compares very well with the observed 1-D fracture frequency of 1.94 fractures per m on actual KAS02 borehole (see Table 5.4). Fracture traces simulated on a 40m square vertical window produced a mean trace length value of 4.32 m and a coefficient of variation of 0.51. When the vertical window size was increased to 55m square, the mean trace length value increased to 4.80m keeping the value of coefficient of variation almost the same. This shows clearly that the mean trace length increases with window size. Note that for infinite size window, a mean trace length of 5m along with a coefficient of variation of 0.5 was used in modeling the fracture size. These numbers validate the used fracture size model. The above findings show that the fracture geometry features of the generated fracture system agree well with the fracture data used to model the 3-D stochastic fracture system.

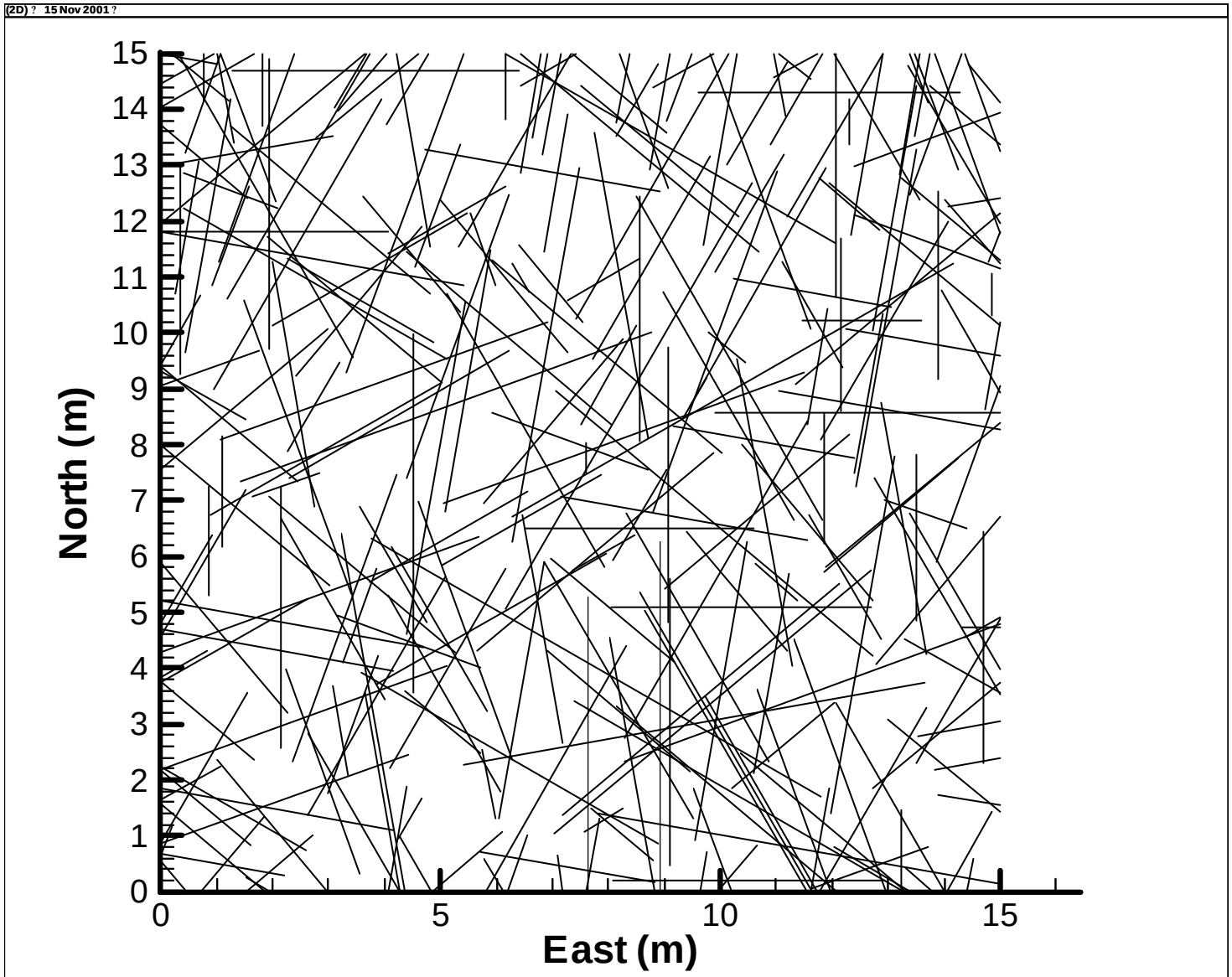

Fig. 5.13 Fracture traces obtained from fracture generation on a horizontal square window of size 15 m placed at the mid level of cube of 30m of Smaland granite rock mass (NGI box #169).

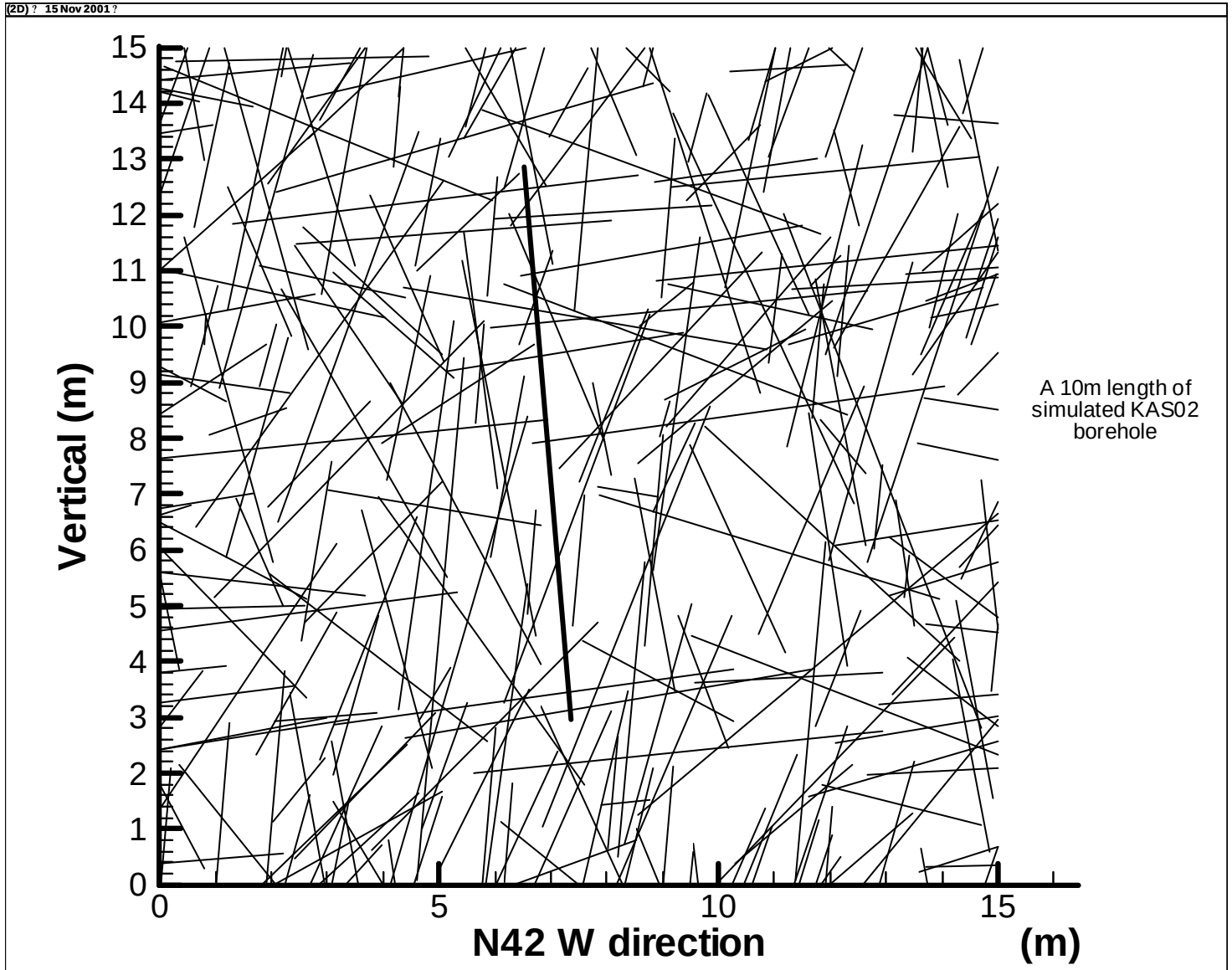

Fig. 5.14 Fracture traces obtained from fracture generation on a vertical square window of size 15 m having strike same as the trend direction of borehole KAS02 placed at the middle of 30m cube of Smaland granite rock mass (NGI box #169).

6 Stochastic 3-D fracture network model for fine-grained granite rock mass (NGI block number 5)

6.1. Number of Fracture Sets and Correction for Orientation Bias

For NGI block number 5, orientation data were obtained from the depth region 384.1-410.3m of borehole KA2598A. The fracture data were analyzed in a similar manner to the analysis conducted for Äspö diorite using the computer program CLUSDEL-BINGHAM. The final results obtained for fracture set delineation are shown in Figure 6.1. Fracture sets 1 and 2 show high variability. This high variability is partly reflected by the **very low number of data** available for orientation analyses. Number of orientation data belonging to each fracture set and the mean directions obtained for the fracture sets are shown in Table 6.1.

The computer program OBIAS1D was applied to study the effect of orientation sampling bias on orientation distribution of each of the 3 fracture sets. The obtained results are shown in Figures 6.2 through 6.4. All three fracture sets intersect with the same borehole KA2598A. Due to lack of fracture size data, the same probability distribution is used to model fracture size of the 3 fracture sets (see section 6.3). Therefore, comparisons between the 3 fracture sets depend only on the relative orientation distribution between the borehole direction and the directions of fractures of each fracture set. Because borehole KA2598A has trend 293° and plunge 32° (Table 2.1), according to the obtained mean orientations of fracture sets (Table 6.1), the intersection probabilities between the borehole and the fracture sets in the order of lowest to highest would be for fracture set 3, 1, and 2. Orientation variability of fracture set 3 is very low compared to that of fracture sets 1 and 2. Orientation variability of fracture set 2 is slightly higher than that of fracture set 1 (see Figure 6.1, Table 6.2 and section 6.2). Fracture sets 1 and 2 have shown some effect with respect to the orientation bias correction (compare a and b plots of Figs.6.2 through 6.3); fracture set 3 has shown very little effect with respect to the sampling bias correction (compare a and b plots of Fig. 6.4).

(Sketch)? 16 Nov 2001 ?

Fig. 6.1 Fracture set delineation results on an upper hemispherical polar equal area projection for fine grained granite (NGI box # 5)

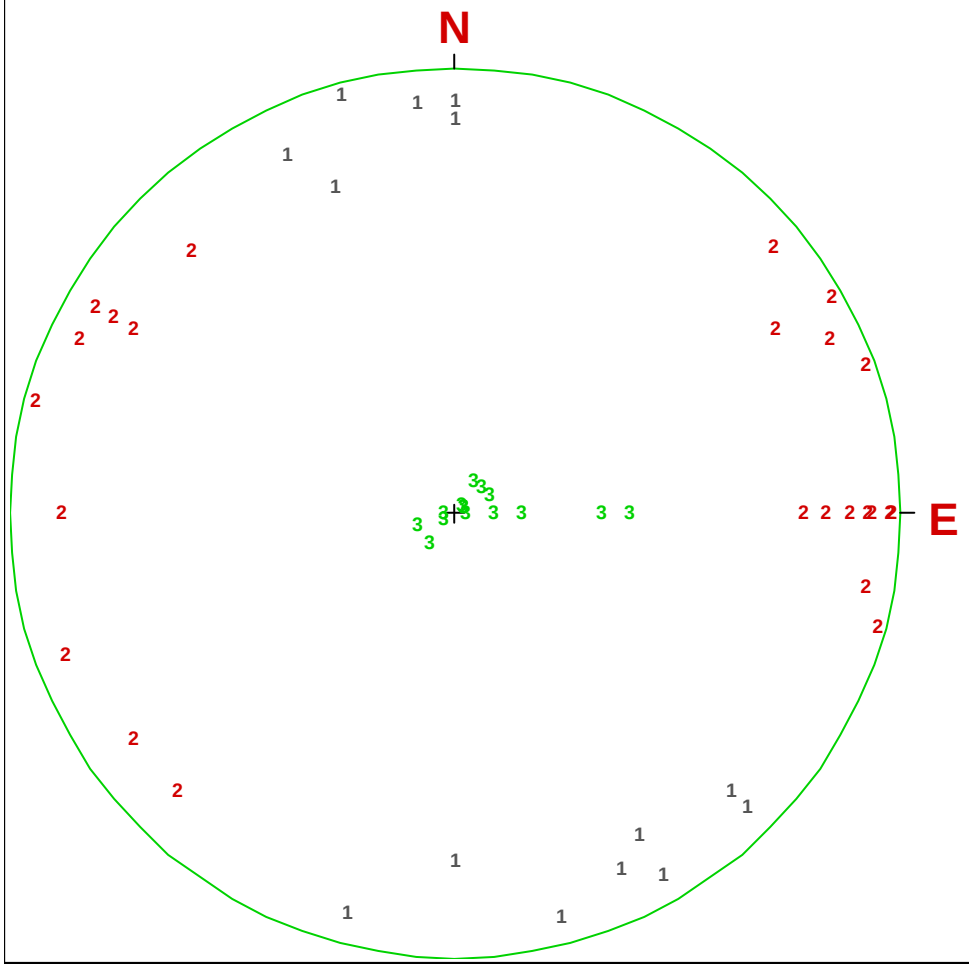

70 POLES

SMALL CIRCLE RADIUS VALUE = 20.00 DEGREES

OBJECTIVE FUNCTION VALUES

F2 = 1.15
F3 = .59
F4 = .51

SYMBOL	FRACTURE SET #	# OF DATA
1	1	19
2	2	34
3	3	17

Table 6.1 Delineated fracture sets and goodness-of-fit results of Bingham distribution for orientation data of fine grained granite

	Fracture		Mu 3		Mu 2		Mu 1		Chi-square Test			
Nobs.	Set	Npts.	Trend (°)	Plunge (°)	Trend (°)	Plunge (°)	Trend (°)	Plunge (°)	D.F.	chi	95chi	P
70	1	19	166.72	5.21	75.84	9.51	285.05	79.13	Data insufficient to perform chi-square test			
	2	34	89.70	3.51	358.97	11.73	198.11	77.74	Data insufficient to perform chi-square test			
	3	17	77.98	84.84	267.86	5.08	177.78	0.88	Data insufficient to perform chi-square test			

Note:

Nobs.=Number of fractures observed on the borehole

Npts.=Number of fractures belonging to the fracture set

Mu3=Mean normal vector direction (upward) of fracture set

Trend of Mu3=Dip direction of fracture set

Plunge of Mu3=90°-Dip angle of fracture set

Mu2=Vector normal to minor axis plane of Bingham distribution

Mu1=Vector normal to major axis plane of Bingham distribution

DF= Degrees of freedom for Chi-square test for Bingham distribution

Chi=Calculated Chi-square value

95Chi=Table Chi-square value at 5% significance level

P=Maximum significance level at which Bingham distribution can be used to represent the statistical distribution of orientation of fracture set

(a minimum of 0.05 is required to represent orientation data by a Bingham distribution)

(3D) ? 16 Nov 2001 ? NGI BOX #5 (Fine Grained Granite)

Fig. 6.2a Observed relative frequency of orientation for fracture set 1 of fine grained granite (NGI box #5).

Based on Line or Borehole(1-D) sampling

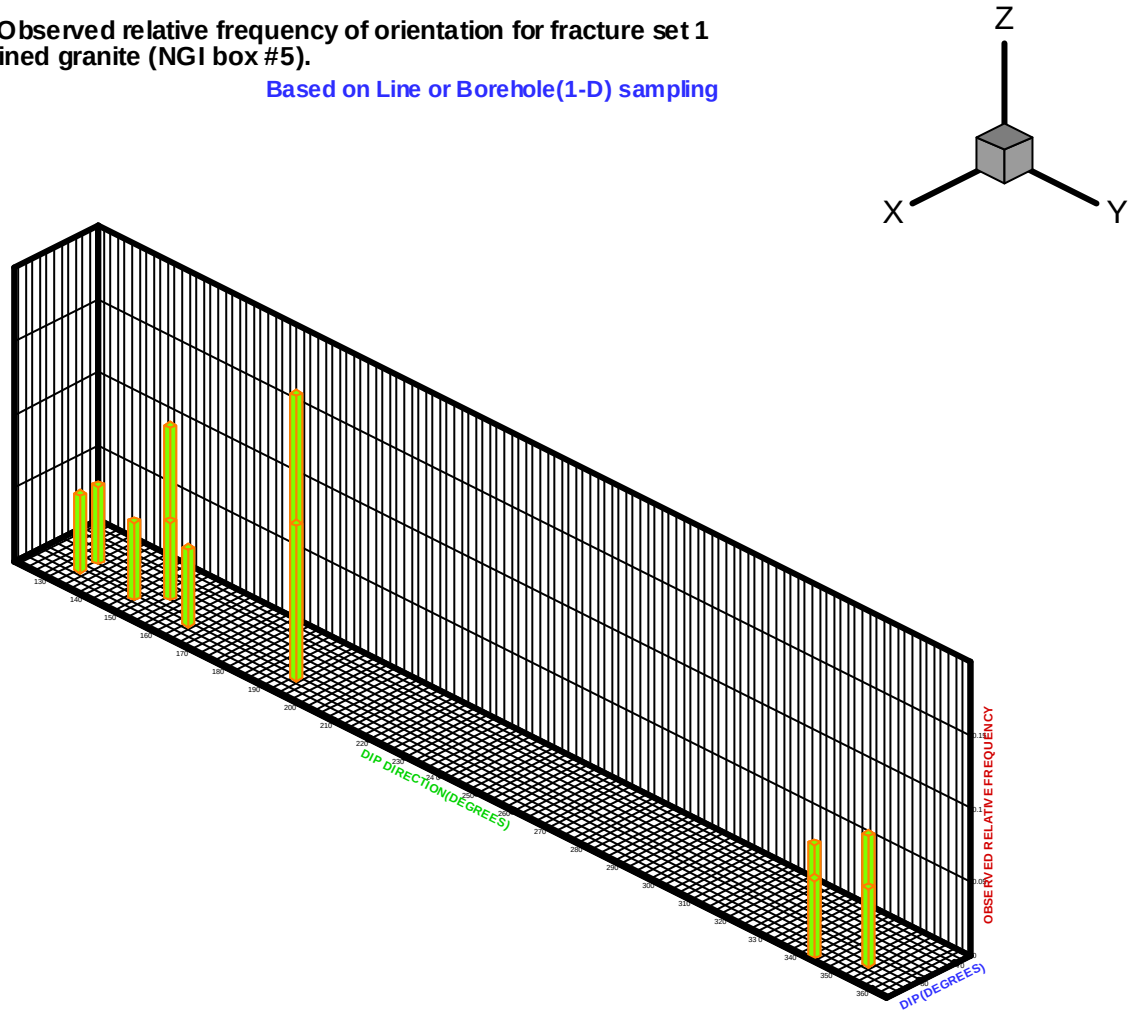

NUMBER OF ORIENTATION DATA = 19
LENGTH OF BOREHOLE = 26.17
TREND OF BOREHOLE = 292.60 (DEG.)
PLUNGE OF BOREHOLE = 32.15 (DEG.)
DIAMETER OF FRACTURE PLANES FROM 5.26 TO 5.26
DIAMETER OF BOREHOLE = .10

A COLUMN REPRESENTS 10 DEGREES(DIP) X 10 DEGREES(DIP DIRE.)
THE MAXIMUM VALUE FOR OBSERVED RELATIVE FREQUENCY = .1579
IT IS LOCATED FROM 65.00 TO 70.00 FOR DIP(DEG.)
AND 175.00 TO 180.00 FOR DIP DIRECTION(DEG.)
THE UNIT FOR LENGTH: Meter

(3D) ? 16 Nov 2001 ? NGI BOX #5 (Fine Grained Granite)

Fig. 6.2b Corrected relative frequency of orientation for fracture set 1 of fine grained granite (NGI box #5).

Based on Line or Borehole(1-D) sampling

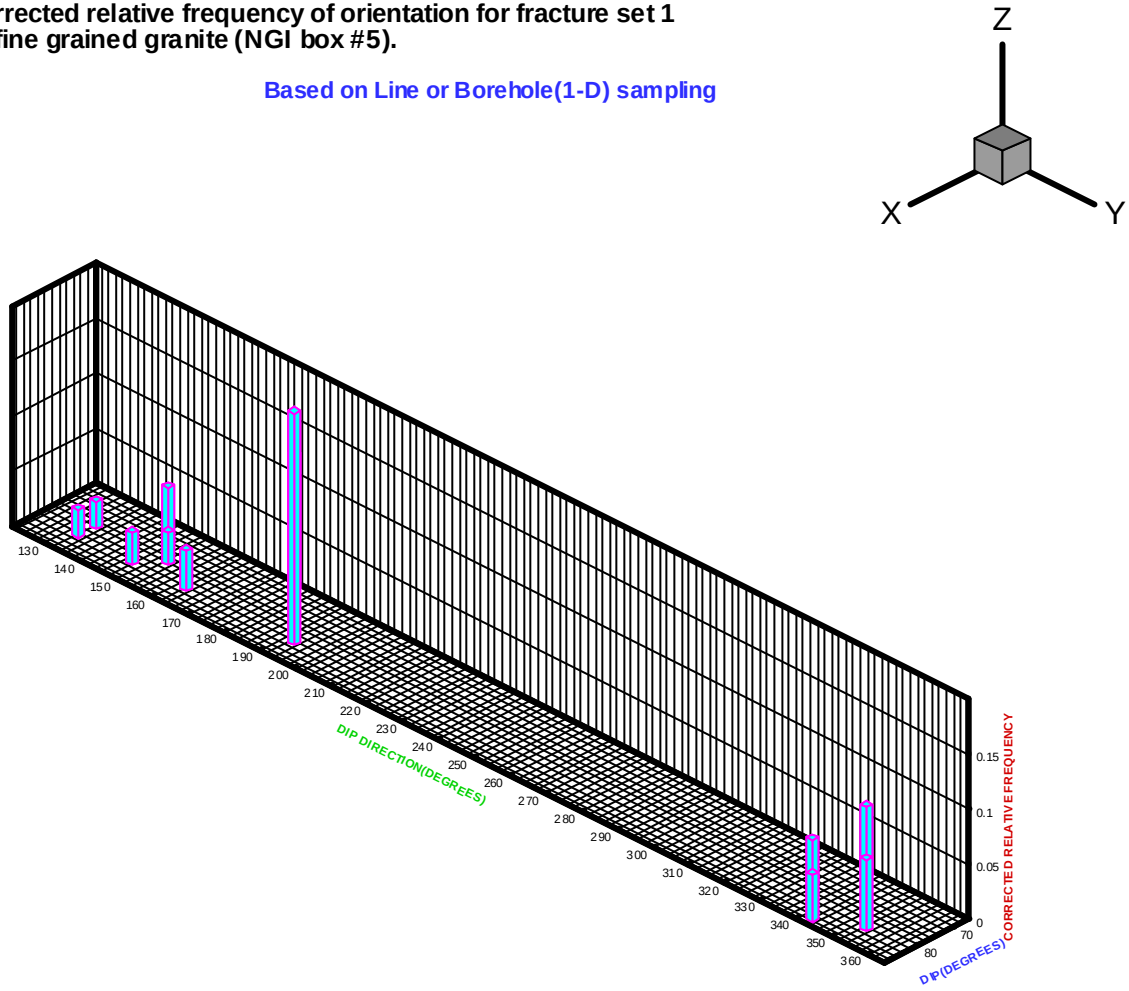

NUMBER OF ORIENTATION DATA = 19
LENGTH OF BOREHOLE = 26.17
TREND OF BOREHOLE = 292.60 (DEG.)
PLUNGE OF BOREHOLE = 32.15 (DEG.)
DIAMETER OF FRACTURE PLANES FROM 5.26 TO 5.26
DIAMETER OF BOREHOLE = .10

A COLUMN REPRESENTS 10 DEGREES(DIP) X 10 DEGREES(DIP DIRE.)
THE MAXIMUM VALUE FOR CORRECTED RELATIVE FREQUENCY = .2105
IT IS LOCATED FROM 80.00 TO 85.00 FOR DIP(DEG.)
AND 190.00 TO 195.00 FOR DIP DIRECTION(DEG.)
THE UNIT FOR LENGTH: Meter

(3D) ? 16 Nov 2001 ? NGI BOX #5 (Fine Grained Granite)

Fig. 6.3a Observed relative frequency of orientation for fracture set 2 of fine grained granite (NGI box #5).

Based on Line or Borehole(1-D) sampling

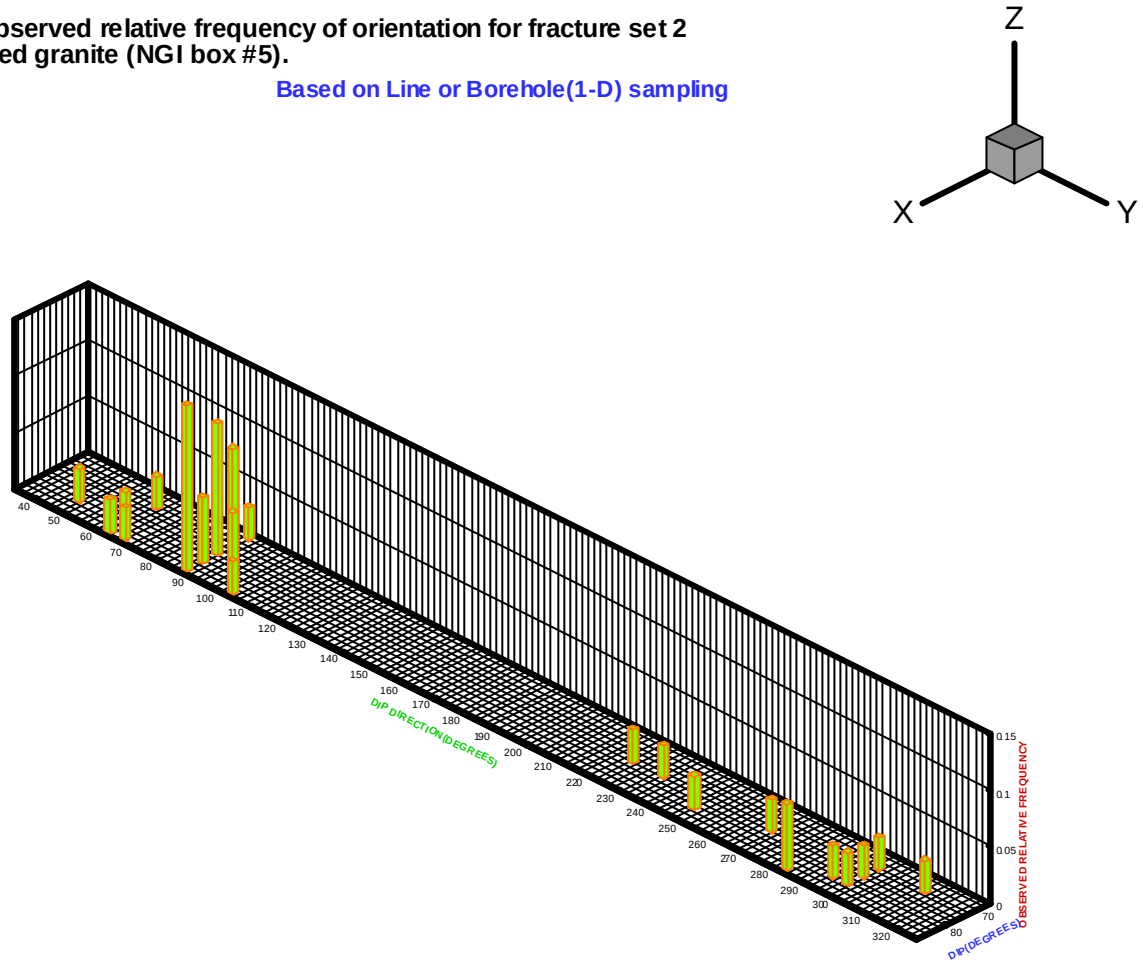

NUMBER OF ORIENTATION DATA = 34
LENGTH OF BOREHOLE = 26.17
TREND OF BOREHOLE = 292.60 (DEG.)
PLUNGE OF BOREHOLE = 32.15 (DEG.)
DIAMETER OF FRACTURE PLANES FROM 5.26 TO 5.26
DIAMETER OF BOREHOLE = .10

A COLUMN REPRESENTS 10 DEGREES(DIP) X 10 DEGREES(DIP DIRE.)
THE MAXIMUM VALUE FOR OBSERVED RELATIVE FREQUENCY = .1471
IT IS LOCATED FROM 85.00 TO 90.00 FOR DIP(DEG.)
AND 85.00 TO 90.00 FOR DIP DIRECTION(DEG.)
THE UNIT FOR LENGTH: Meter

Fig. 6.3b Corrected relative frequency of orientation for fracture set 2 of fine grained granite (NGI box #5).

Based on Line or Borehole(1-D) sampling

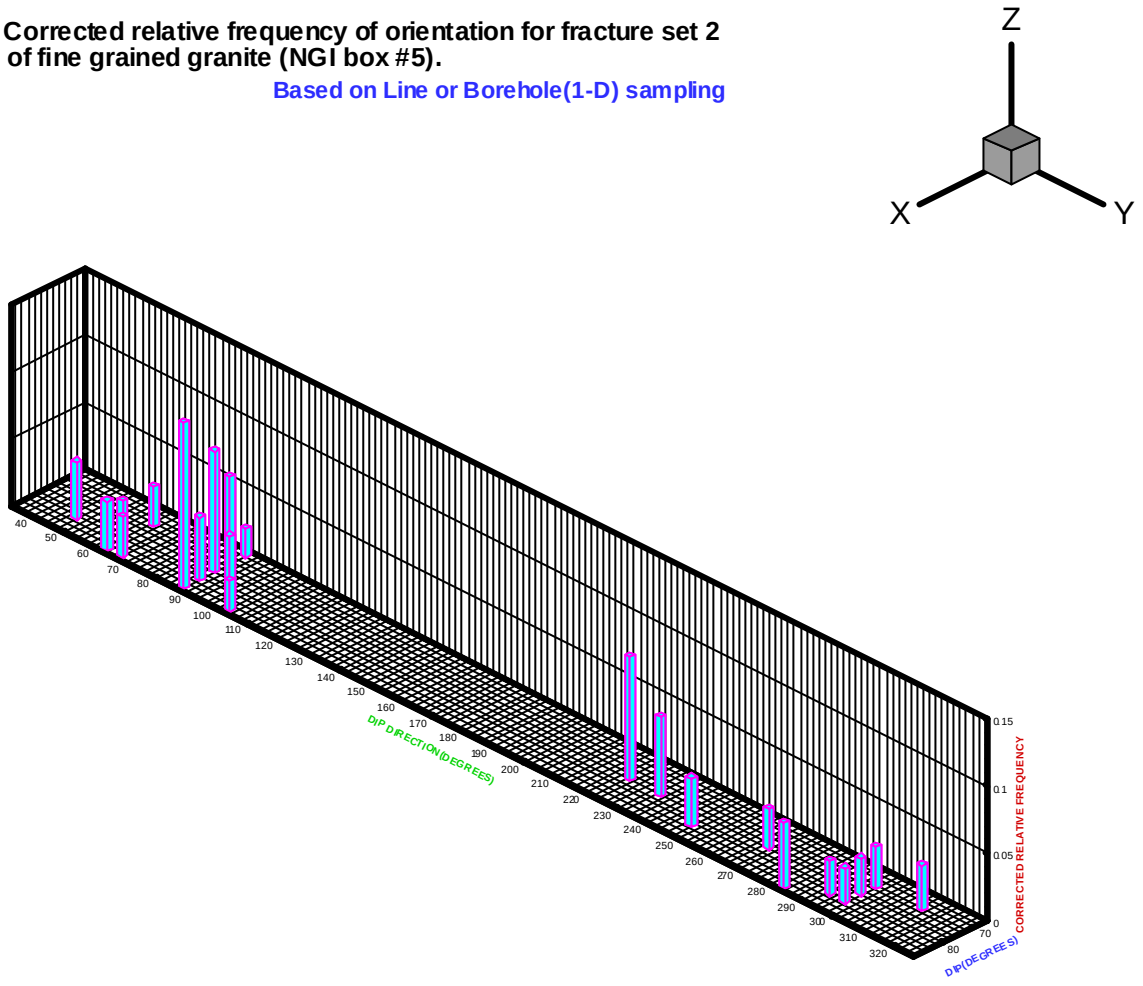

NUMBER OF ORIENTATION DATA = 34
LENGTH OF BOREHOLE = 26.17
TREND OF BOREHOLE = 292.60 (DEG.)
PLUNGE OF BOREHOLE = 32.15 (DEG.)
DIAMETER OF FRACTURE PLANES FROM 5.26 TO 5.26
DIAMETER OF BOREHOLE = .10

A COLUMN REPRESENTS 10 DEGREES(DIP) X 10 DEGREES(DIP DIRE.)
THE MAXIMUM VALUE FOR CORRECTED RELATIVE FREQUENCY = .1234
IT IS LOCATED FROM 85.00 TO 90.00 FOR DIP(DEG.)
AND 85.00 TO 90.00 FOR DIP DIRECTION(DEG.)
THE UNIT FOR LENGTH: Meter

(3D) ? 16 Nov 2001 ? NGI BOX #5 (Fine Grained Granite)

Fig. 6.4a Observed relative frequency of orientation for fracture set 3 of fine grained granite (NGI box #5).

Based on Line or Borehole(1-D) sampling

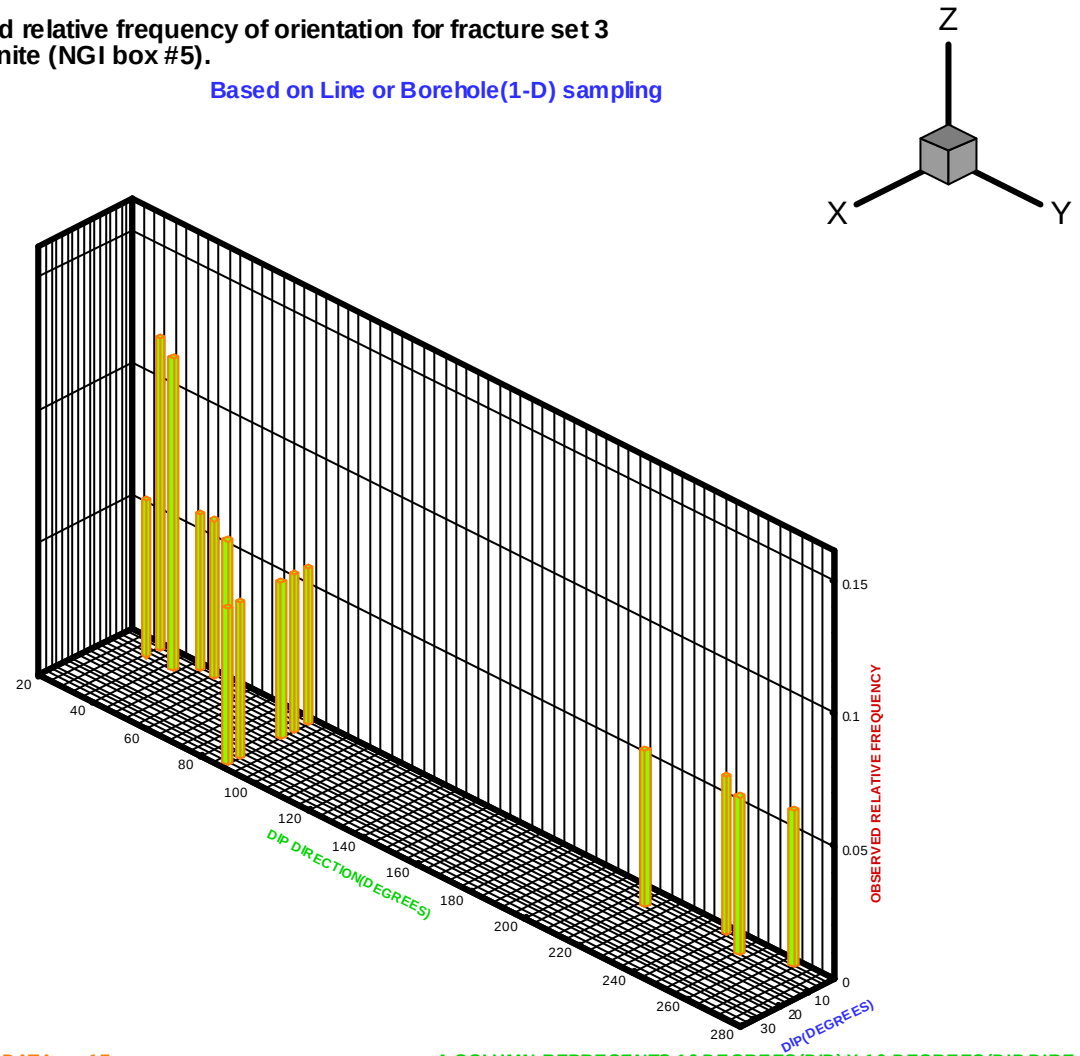

NUMBER OF ORIENTATION DATA = 17
LENGTH OF BOREHOLE = 26.17
TREND OF BOREHOLE = 292.60 (DEG.)
PLUNGE OF BOREHOLE = 32.15 (DEG.)
DIAMETER OF FRACTURE PLANES FROM 5.26 TO 5.26
DIAMETER OF BOREHOLE = .10

A COLUMN REPRESENTS 10 DEGREES(DIP) X 10 DEGREES(DIP DIRE.)
THE MAXIMUM VALUE FOR OBSERVED RELATIVE FREQUENCY = .1176
IT IS LOCATED FROM .00 TO 5.00 FOR DIP(DEG.)
AND 30.00 TO 35.00 FOR DIP DIRECTION(DEG.)
THE UNIT FOR LENGTH: Meter

(3D) ? 16 Nov 2001 ?NGI BOX #5 (Fine Grained Granite)

Fig. 6.4b Corrected relative frequency of orientation for fracture set 3 of fine grained granite (NGI box #5).

Based on Line or Borehole(1-D) sampling

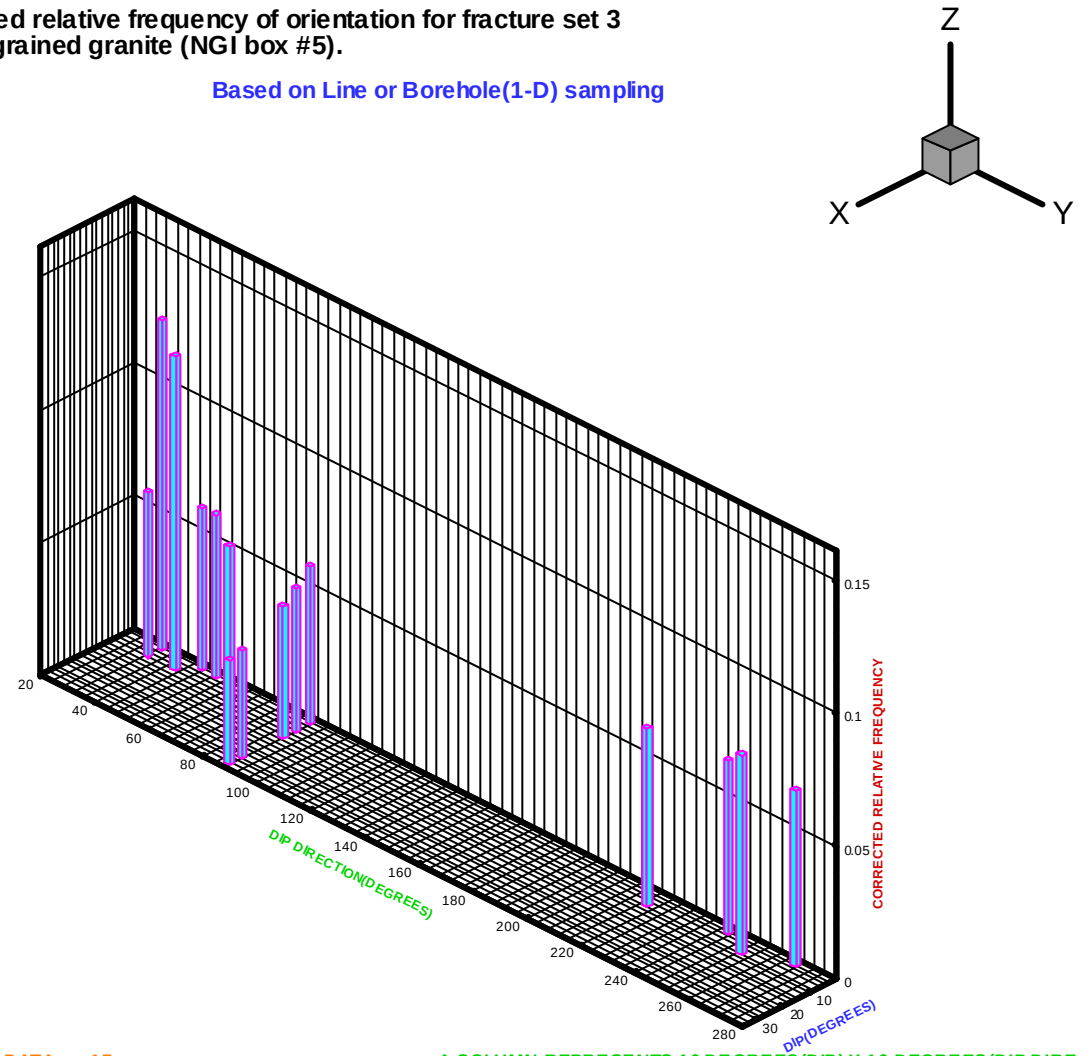

NUMBER OF ORIENTATION DATA = 17
LENGTH OF BOREHOLE = 26.17
TREND OF BOREHOLE = 292.60 (DEG.)
PLUNGE OF BOREHOLE = 32.15 (DEG.)
DIAMETER OF FRACTURE PLANES FROM 5.26 TO 5.26
DIAMETER OF BOREHOLE = .10

A COLUMN REPRESENTS 10 DEGREES(DIP) X 10 DEGREES(DIP DIRE.)
THE MAXIMUM VALUE FOR CORRECTED RELATIVE FREQUENCY = .1243
IT IS LOCATED FROM .00 TO 5.00 FOR DIP(DEG.)
AND 30.00 TO 35.00 FOR DIP DIRECTION(DEG.)
THE UNIT FOR LENGTH: Meter

6.2 Orientation Distribution for Each Fracture Set

Goodness-of-fit of hemispherical normal distribution was performed for both the raw and corrected orientation data of each fracture set using the computer program HEMISPHN. For fracture sets 1 and 2 the mean normal vector direction and the distribution of the orientation have changed to some extent due to the orientation bias correction (compare plots a and b of Figs. 6.5 through 6.6). This indicates the importance of applying the orientation sampling bias correction in modeling joint orientation distribution. Effect of sampling bias correction on fracture set 3 is very small (Figs 6.7a and b). The summary results (Table 6.2) indicate that hemispherical normal distribution is not suitable to represent the statistical distribution of orientation for the 3 fracture sets. According to the spherical variance and k values in Table 6.2, in the increasing order of orientation variability the fracture sets can be arranged as fracture sets 3, 1 and 2.

Goodness-of-fit of Bingham distribution was performed for the orientation data of each fracture set using the computer program CLUSDEL-BINGHAM. The results (Table6.1) provide mean normal vectors for the fracture sets and show that the number of data available for each of the 3 fracture sets is too small to perform Chi-square goodness-of-fit test for Bingham distribution.

The aforementioned results show that the available theoretical probability distributions (hemispherical normal and Bingham distributions) cannot be used to represent the statistical distribution of orientation of the three fracture sets. For a fracture set that cannot be represented by a theoretical orientation probability distribution, the empirical orientation distribution obtained from the corrected relative frequency data can be used for generation of orientation values.

6.3 Trace Length and Size Distributions for Each Fracture Set

As mentioned before, no fracture trace data were provided for this project to model fracture trace length distribution and size distribution in 3-D. Due to lack of reliable data on fracture traces, the same gamma distribution (mean=5m and coefficient of variation=0.5) used for Äspö diorite is also used to represent the fracture trace length distribution in 2-D for all 3 fracture sets. As for Äspö diorite, the equivalent fracture diameter in 3-D for all three fracture sets is represented by the gamma distribution with mean = 5.26m and standard deviation = 2.25m.

Fig. 6.5a Results of hemispherical normal distribution fit for observed orientation data of fracture set 1 of fine grained granite (NGI box #5).

Probability(Confidence) Contours for the
Hemispherical Normal Distribution of Fracture Normals

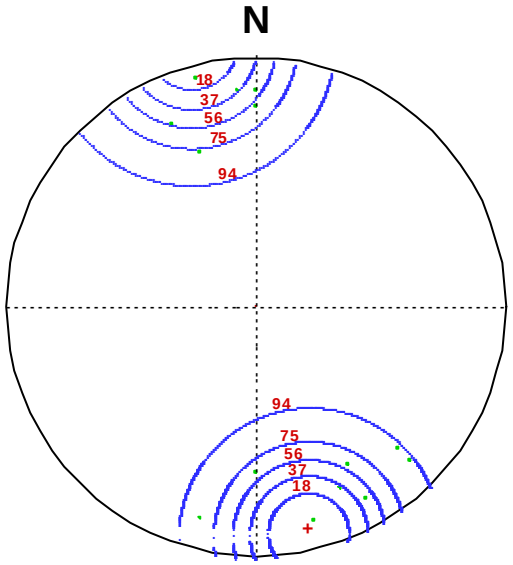

The number given for the contour is the percent(%) confidence

Maximum significance level at which the hemispherical normal distribution is suitable to represent the statistical distribution of joint orientation data : < 0.005

Number of Joint Data = 19

Average L = .9687
Average M = .2307
Average N = -.0915

Magnitude of Mean Vector = .9280
Mean Plunge(up) = 5.2480 (deg.)
Mean Trend = 166.6067 (deg.)
K Value of the Distribution = 13.1583
Spherical Variance = .0720

The small . indicate the joint normal vectors
The small + indicates the mean normal vector to the joint set

Upper-Hemispherical Stereographic Projection

Fig. 6.5b Results of hemispherical normal distribution fit for orientation data of fracture set 1 of fine grained granite (NGI box #5) corrected for sampling bias.

Probability(Confidence) Contours for the
Hemispherical Normal Distribution of Fracture Normals

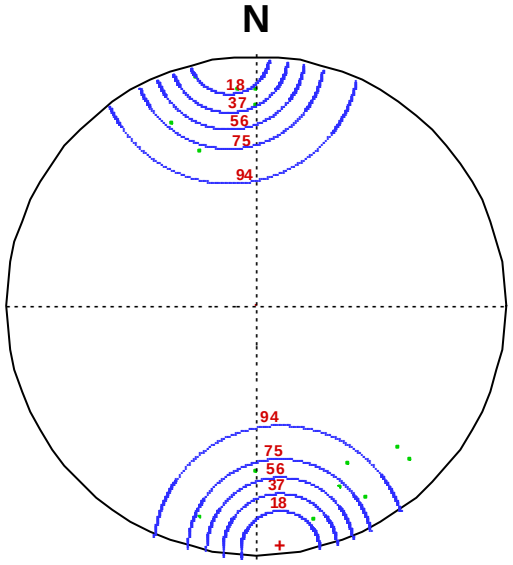

The number given for the contour is the percent(%) confidence

Maximum significance level at which the hemispherical normal distribution is suitable to represent the statistical distribution of joint orientation data : < 0.005

Number of Joint Data = 19

Average L = .9942
Average M = .1022
Average N = -.0326

Magnitude of Mean Vector = .9339
Mean Plunge(up) = 1.8654 (deg.)
Mean Trend = 174.1326 (deg.)
K Value of the Distribution = 14.3340
Spherical Variance = .0661

The small . indicate the joint normal vectors
The small + indicates the mean normal vector to the joint set

Upper-Hemispherical Stereographic Projection

Fig. 6.6a Results of hemispherical normal distribution fit for observed orientation data of fracture set 2 of fine grained granite (NGI box #5).

Probability(Confidence) Contours for the
Hemispherical Normal Distribution of Fracture Normals

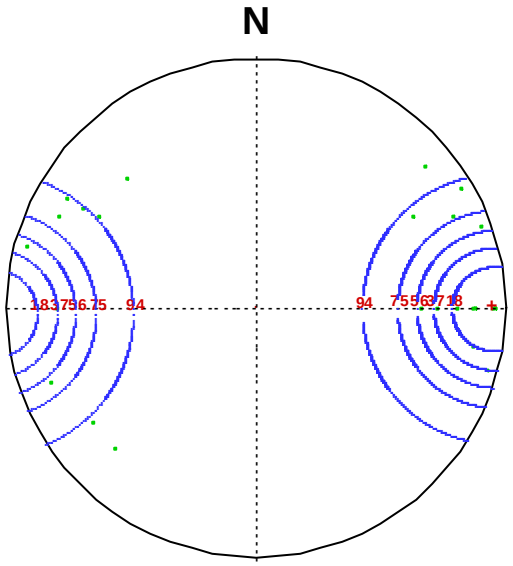

The number given for the contour is the percent(%) confidence

Maximum significance level at which the hemispherical normal distribution is suitable to represent the statistical distribution of joint orientation data : < 0.005

Number of Joint Data = 34

Average L = .0093
Average M = -.9987
Average N = .0499

Magnitude of Mean Vector = .9215
Mean Plunge(up) = 2.8620 (deg.)
Mean Trend = 89.4685 (deg.)
K Value of the Distribution = 12.3700
Spherical Variance = .0785

The small . indicate the joint normal vectors
The small + indicates the mean normal vector to the joint set

Upper-Hemispherical Stereographic Projection

Fig. 6.6b Results of hemispherical normal distribution fit for orientation data of fracture set 2 of fine grained granite (NGI box #5) corrected for sampling bias.

Probability(Confidence) Contours for the
Hemispherical Normal Distribution of Fracture Normals

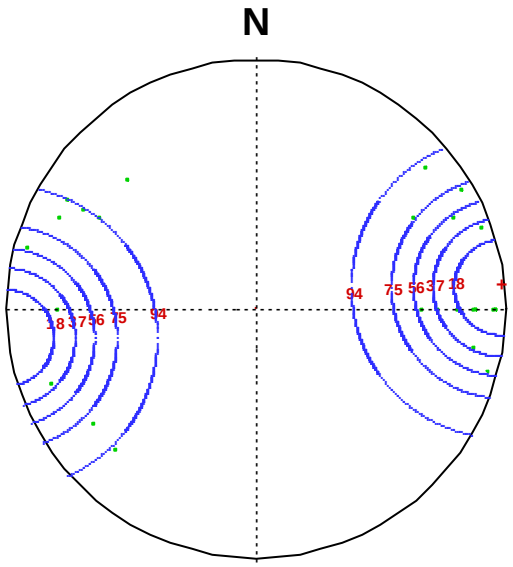

The number given for the contour is the percent(%) confidence

Maximum significance level at which the hemispherical normal distribution is suitable to represent the statistical distribution of joint orientation data : < 0.005

Number of Joint Data = 34

Average L = .1012
Average M = -.9948
Average N = .0073

Magnitude of Mean Vector = .8970
Mean Plunge(up) = .4171 (deg.)
Mean Trend = 84.1941 (deg.)
K Value of the Distribution = 9.4243
Spherical Variance = .1030

The small . indicate the joint normal vectors
The small + indicates the mean normal vector to the joint set

Upper-Hemispherical Stereographic Projection

Fig. 6.7a Results of hemispherical normal distribution fit for observed orientation data of fracture set 3 of fine grained granite (NGI box #5).

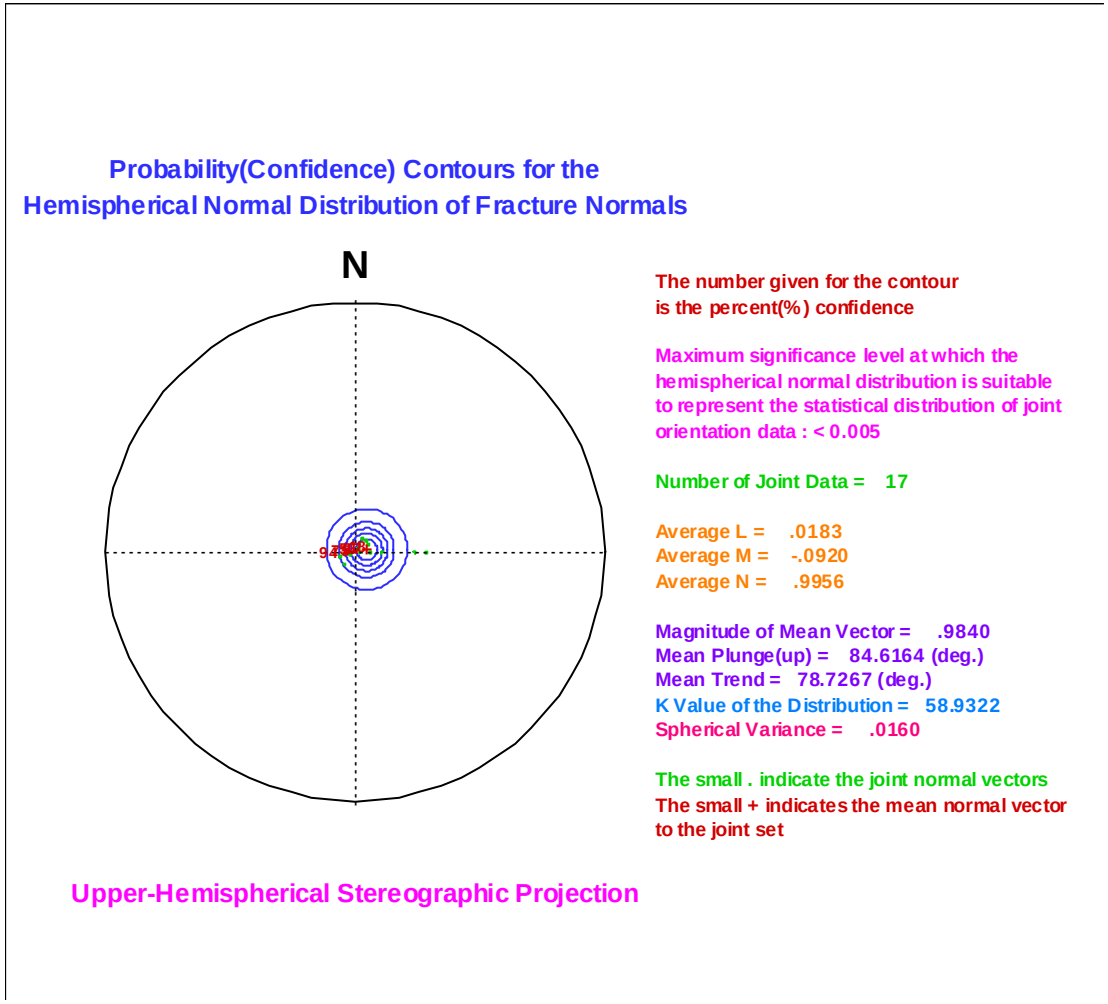

Fig. 6.7b Results of hemispherical normal distribution fit for orientation data of fracture set 3 of fine grained granite (NGI box #5) corrected for sampling bias.

Probability(Confidence) Contours for the
Hemispherical Normal Distribution of Fracture Normals

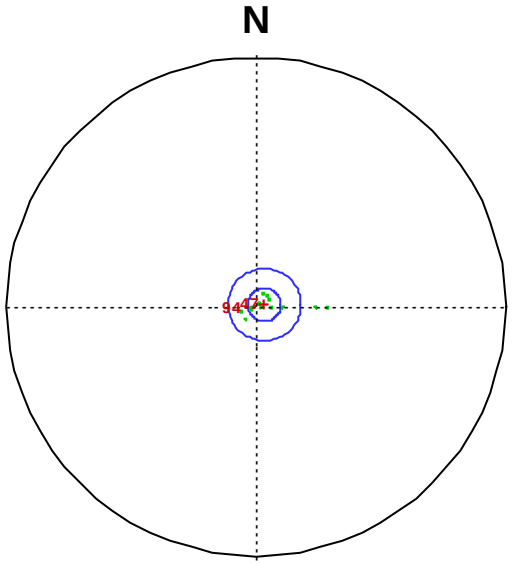

The number given for the contour
is the percent(%) confidence

Maximum significance level at which the hemispherical normal distribution is suitable to represent the statistical distribution of joint orientation data : < 0.005

Number of Joint Data = 17

Average L = .0174
Average M = -.0675
Average N = .9976

Magnitude of Mean Vector = .9871
Mean Plunge(up) = 86.0052 (deg.)
Mean Trend = 75.5383 (deg.)
K Value of the Distribution = 73.0668
Spherical Variance = .0129

The small . indicate the joint normal vectors
The small + indicates the mean normal vector to the joint set

Upper-Hemispherical Stereographic Projection

Table 6.2 Goodness-of-fit results of hemispherical normal distribution for orientation data of fine grained granite.

(a) Raw orientation data

Nobs.	Fracture set #	Npts.	Upward mean normal vector		K	Sp. Var.	P
			Trend (°)	Plunge (°)			
70	1	19	166.61	5.25	13.16	0.0720	<0.005
	2	34	89.47	2.86	12.37	0.0785	<0.005
	3	17	78.73	84.62	58.93	0.0160	<0.005

(b) Data corrected for sampling bias

Nobs.	Fracture set #	Npts.	Upward mean normal vector		K	Sp. Var.	P
			Trend (°)	Plunge (°)			
70	1	19	174.13	1.87	14.33	0.0661	<0.005
	2	34	84.19	0.42	9.42	0.1030	<0.005
	3	17	75.54	86.01	73.07	0.0129	<0.005

Nobs.=Number of fractures observed on the borehole
Npts.=Number of fractures belonging to the fracture set
K=A parameter in the hemispherical normal distribution
Sp. Var.=Spherical variance
P=Maximum significance level at which the hemispherical normal distribution is suitable to represent the statistical distribution of fracture orientation data
(a minimum of 0.05 is required to represent orientation data by a hemispherical normal distribution)

6.4 Spacing Distribution and 1-D Fracture frequency for Each Fracture Set

Fracture spacing data were obtained from the depth region 384.1-410.3m of borehole KA2598A. Goodness-of-fit tests were performed using GDFT computer program to find the suitable probability distributions as well as the best probability distribution to represent the statistical distribution of spacing for each fracture set. The results (Table 6.3) indicate that all three probability distributions lognormal, gamma and exponential are highly suitable to represent the statistical distribution of spacing for any of the 3 fracture sets. Each of the three probability distributions was found to be the best distribution for 1 fracture set and the 2nd best distribution for 1 fracture set.

The estimation of mean spacing and 1-D fracture frequency along the borehole direction and mean normal vector direction of each fracture set was conducted in the same way it was done for Äspö diorite rock mass using the computer program COR1DFM1 The obtained results are given in Table 6.4. Note that for each of the 3 fracture sets, the angle between the borehole direction and the mean normal vector direction of the fracture set turned out to be less than 60 degrees (Table 6.4). Therefore, for each of the 3 fracture sets, the calculated 1-D fracture frequency along the mean normal vector direction has good reliability.

Table 6.3 Goodness-of-fit test results for spacing of the three fracture sets of fine grained granite (NGI box #5)

Fracture set #	No. of data	Mean (m)	Var (m^2)	Probability Distribution	*K-S* $_{stat}$ Value	df	*P* -value	Best Distribution Rank
1	18	1.4539	2.8805	Exponential	0.0355	4	>0.2	2
				Gamma	0.0256	4	>0.2	1
				LogNormal	0.0889	4	>0.2	3
2	33	0.7270	1.2724	Exponential	0.0332	5	>0.2	1
				Gamma	0.0787	5	>0.2	3
				LogNormal	0.0346	5	>0.2	2
3	16	1.1050	3.3477	Exponential	0.1204	4	>0.2	3
				Gamma	0.0945	4	>0.2	2
				LogNormal	0.0673	4	>0.2	1

Note: A minimum P value of 0.05 is required to accept the tried probability distribution to represent the spacing distribution of the fracture set.

Table 6.4 Mean spacings and linear frequencies along the borehole KA2598A and mean normal vector directions for fracture sets of fine grained granite (NGI box #5)

Fracture set #	Orientation of fracture set		Dir. of borehole		Obs. mean spacing along borehole (m)	Length of borehole (m)	Corr. mean spacing along borehole (m)	1-D fracture frequency along borehole (# per m)	Angle between borehole & MNV (deg.)	1-D fracture frequency along MNV (# per m)
	Dip dir. (degs.)	Dip (degs.)	Trend (degs.)	Plunge (degs.)						
1	167	85	293	32	1.45	26.17	1.45	0.69	57.15	1.27
2	090	86	293	32	0.73	26.17	0.73	1.38	35.80	1.70
3	078	5	293	32	1.11	26.17	1.11	0.91	53.66	1.53

MNV = Mean Normal Vector of fracture set

6.5 1-D Fracture frequency in any Direction in 3-D

The 1-D fracture frequencies obtained along the mean normal vector directions of fracture sets were then used to estimate the 1-D fracture frequency in all the directions in 3-D by using the computer program FREQ1DALLDIR. Figure 6.8 shows the obtained results. This figure also pin points the directions and magnitudes for the minimum and maximum fracture frequencies for the fine-grained granite rock mass.

6.6 Mean Estimates for Block Size, Number of Blocks per Unit Volume and Number of Fractures per Unit Volume

The spacing distributions obtained along the mean normal vector directions for the 3 fracture sets were used along with the orientation distributions of the fracture sets in generating rock blocks in 3-D using the Monte-Carlo simulation procedure. This was performed using the computer program FREQ3DMVDJS. Orientations for the fracture sets were generated according to the obtained empirical orientation distributions. The obtained results for the distribution of volume of equivalent matrix block at a trimming level of 30% are shown in Figure 6.9 along with the trimmed mean value. Similar results for the number of matrix blocks per unit volume are shown in Figure 6.10.

Volumetric fracture frequencies for the 3 fracture sets were estimated in a similar manner to it was conducted for the Äspö diorite rock mass using the computer program 3DINTF1D. Obtained results are given in Table 6.5.

(2D) ? 16 Nov 2001 ?

Fig. 6.8 1-D fracture frequency distribution in 3-D on an equal-angle equatorial upper hemispherical projection for fine grained granite rock mass (NGI box #5).

Length Unit: Meter

Minimum Fracture Frequency:		Maximum Fracture Frequency:	
Magnitude(#/Length Unit):	1.2342	Magnitude(#/Length Unit):	2.9942
Trend(Deg.):	179.7700	Trend(Deg.):	119.3500
Plunge(Deg.):	1.0600	Plunge(Deg.):	35.6000

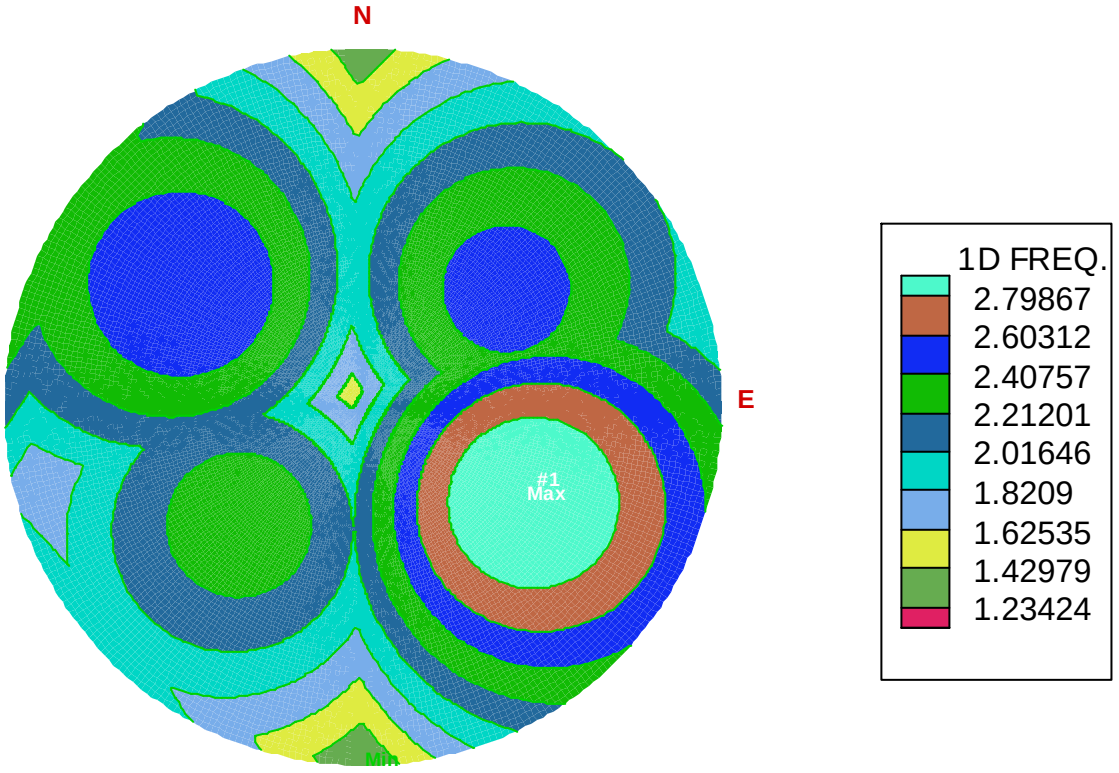

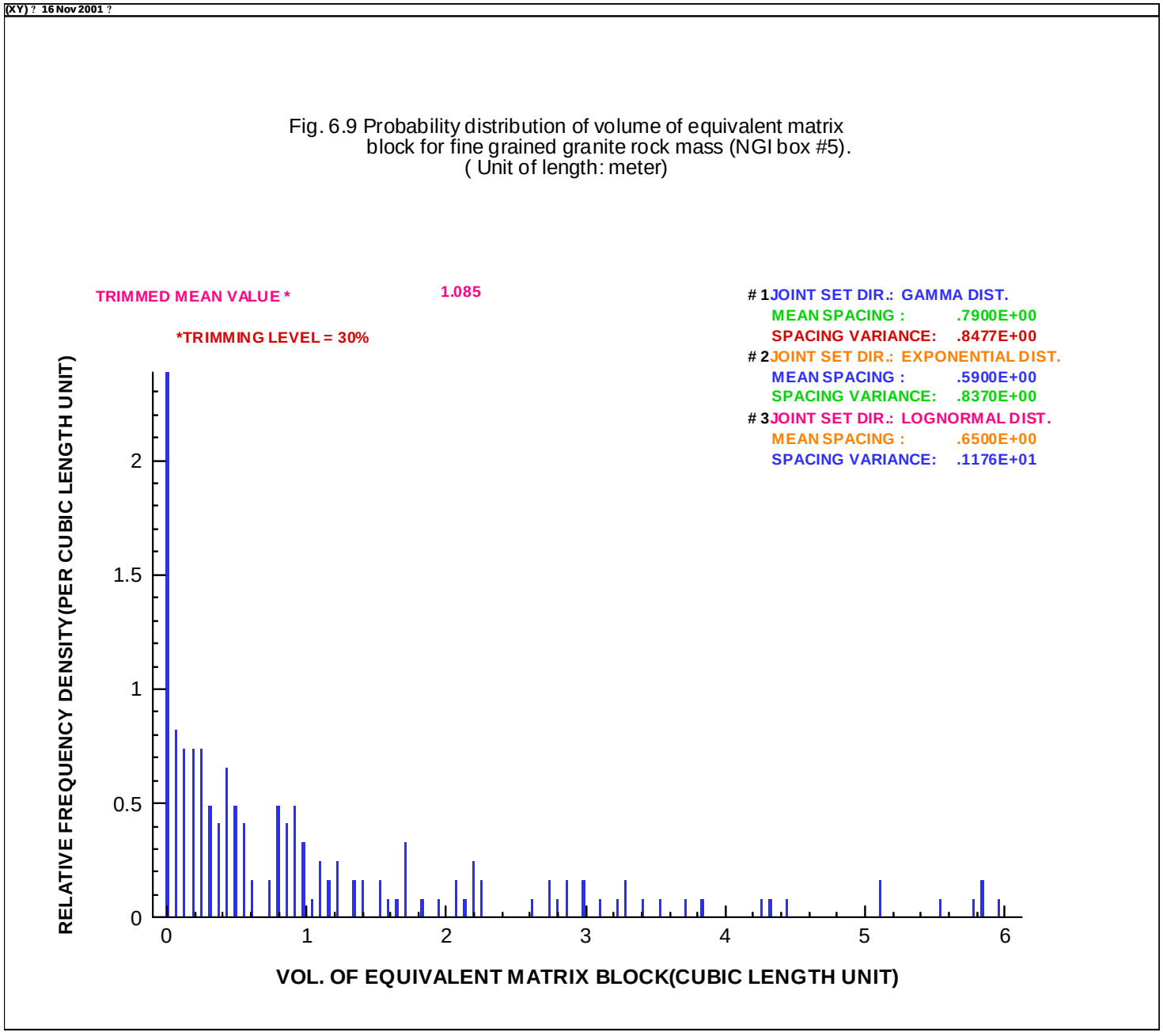

Fig. 6.9 Probability distribution of volume of equivalent matrix block for fine grained granite rock mass (NGI box #5). (Unit of length: meter)

(XY) ? 16 Nov 2001 ?

Fig. 6.10 Probability distribution of number of blocks per unit volume for fine grained granite rock mass (NGI box #5). (Unit: #/cubic meter)

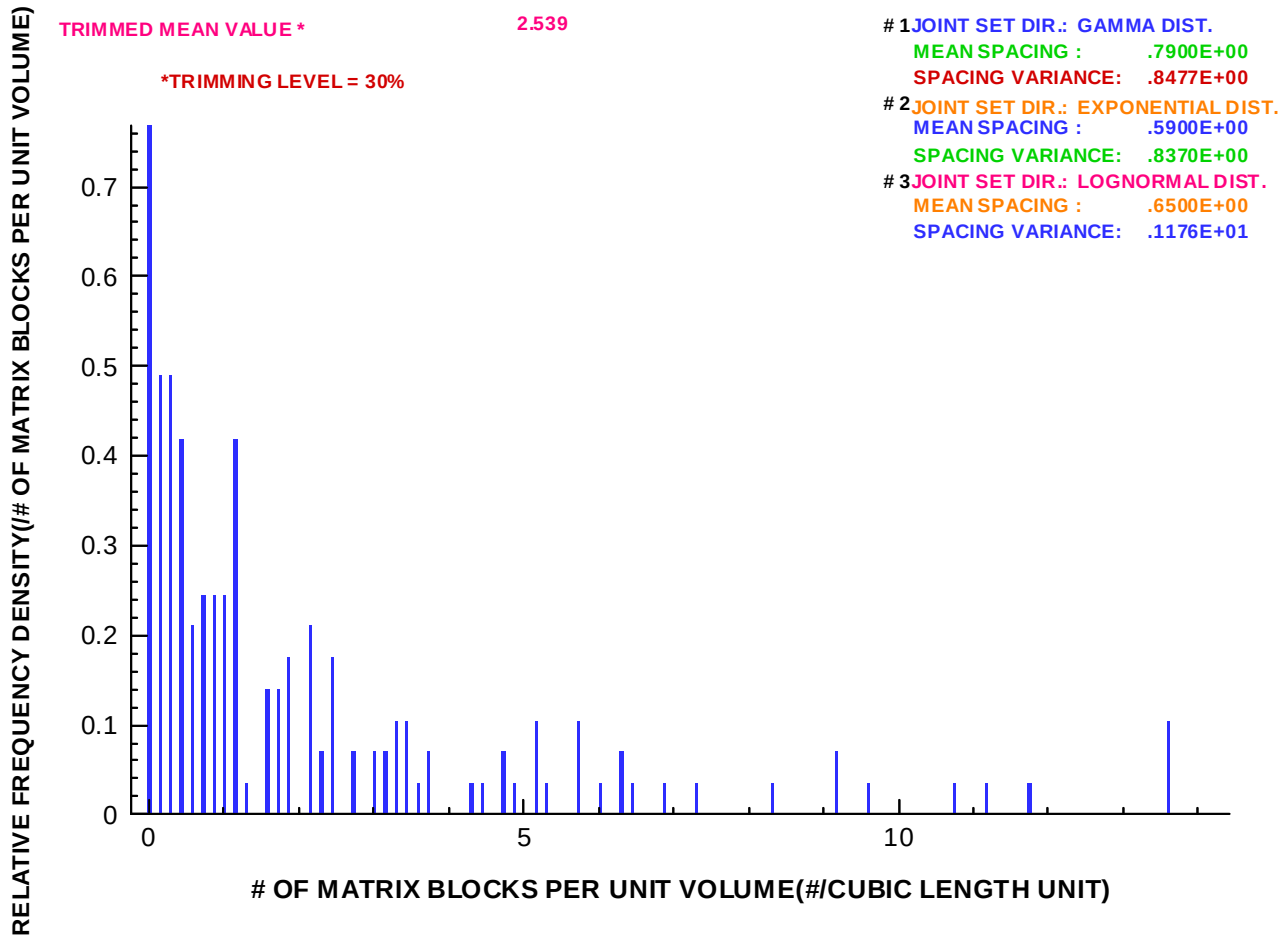

Table 6.5 Volumetric fracture frequency results for fine grained granite (NGI box #5) fracture sets

Fracture set #	1D-Intensity (#/m)	E(n·i)	$E(D^2)$ (m^2)	3D-Intensity ($\#/m^3$)
1	1.27	0.60	32.75	0.0823
2	1.70	0.60	32.75	0.1102
3	1.53	0.60	32.75	0.0991

Note: Lowest E(n·i) is limited to 0.6

6.7 Fracture System Generation in 3-D and Validation

Three-dimensional fracture system for a 30m cube of fine-grained granite rock mass (NGI block # 5) was generated similar to the way it was generated for Äspö diorite rock mass using the computer program GENERATE. Figure 6.11 shows the fracture traces obtained from the fracture generation in 3-D on a horizontal square window of 15m placed at the mid-level of the 30m cube. Fracture sets 1 and 2 are almost vertical and fracture set 3 is almost horizontal (see Table 6.2). Therefore fracture sets 1 and 2 should intersect the horizontal window quite well; fracture set 3 has a very low chance of intersecting the horizontal window. According to Table 6.2b, the mean strike values of the fracture sets 1and 2 are N 84° E and N 06° W, respectively. Strike directions around these two mean strike values can be seen very well in Figure 6.11. Figure 6.12 shows the fracture traces obtained from the fracture generation on a vertical square window of size 15m having the strike direction same as the trend direction of borehole KA2598A (293°) and placed at the middle of the 30m cube. Fracture set 1 strikes N 84° E and dips 88° S. Therefore, fracture set 1 should intersect the chosen vertical window well and produce traces having high apparent dips. Such traces can be seen very well on Figure 6.12. Fracture set 2 strikes N 06° W and dips almost vertical. Therefore, fracture set 2 should intersect the chosen vertical window very well and produce traces having high apparent dip angles. Figure 6.12 shows such traces very well. Fracture set 3 is almost horizontal. Therefore, fracture set 3 should intersect the chosen vertical window very well and produce sub-horizontal traces. Figure 6.12 shows such traces very well. A 10m length of KA2598A borehole is simulated on Figure 6.12. The 1-D fracture frequency on this simulated borehole is about 3.0 fractures per m. This number compares extremely well with the observed 1-D fracture frequency of 2.98 fractures per m on actual KA2598A borehole (see Table6.4).). Fracture traces simulated on a 40m square vertical window produced a mean trace length value of 4.28 m and a coefficient of variation of 0.50. When the vertical window size was increased to 55m square, the mean trace length value increased to 4.75m keeping the value of coefficient of variation almost the same. This shows clearly that the mean trace length increases with window size. Note that for infinite size window, a mean trace length of 5m along with a coefficient of variation of 0.5 was used in modeling the fracture size. These numbers validate the used fracture size model. The above findings show that the fracture geometry features of the generated fracture system agree well with the fracture data used to model the 3-D stochastic fracture system.

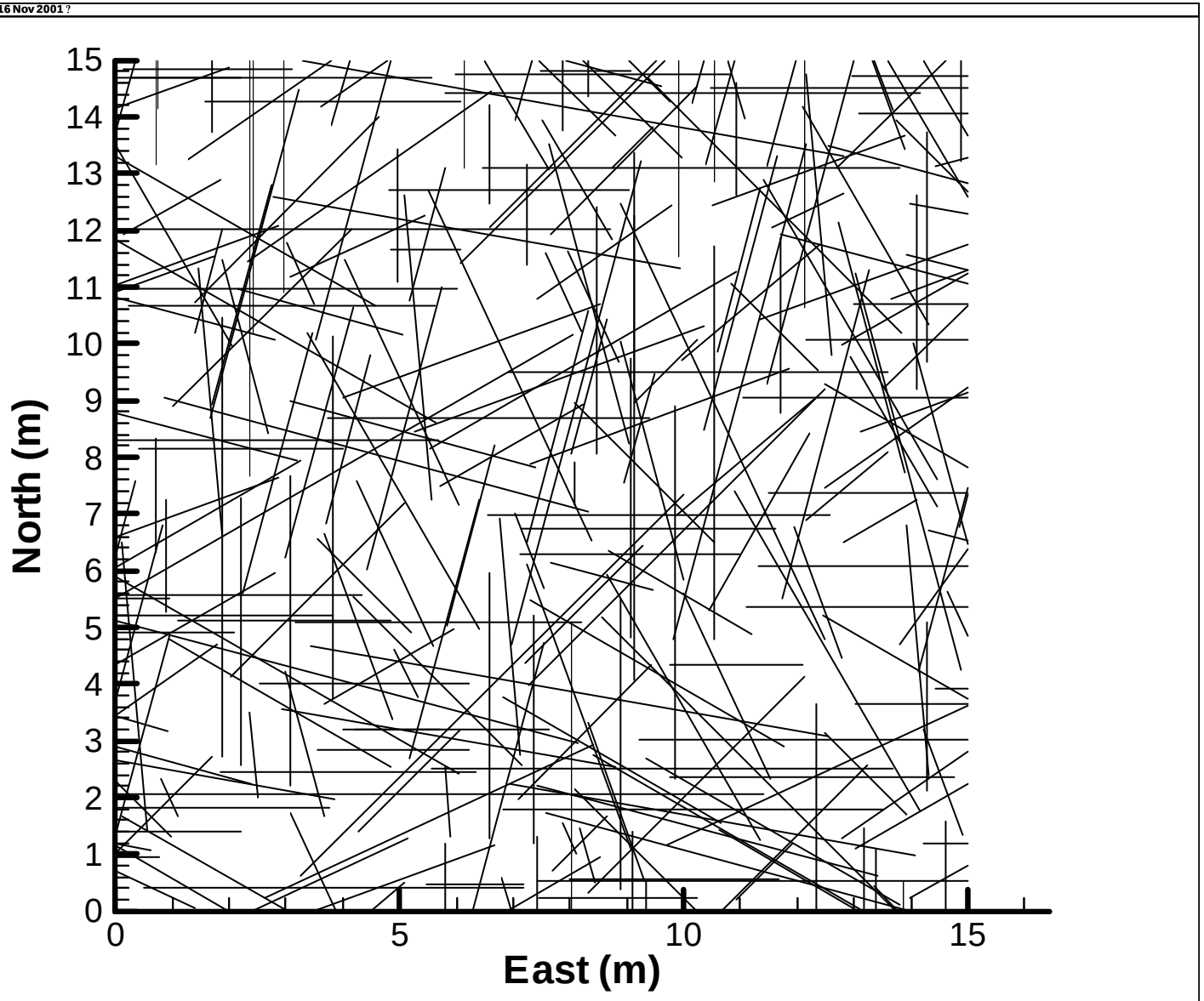

Fig. 6.11 Fracture traces obtained from fracture generation on a horizontal square window of size 15 m placed at the mid level of cube of 30m of fine grained granite rock mass (NGI box #5).

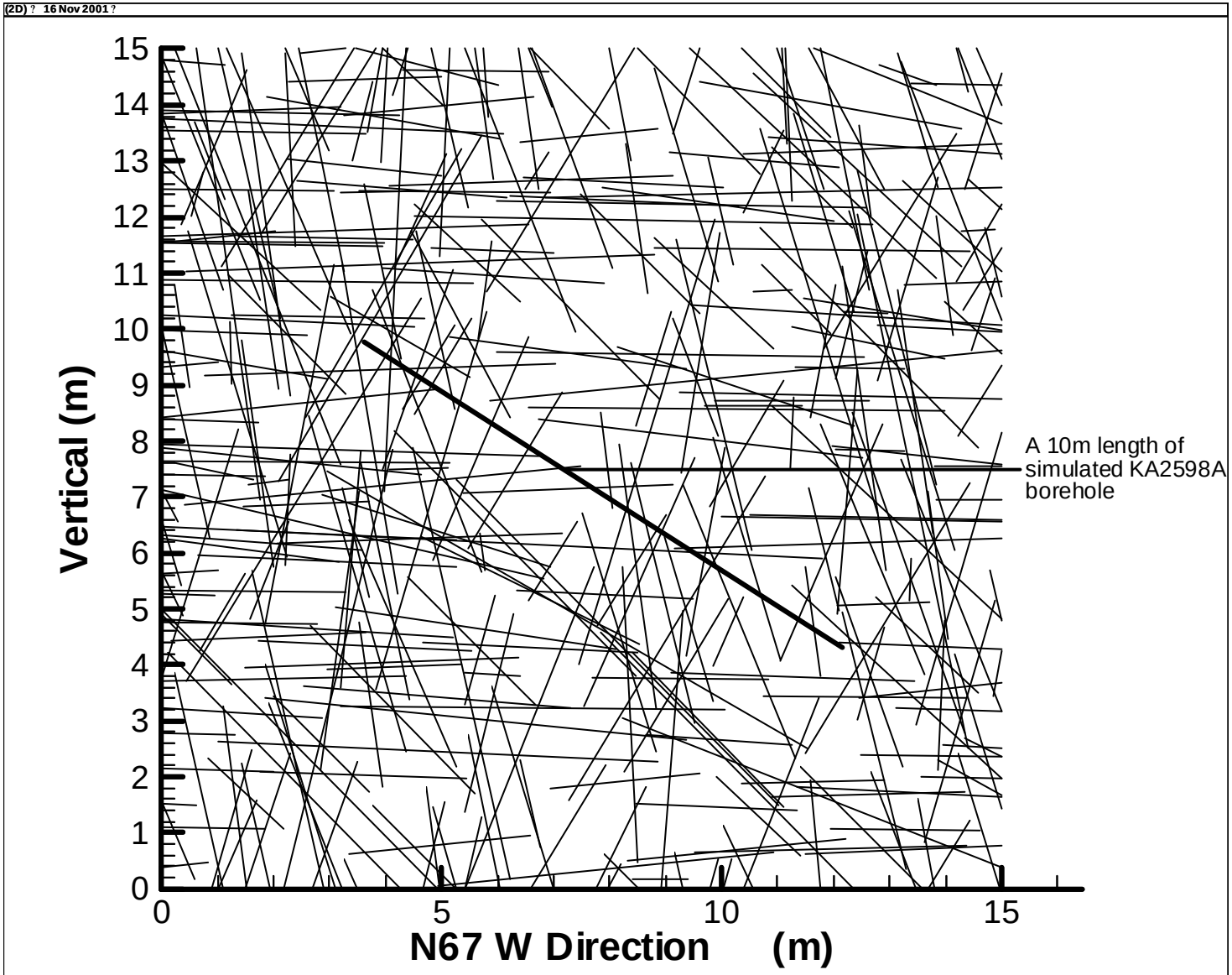

Fig. 6.12 Fracture traces obtained from fracture generation on a vertical square window of size 15 m having strike same as the trend direction of borehole KA2598A placed at the middle of 30m cube of fine grained granite rock mass (NGI box #5).

7 Stochastic 3-D fracture network model for NGI block number 49

7.1 Number of Fracture Sets and Correction for Orientation Bias

NGI block number 49 is located in the depth region of 380-410m of borehole KAS02. To enlarge the fracture data base slightly, orientation data were obtained from the depth region 375.4-414.5m of borehole KAS02. The fracture data were analyzed in a similar manner to the analysis conducted for Äspö diorite using the computer program CLUSDEL-BINGHAM. The final results obtained for fracture set delineation are shown in Figure 7.1. All three fracture sets show high variability. This high variability is partly reflected by the low number of data available for orientation analyses. Number of orientation data belonging to each fracture set and the mean directions obtained for the fracture sets are shown in Table 7.1.

The computer program OBIAS1D was applied to study the effect of orientation sampling bias on orientation distribution of each of the 3 fracture sets. The obtained results are shown in Figures 7.2 through 7.4. All three fracture sets intersect with the same borehole KAS02. Due to lack of fracture size data, the same probability distribution is used to model fracture size of the 4 fracture sets (see section 7.3). Therefore, comparisons between the 3 fracture sets depend only on the relative orientation distribution between the borehole direction and the directions of fractures of each fracture set. Borehole KAS02 is almost vertical. Fracture set 1 is almost vertical and fracture set 2 has a dip angle of 80°. Fracture set 3 has a dip angle of 25°. Therefore, fracture sets 1 and 2 have a less chance of intersection with the borehole compared to fracture set 3. Out of the three fracture sets, fracture set 1 has the lowest chance of intersection with the borehole. With respect to the orientation variability, in the increasing order the 3 fracture sets can be arranged as fracture set 1, 2 and 3 (see Figure 7.1, Table 7.2 and section 7.2). However, the difference in the variability between the fracture sets is small. Therefore, fracture sets 1 and 2 should have slightly higher effects than fracture set 3 with respect to the orientation bias correction (compare a and b plots of Figs. 7.2 through 7.4).

(Sketch) ? 16 Nov 2001 ?

Fig. 7.1 Fracture set delineation results on an upper hemispherical polar equal area projection for mixed lithology (NGI box # 49)

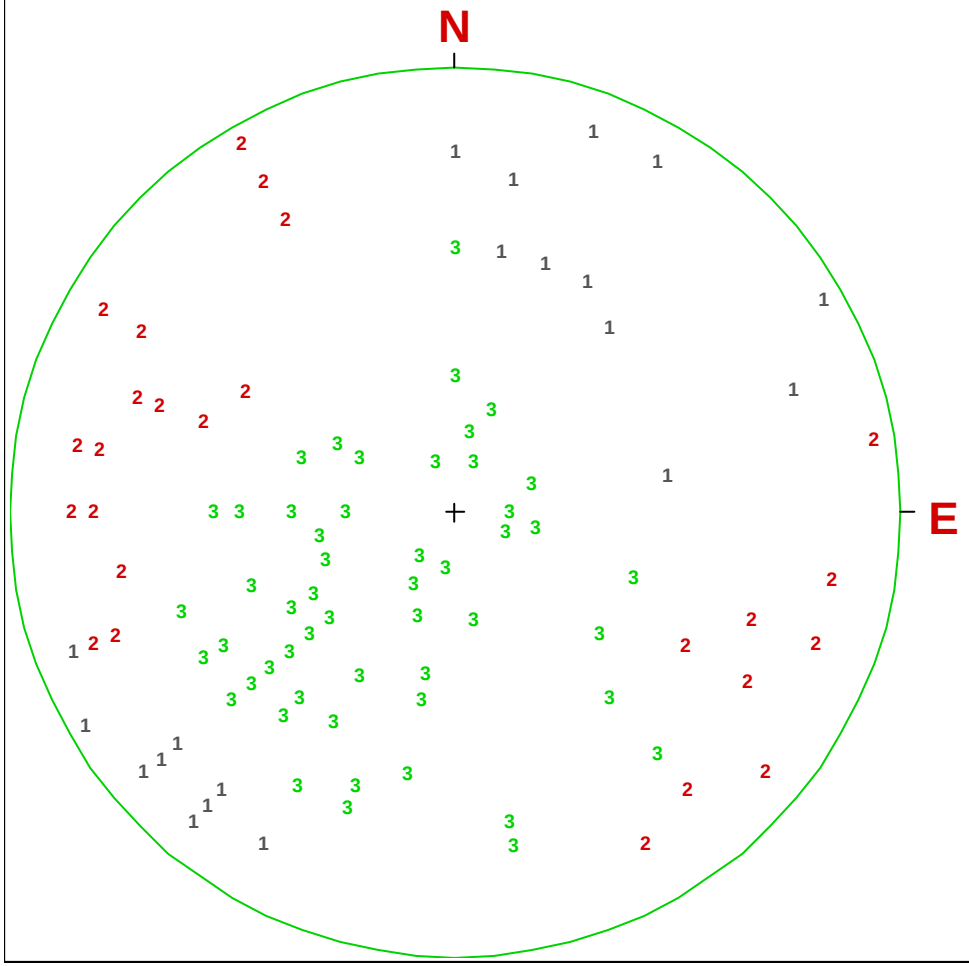

111 POLES

SMALL CIRCLE RADIUS VALUE =
14.05 DEGREES

OBJECTIVE FUNCTION VALUES

F2 =	3.28
F3 =	.65
F4 =	.20

SYMBOL	FRACTURE SET #	# OF DATA
1	1	24
2	2	28
3	3	59

Table 7.1 Delineated fracture sets and goodness-of-fit results of Bingham distribution for orientation data of mixed lithology (NGI box 49)

	Fracture		Mu 3		Mu 2		Mu 1		Chi-square Test			
Nobs.	Set	Npts.	Trend (°)	Plunge (°)	Trend (°)	Plunge (°)	Trend (°)	Plunge (°)	D.F.	chi	95chi	P
111	1	24	43.15	3.12	306.21	65.71	134.54	24.07				
	2	28	287.73	10.40	190.20	35.53	31.58	52.52				
	3	59	221.37	64.51	22.38	24.27	115.71	7.33	6	17.35	12.57	0.008

Note:

Nobs.=Number of fractures observed on the borehole

Npts.=Number of fractures belonging to the fracture set

Mu3=Mean normal vector direction (upward) of fracture set

Trend of Mu3=Dip direction of fracture set

Plunge of Mu3=90°-Dip angle of fracture set

Mu2=Vector normal to minor axis plane of Bingham distribution

Mu1=Vector normal to major axis plane of Bingham distribution

DF= Degrees of freedom for Chi-square test for Bingham distribution

Chi=Calculated Chi-square value

95Chi=Table Chi-square value at 5% significance level

P=Maximum significance level at which Bingham distribution can be used to represent the statistical distribution of orientation of fracture set

(a minimum of 0.05 is required to represent orientation data by a Bingham distribution)

(3D) ? 16 Nov 2001 ? NGI BOX #49

Fig. 7.2a Observed relative frequency of orientation for fracture set 1 of mixed lithology (NGI box #49).

Based on Line or Borehole(1-D) sampling

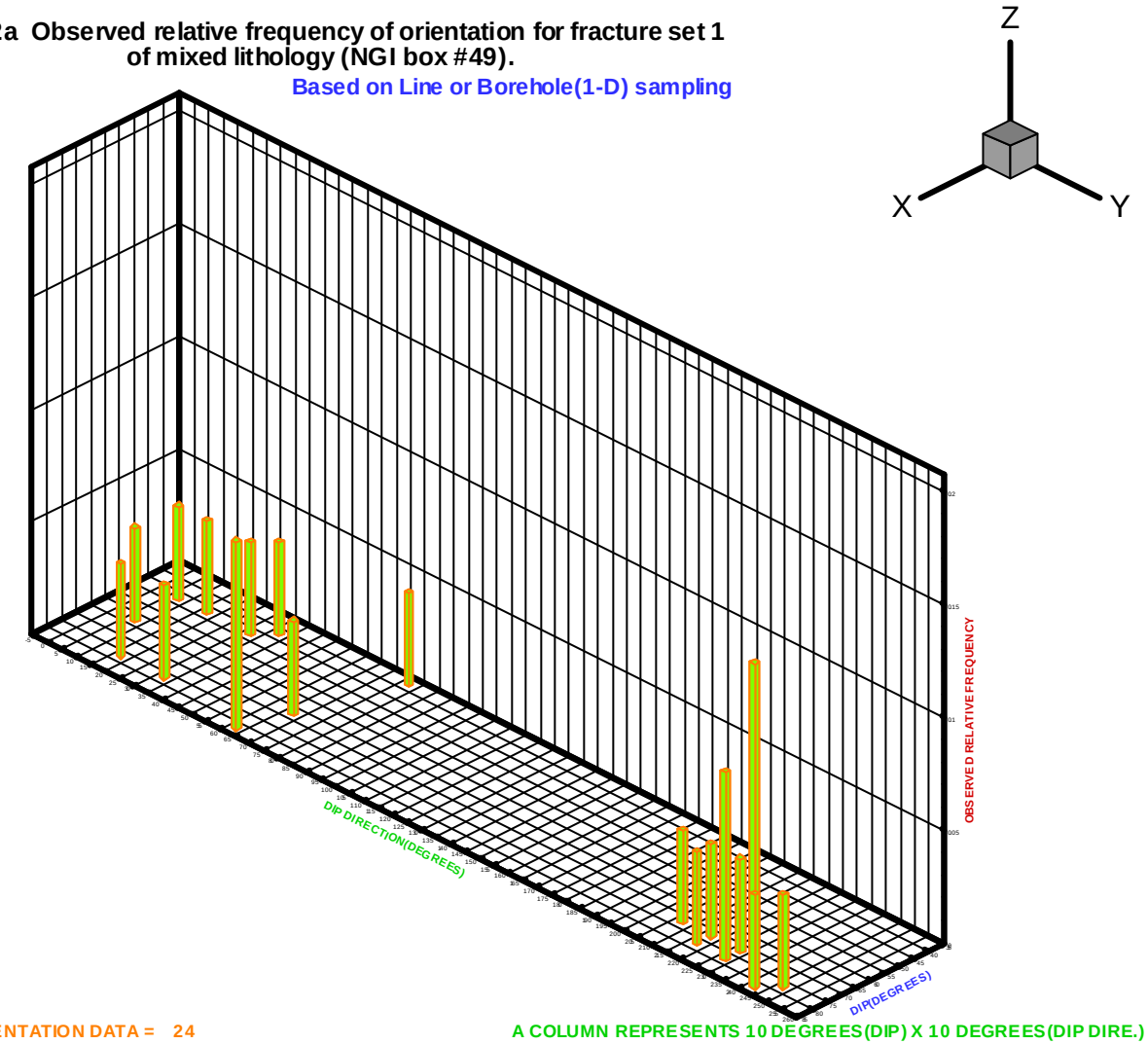

NUMBER OF ORIENTATION DATA = 24
LENGTH OF BOREHOLE = 39.08
TREND OF BOREHOLE = 318.00 (DEG.)
PLUNGE OF BOREHOLE = 85.00 (DEG.)
DIAMETER OF FRACTURE PLANES FROM 5.26 TO 5.26
DIAMETER OF BOREHOLE = .10

A COLUMN REPRESENTS 10 DEGREES(DIP) X 10 DEGREES(DIP DIRE.)
THE MAXIMUM VALUE FOR OBSERVED RELATIVE FREQUENCY = .1250
IT IS LOCATED FROM 65.00 TO 70.00 FOR DIP(DEG.)
AND 225.00 TO 230.00 FOR DIP DIRECTION(DEG.)
THE UNIT FOR LENGTH: Meter

(3D) ? 16 Nov 2001 ? NGI BOX #49

Fig. 7.2b Corrected relative frequency of orientation for fracture set 1 of mixed lithology (NGI box #49).

Based on Line or Borehole(1-D) sampling

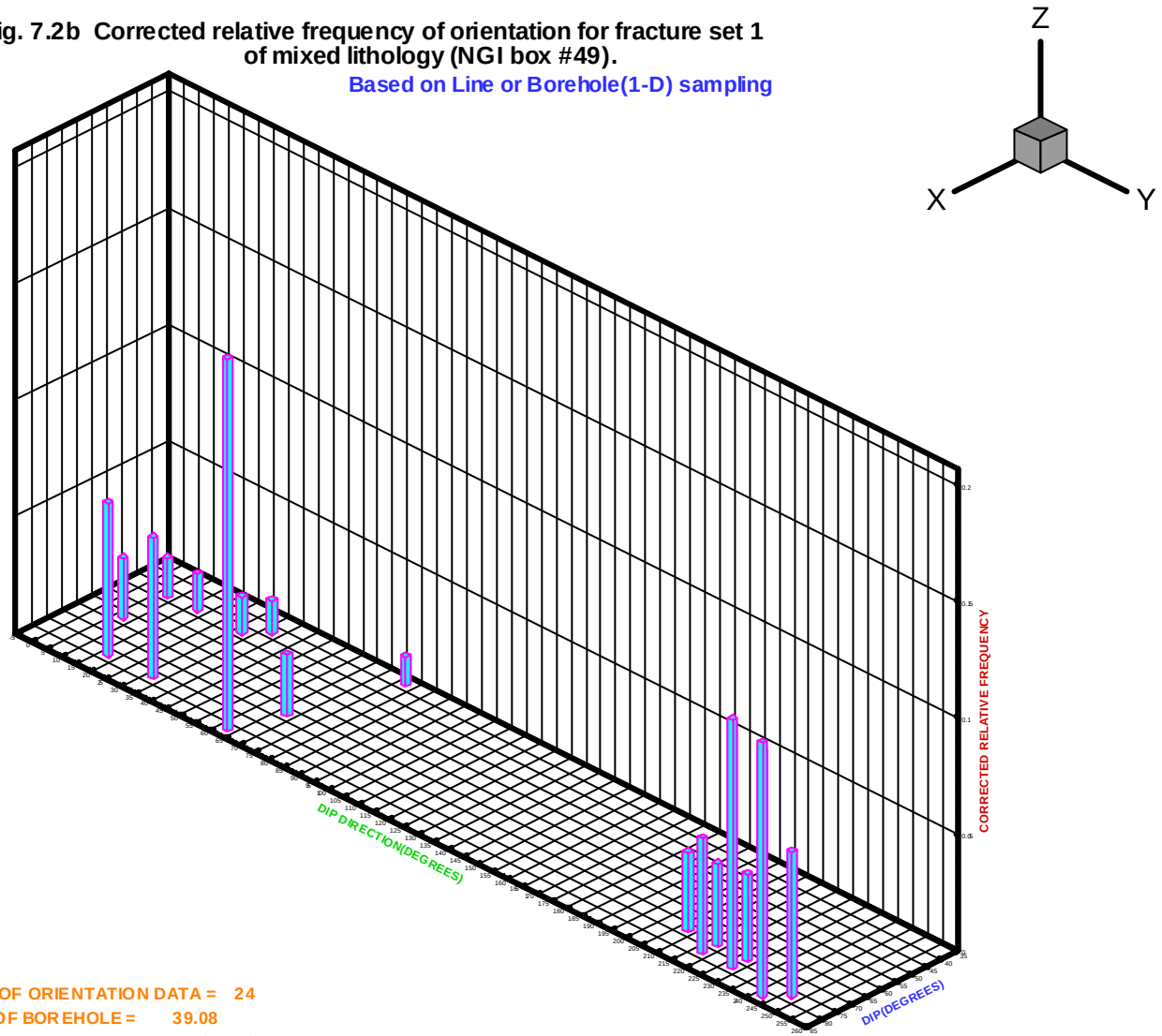

NUMBER OF ORIENTATION DATA = 24
LENGTH OF BOREHOLE = 39.08
TREND OF BOREHOLE = 318.00 (DEG.)
PLUNGE OF BOREHOLE = 85.00 (DEG.)
DIAMETER OF FRACTURE PLANES FROM 5.26 TO 5.26
DIAMETER OF BOREHOLE = .10

A COLUMN REPRESENTS 10 DEGREES(DIP) X 10 DEGREES(DIP DIRE.)
THE MAXIMUM VALUE FOR CORRECTED RELATIVE FREQUENCY = .1597
IT IS LOCATED FROM 80.00 TO 85.00 FOR DIP(DEG.)
AND 60.00 TO 65.00 FOR DIP DIRECTION(DEG.)
THE UNIT FOR LENGTH: Meter

(3D) ? 16 Nov 2001 ? NGI BOX #49

Fig. 7.3a Observed relative frequency of orientation for fracture set 2 of mixed lithology (NGI box #49).

Based on Line or Borehole(1-D) sampling

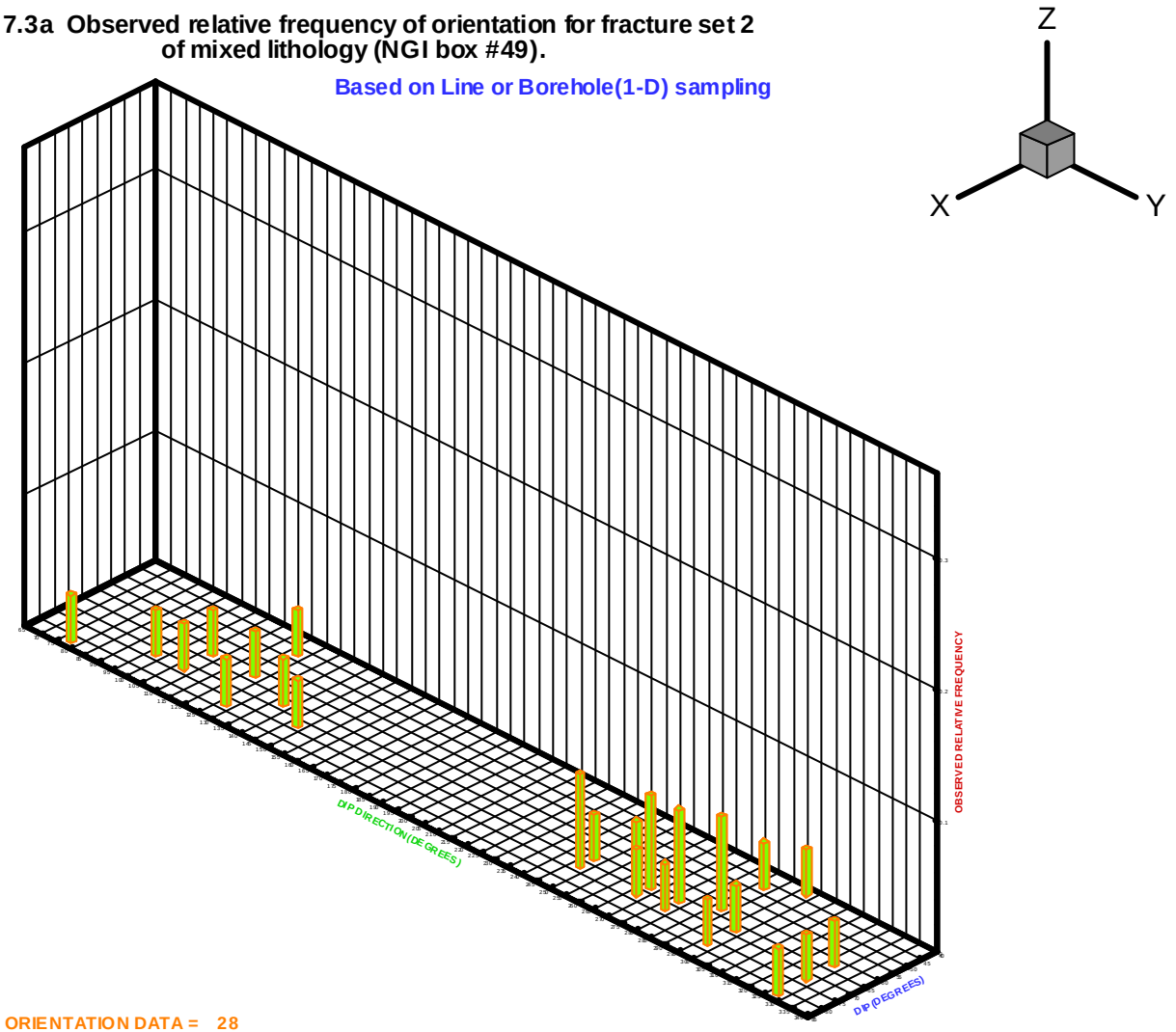

NUMBER OF ORIENTATION DATA = 28
LENGTH OF BOREHOLE = 39.08
TREND OF BOREHOLE = 318.00 (DEG.)
PLUNGE OF BOREHOLE = 85.00 (DEG.)
DIAMETER OF FRACTURE PLANES FROM 5.26 TO 5.26
DIAMETER OF BOREHOLE = .10

A COLUMN REPRESENTS 10 DEGREES(DIP) X 10 DEGREES(DIP DIRE.)
THE MAXIMUM VALUE FOR OBSERVED RELATIVE FREQUENCY = .0714
IT IS LOCATED FROM 60.00 TO 65.00 FOR DIP(DEG.)
AND 285.00 TO 290.00 FOR DIP DIRECTION(DEG.)
THE UNIT FOR LENGTH: Meter

(3D) ? 16 Nov 2001 ? NGI BOX #49

Fig. 7.3b Corrected relative frequency of orientation for fracture set 2 of mixed lithology (NGI box #49).

Based on Line or Borehole(1-D) sampling

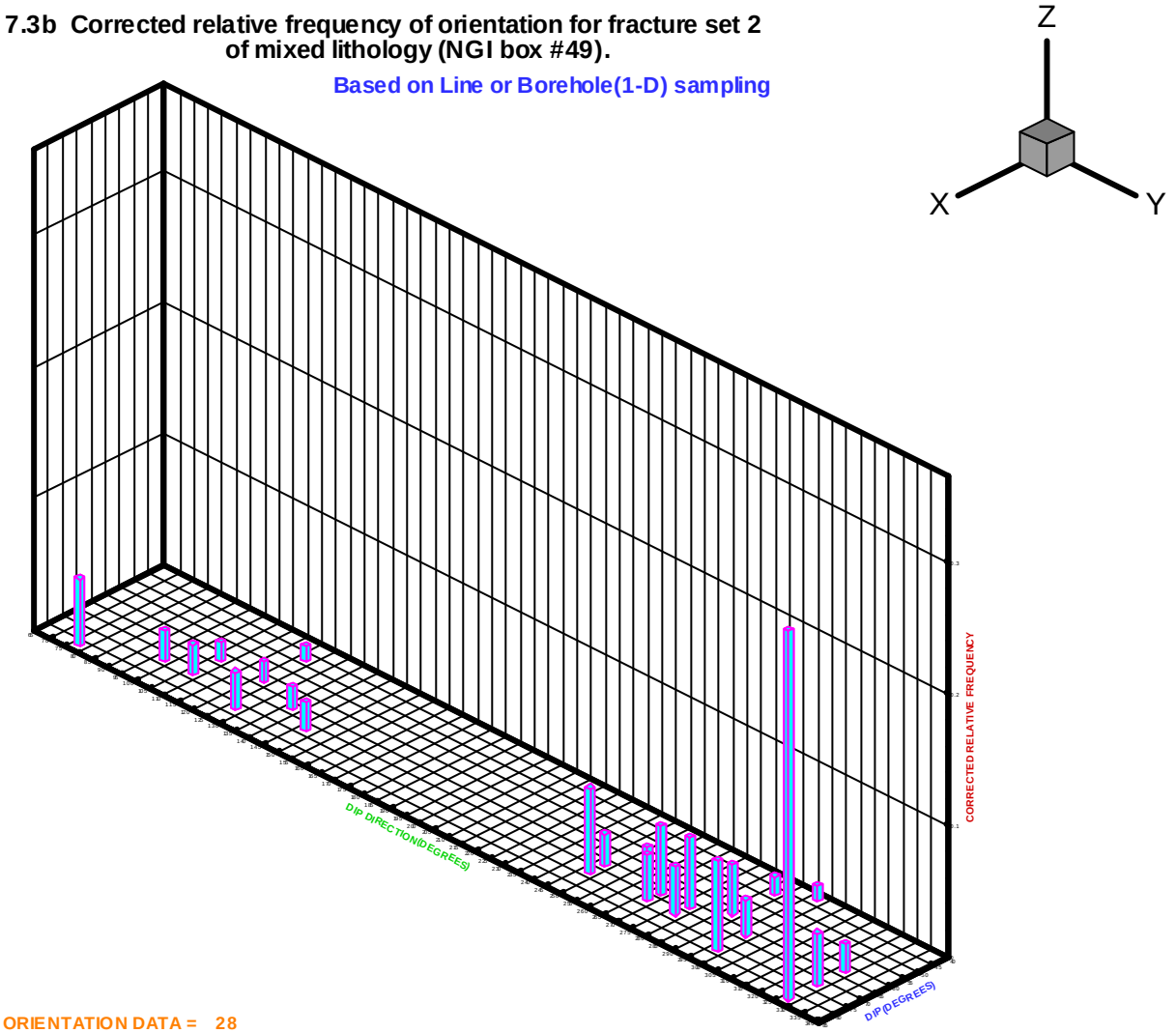

NUMBER OF ORIENTATION DATA = 28
LENGTH OF BOREHOLE = 39.08
TREND OF BOREHOLE = 318.00 (DEG.)
PLUNGE OF BOREHOLE = 85.00 (DEG.)
DIAMETER OF FRACTURE PLANES FROM 5.26 TO 5.26
DIAMETER OF BOREHOLE = .10

A COLUMN REPRESENTS 10 DEGREES(DIP) X 10 DEGREES(DIP DIRE.)
THE MAXIMUM VALUE FOR CORRECTED RELATIVE FREQUENCY = .2811
IT IS LOCATED FROM 80.00 TO 85.00 FOR DIP(DEG.)
AND 325.00 TO 330.00 FOR DIP DIRECTION(DEG.)
THE UNIT FOR LENGTH: Meter

(3D) ? 16 Nov 2001 ? NGI BOX #49

Fig. 7.4a Observed relative frequency of orientation for fracture set 3 of mixed lithology (NGI box #49).

Based on Line or Borehole(1-D) sampling

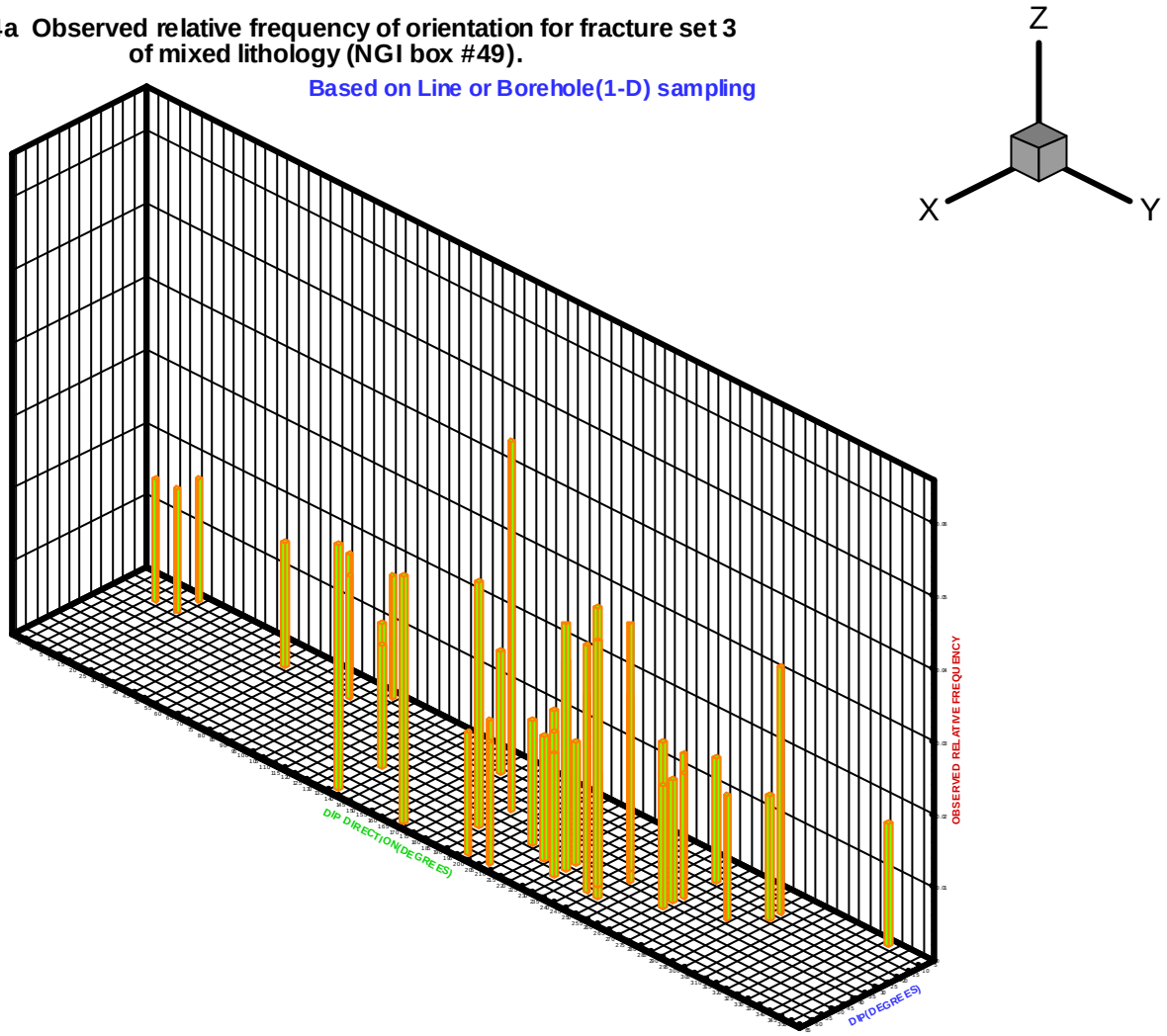

NUMBER OF ORIENTATION DATA = 59
LENGTH OF BOREHOLE = 39.08
TREND OF BOREHOLE = 318.00 (DEG.)
PLUNGE OF BOREHOLE = 85.00 (DEG.)
DIAMETER OF FRACTURE PLANES FROM 5.26 TO 5.26
DIAMETER OF BOREHOLE = .10

A COLUMN REPRESENTS 10 DEGREES(DIP) X 10 DEGREES(DIP DIRE.)
THE MAXIMUM VALUE FOR OBSERVED RELATIVE FREQUENCY = .0508
IT IS LOCATED FROM 30.00 TO 35.00 FOR DIP(DEG.)
AND 185.00 TO 190.00 FOR DIP DIRECTION(DEG.)
THE UNIT FOR LENGTH: Meter

Fig. 7.4b Corrected relative frequency of orientation for fracture set 3 of mixed lithology (NGI box #49).

Based on Line or Borehole(1-D) sampling

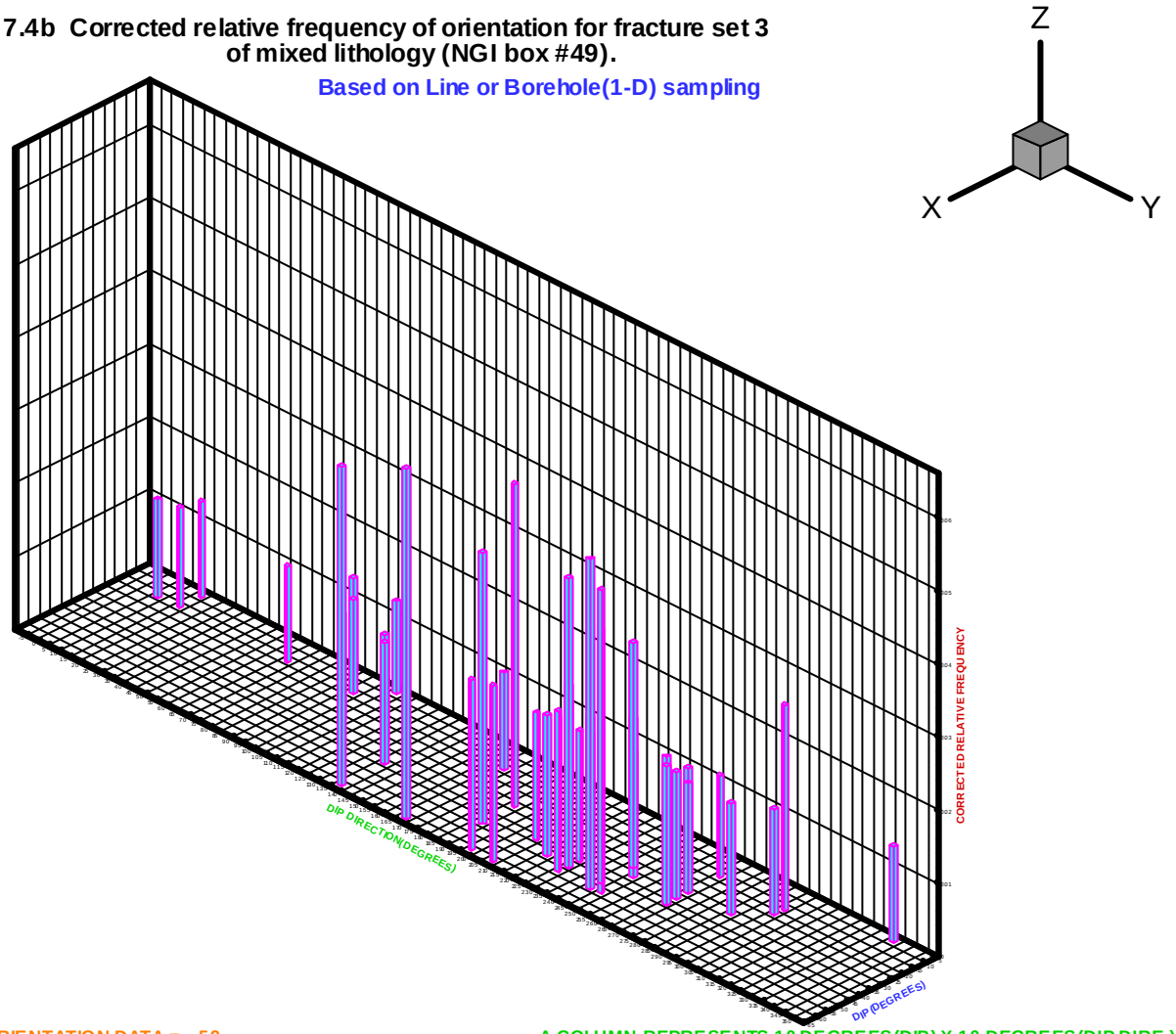

NUMBER OF ORIENTATION DATA = 59
LENGTH OF BOREHOLE = 39.08
TREND OF BOREHOLE = 318.00 (DEG.)
PLUNGE OF BOREHOLE = 85.00 (DEG.)
DIAMETER OF FRACTURE PLANES FROM 5.26 TO 5.26
DIAMETER OF BOREHOLE = .10

A COLUMN REPRESENTS 10 DEGREES(DIP) X 10 DEGREES(DIP DIRE.)
THE MAXIMUM VALUE FOR CORRECTED RELATIVE FREQUENCY = .0479
IT IS LOCATED FROM 60.00 TO 65.00 FOR DIP(DEG.)
AND 165.00 TO 170.00 FOR DIP DIRECTION(DEG.)
THE UNIT FOR LENGTH: Meter

7.2 Orientation Distribution for Each Fracture Set

Goodness-of-fit of hemispherical normal distribution was performed for both the raw and corrected orientation data of each fracture set using the computer program HEMISPHN. For all three fracture sets the mean normal vector direction and the distribution of the orientation have changed to some extent due to the orientation bias correction (compare plots a and b of Figs. 7.5 through 7.7). This indicates the importance of applying the orientation sampling bias correction in modeling joint orientation distribution. The summary results (Table 7.2) indicate that hemispherical normal distribution is not suitable to represent the statistical distribution of orientation of all 3 fracture sets. According to the spherical variance and *k* values in Table7.2, in the increasing order of orientation variability the fracture sets can be arranged as fracture sets 1, 2 and 3.

Goodness-of-fit of Bingham distribution was performed for the orientation data of each fracture set using the computer program CLUSDEL-BINGHAM. The results (Table 7.1) provide mean normal vectors for the fracture sets and also show that the number of data available for fracture set 1 and 2 is too small to perform Chi-square goodness-of-fit test for Bingham distribution. The results also show that the Bingham distribution is unsuitable to represent the orientation distribution of fracture set 3.

The aforementioned results show that the available theoretical probability distributions (hemispherical normal and Bingham distributions) cannot be used to represent the statistical distribution of orientation of all three fracture sets. Therefore, the empirical orientation distribution obtained from the corrected relative frequency data is used to generate orientation values for each of the three fracture sets.

7.3 Trace Length and Size Distributions for Each Fracture Set

As mentioned before, no fracture trace data were provided for this project to model fracture trace length distribution and size distribution in 3-D. Due to lack of reliable data on fracture traces, the same gamma distribution (mean=5m and coefficient of variation=0.5) used for Äspö diorite is also used to represent the fracture trace length distribution in 2-D for all 3 fracture sets. As for Äspö diorite, the equivalent fracture diameter in 3-D for all three fracture sets is represented by the gamma distribution with mean = 5.26m and standard deviation = 2.25m.

Fig. 7.5a Results of hemispherical normal distribution fit for observed orientation data of fracture set 1 of mixed lithology (NGI box #49).

Probability(Confidence) Contours for the
Hemispherical Normal Distribution of Fracture Normals

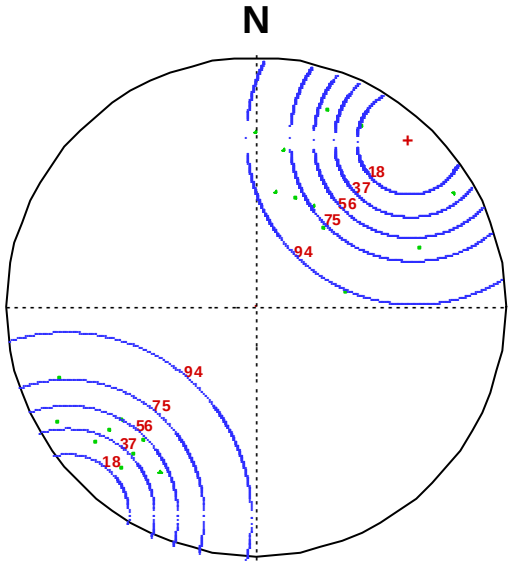

The number given for the contour is the percent(%) confidence

Maximum significance level at which the hemispherical normal distribution is suitable to represent the statistical distribution of joint orientation data : < 0.005

Number of Joint Data = 24

Average L = .7341
Average M = -.6715
Average N = .1009

Magnitude of Mean Vector = .8686
Mean Plunge(up) = 5.7913 (deg.)
Mean Trend = 42.4486 (deg.)
K Value of the Distribution = 7.2932
Spherical Variance = .1314

The small . indicate the joint normal vectors
The small + indicates the mean normal vector to the joint set

Upper-Hemispherical Stereographic Projection

Fig. 7.5b Results of hemispherical normal distribution fit for orientation data of fracture set 1 of mixed lithology (NGI box #49) corrected for sampling bias.

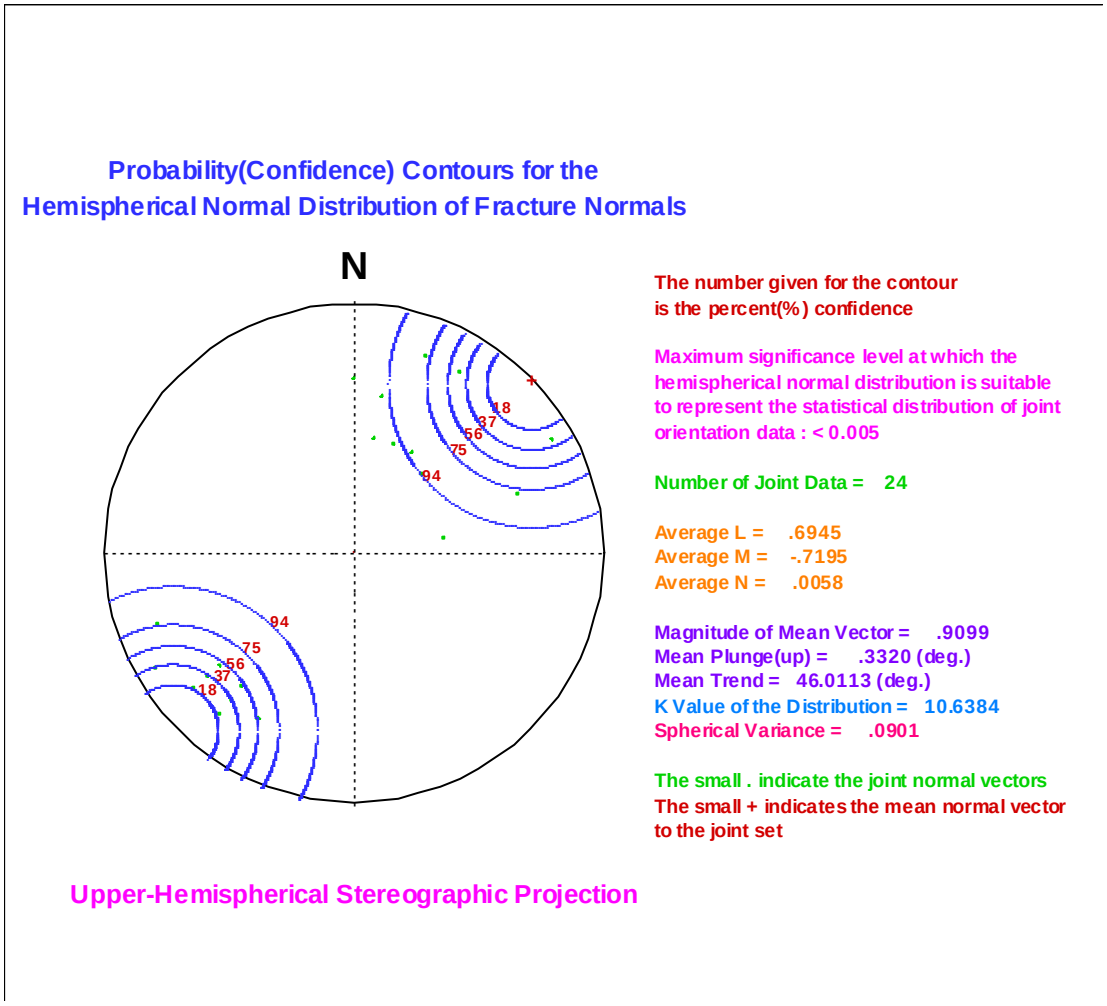

Fig. 7.6a Results of hemispherical normal distribution fit for observed orientation data of fracture set 2 of mixed lithology (NGI box #49).

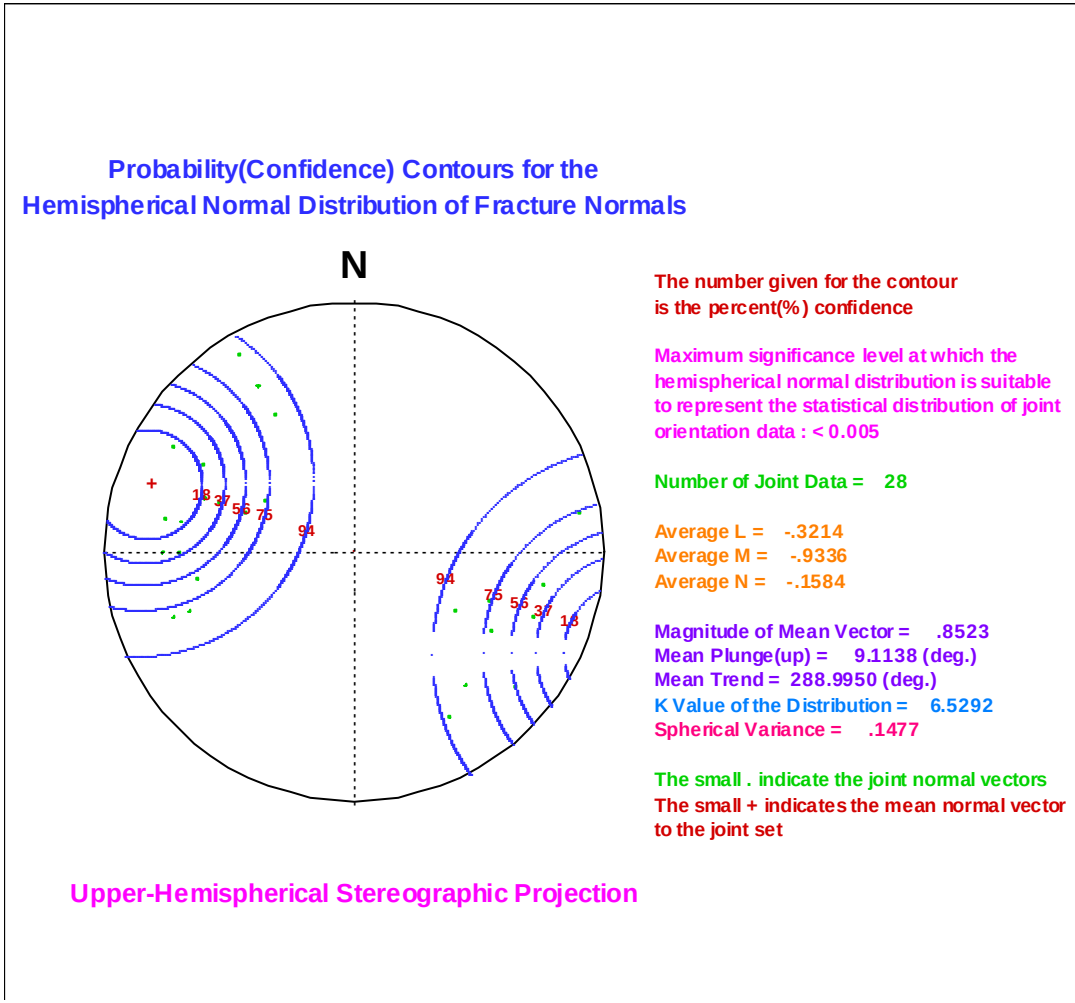

Fig. 7.6b Results of hemispherical normal distribution fit for orientation data of fracture set 2 of mixed lithology (NGI box #49) corrected for sampling bias.

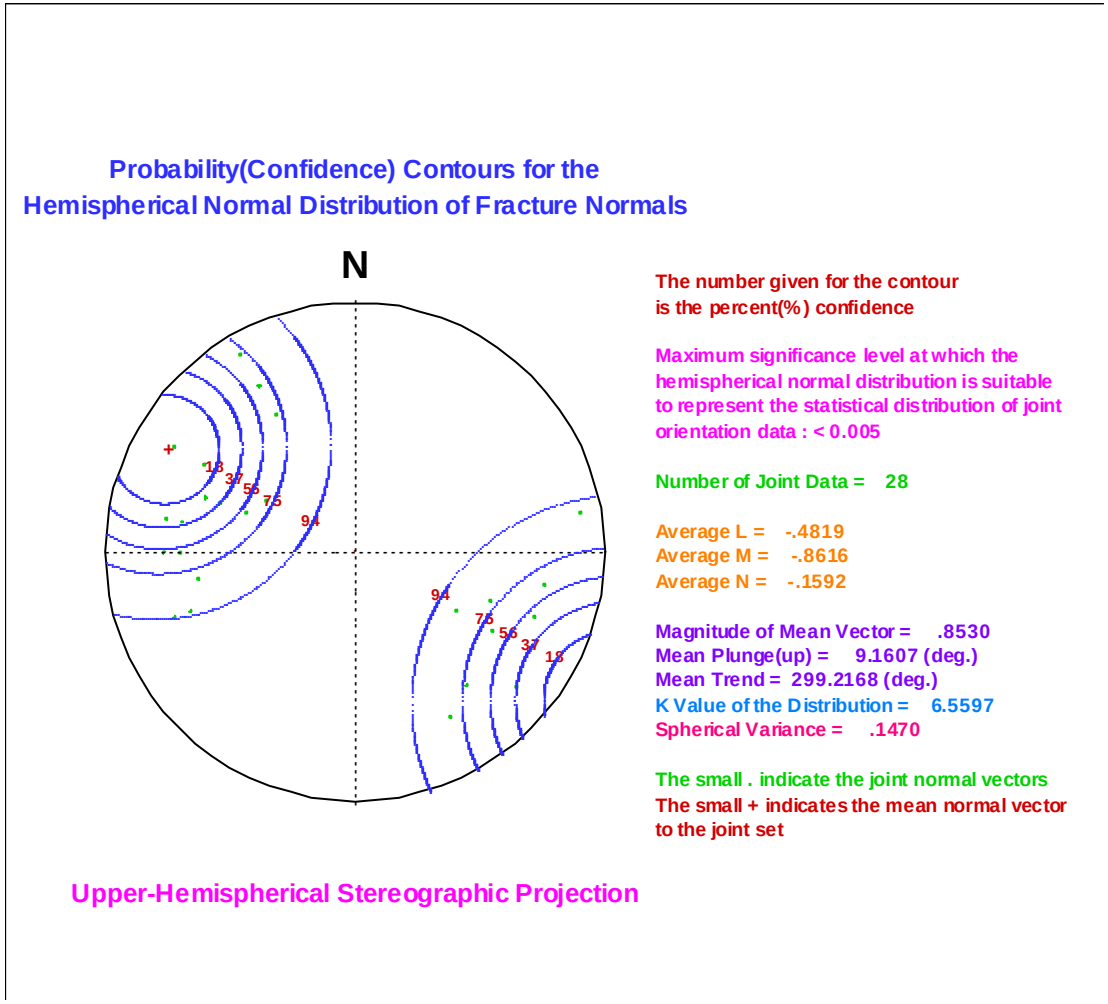

Fig. 7.7a Results of hemispherical normal distribution fit for observed orientation data of fracture set 3 of mixed lithology (NGI box #49).

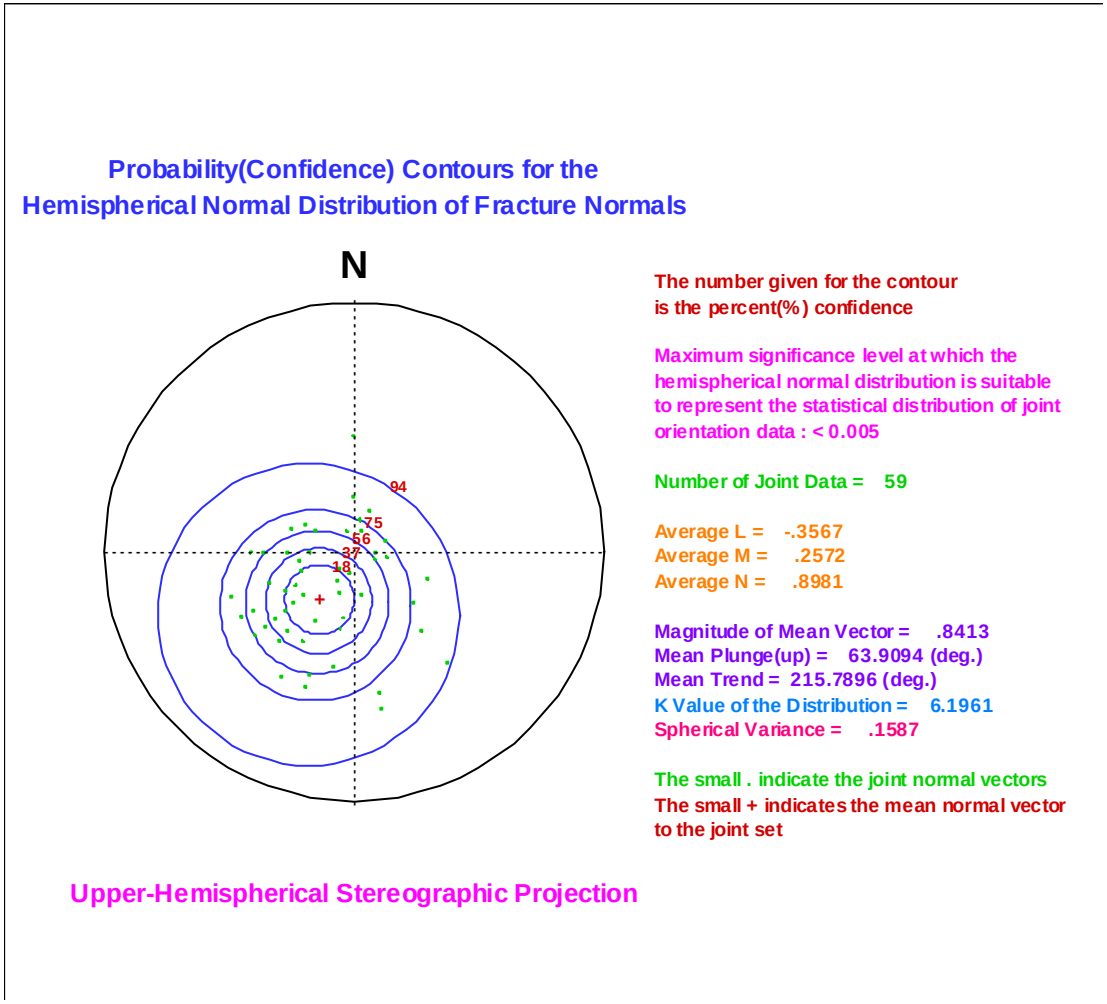

Fig. 7.7b Results of hemispherical normal distribution fit for orientation data of fracture set 3 of mixed lithology (NGI box #49) corrected for sampling bias.

Probability(Confidence) Contours for the
Hemispherical Normal Distribution of Fracture Normals

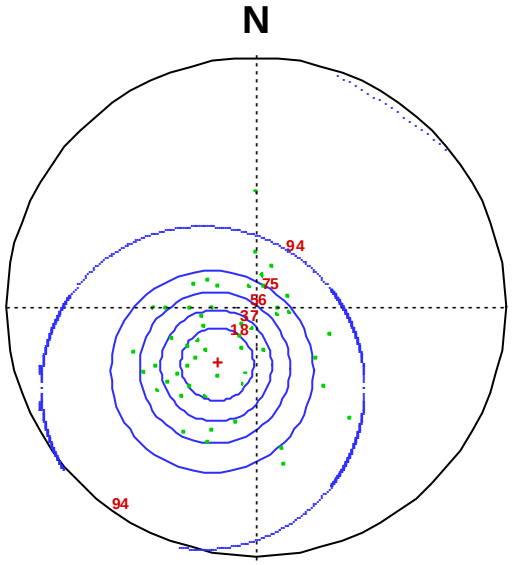

The number given for the contour is the percent(%) confidence

Maximum significance level at which the hemispherical normal distribution is suitable to represent the statistical distribution of joint orientation data : < 0.005

Number of Joint Data = 59

Average L = -.4190
Average M = .2844
Average N = .8623

Magnitude of Mean Vector = .8312
Mean Plunge(up) = 59.5769 (deg.)
Mean Trend = 214.1692 (deg.)
K Value of the Distribution = 5.8240
Spherical Variance = .1688

The small . indicate the joint normal vectors
The small + indicates the mean normal vector to the joint set

Upper-Hemispherical Stereographic Projection

Table 7.2 Goodness-of-fit results of hemispherical normal distribution for orientation data of mixed lithology (NGI box #49)

(a) Raw orientation data

Nobs.	Fracture set #	Npts.	Upward mean normal vector		K	Sp. Var.	P
			Trend (°)	Plunge (°)			
111	1	24	42.45	5.79	7.29	0.1314	<0.005
	2	28	289.00	9.11	6.53	0.1477	<0.005
	3	59	215.79	63.91	6.20	0.1587	<0.005

(b) Data corrected for sampling bias

Nobs.	Fracture set #	Npts.	Upward mean normal vector		K	Sp. Var.	P
			Trend (°)	Plunge (°)			
111	1	24	46.01	0.33	10.64	0.0901	<0.005
	2	28	299.22	9.16	6.56	0.1470	<0.005
	3	59	214.17	59.58	5.82	0.1688	<0.005

Nobs.=Number of fractures observed on the borehole
Npts.=Number of fractures belonging to the fracture set
K=A parameter in the hemispherical normal distribution
Sp. Var.=Spherical variance
P=Maximum significance level at which the hemispherical normal distribution is suitable to represent the statistical distribution of fracture orientation data
(a minimum of 0.05 is required to represent orientation data by a hemispherical normal distribution)

7.4 Spacing Distribution and 1-D Fracture frequency for Each Fracture Set

Fracture spacing data were obtained from the depth region 375.4-414.5m of borehole KAS02. Goodness-of-fit tests were performed using GDFT computer program to find the suitable probability distributions as well as the best probability distribution to represent the statistical distribution of spacing for each fracture set. The results (Table 7.3) indicate that all three probability distributions lognormal, gamma and exponential are highly suitable to represent the statistical distribution of spacing for any of the 3 fracture sets. The lognormal distribution was found to be the best distribution for 2 fracture sets. The gamma distribution turned out to be the best distribution for 1 fracture set and 2nd best distribution for 1 fracture set. The exponential distribution was found to be the 2nd best distribution for 2 fracture sets.

The estimation of mean spacing and 1-D fracture frequency along the borehole direction and mean normal vector direction of each fracture set were conducted in the same way it was done for Äspö diorite rock mass using the computer program COR1DFM1 The obtained results are given in Table 7.4. Note that for fracture sets 1 and 2, the angle between the borehole direction and the mean normal vector direction of the fracture set is greater than 70 degrees (Table 7.4). Because of the reasons mentioned in section 4.4, for these two fracture sets the 1-D fracture frequency along the mean normal vector direction is estimated by limiting the aforementioned angle to 70 degrees.

Table 7.3 Goodness-of-fit test results for spacing of the three fracture sets of mixed lithology (NGI box # 49)

Fracture set #	No. of data	Mean (m)	Var (m^2)	Probability Distribution	*K-S* $_{stat}$ Value	df	*P* -value	Best Distribution Rank
1	23	1.6483	5.4226	Exponential	0.1505	6	>0.2	3
				Gamma	0.0843	6	>0.2	2
				LogNormal	0.0609	6	>0.2	1
2	27	1.4237	6.1471	Exponential	0.0753	6	>0.2	2
				Gamma	0.0800	6	>0.2	3
				LogNormal	0.0467	6	>0.2	1
3	58	0.5650	0.3825	Exponential	0.0522	7	>0.2	2
				Gamma	0.0310	7	>0.2	1
				LogNormal	0.0540	7	>0.2	3

Note: A minimum P value of 0.05 is required to accept the tried probability distribution to represent the spacing distribution of the fracture set.

Table 7.4 Mean spacings and linear frequencies along the borehole KAS02 and mean normal vector directions for fracture sets of mixed lithology (NGI box #49)

Fracture set #	Orientation of fracture set		Dir. of borehole		Obs. mean spacing along borehole	Length of borehole	Corr. mean spacing along borehole	1-D fracture frequency along borehole	Angle between borehole & MNV	1-D fracture frequency along MNV
	Dip dir. (degs.)	Dip (degs.)	Trend (degs.)	Plunge (degs.)	(m)	(m)	(m)	(# per m)	(deg.)	(# per m)
1	043	87	318	85	1.65	39.08	1.65	0.61	*70 (87.36)	1.77
2	287	80	318	85	1.42	39.08	1.42	0.70	*70 (84.36)	2.05
3	221	25	318	85	0.57	39.08	0.57	1.77	25.41	1.96

MNV = Mean Normal Vector of fracture set

* = Actual angle is greater than 70°; however the angle was limited to 70° to calculate the 1-D fracture frequency along MNV direction

7.5 1-D Fracture frequency in any Direction in 3-D

The 1-D fracture frequencies obtained along the mean normal vector directions of fracture sets were then used to estimate the 1-D fracture frequency in all the directions in 3-D by using the computer program FREQ1DALLDIR. Figure 7.8 shows the obtained results. This figure also pin points the directions and magnitudes for the minimum and maximum fracture frequencies for the rock mass in NGI block number 49.

7.6 Mean Estimates for Block Size, Number of Blocks per Unit Volume and Number of Fractures per Unit Volume

The spacing distributions obtained along the mean normal vector directions for the 3 fracture sets were used along with the orientation distributions of the fracture sets in generating rock blocks in 3-D using the Monte-Carlo simulation procedure. This was performed using the computer program FREQ3DMVDJS. Orientations for the fracture sets were generated according to the obtained empirical orientation distributions. The obtained results for the distribution of volume of equivalent matrix block at a trimming level of 30% are shown in Figure 7.9 along with the trimmed mean value. Similar results for the number of matrix blocks per unit volume are shown in Figure 7.10.

Volumetric fracture frequencies for the 3 fracture sets were estimated in a similar manner to it was conducted for the Äspö diorite rock mass using the computer program 3DINTF1D. Obtained results are given in Table 7.5.

Table 7.5 Volumetric fracture frequency results for mixed lithology (NGI box #49) fracture sets

Fracture set #	1D-Intensity (#/m)	E(n·i)	$E(D^2)$ (m^2)	3D-Intensity ($\#/m^3$)
1	1.77	0.6000	32.75004	0.1147
2	2.05	0.6000	32.75004	0.1328
3	1.96	0.6000	32.75004	0.1270

Note: Lowest E(n·i) is limited to 0.6

(2D) ? 16 Nov 2001 ?

Fig. 7.8 1-D fracture frequency distribution in 3-D on an equal-angle equatorial net on the upper hemispherical for mixed lithology rock mass (NGI box #49).

Length Unit: Meter

Minimum Fracture Frequency:		Maximum Fracture Frequency:	
Magnitude(#/Length Unit):	1.5470	Magnitude(#/Length Unit):	4.4134
Trend(Deg.):	22.4800	Trend(Deg.):	250.4700
Plunge(Deg.):	24.2800	Plunge(Deg.):	27.5700

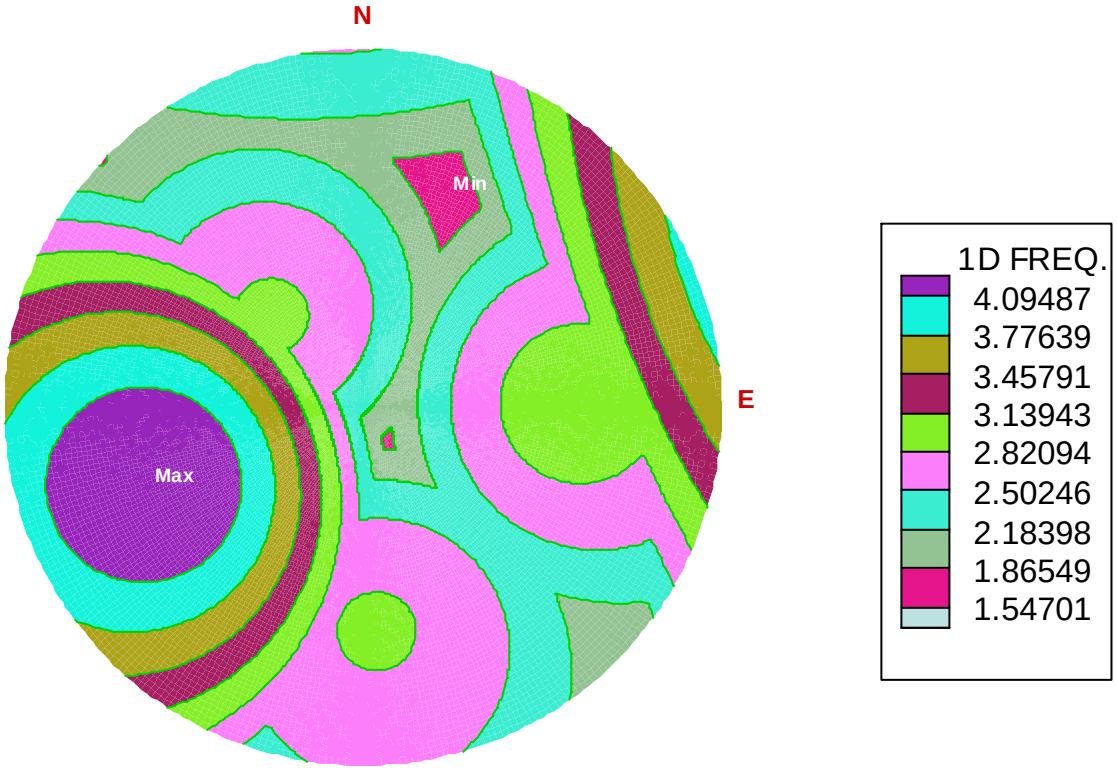

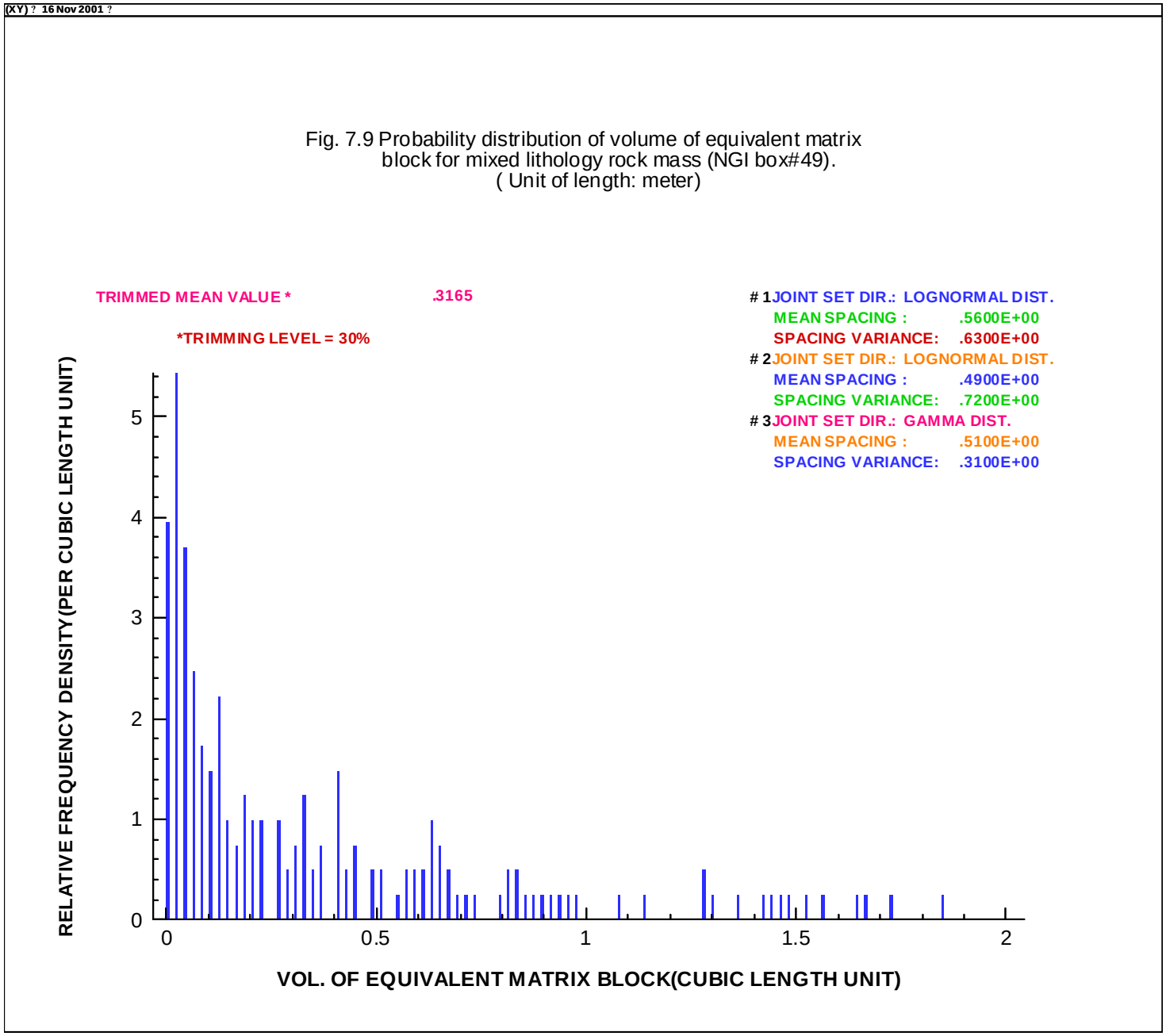

Fig. 7.9 Probability distribution of volume of equivalent matrix block for mixed lithology rock mass (NGI box#49). (Unit of length: meter)

(XY) ? 16 Nov 2001 ?

Fig. 7.10 Probability distribution of number of blocks per unit volume for mixed lithology rock mass (NGI box #49). (Unit: #/cubic meter)

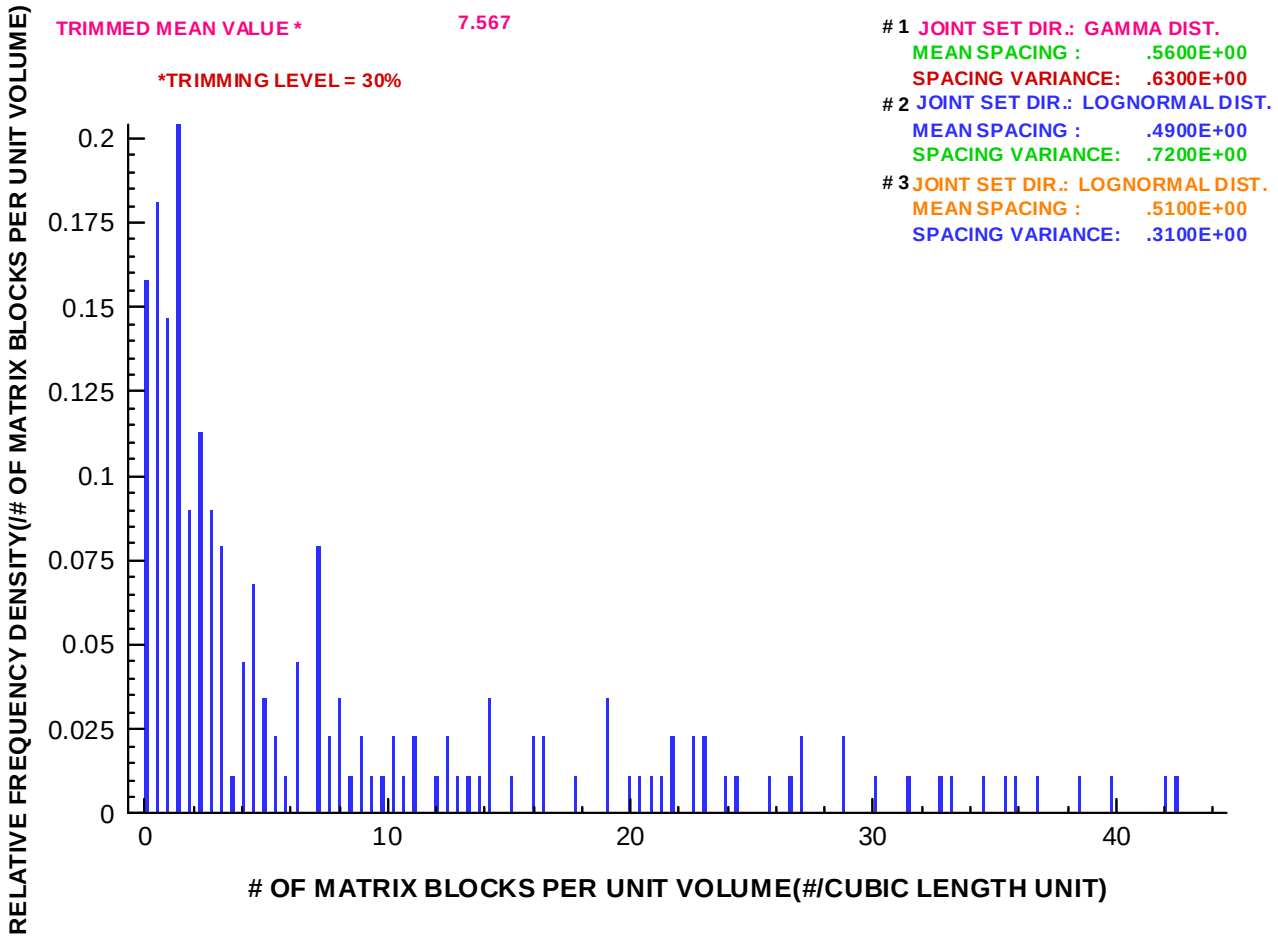

7.7 Fracture System Generation in 3-D and Validation

Three-dimensional fracture system for NGI block # 49 of size 30m cube was generated similar to the way it was generated for Äspö diorite rock mass using the computer program GENERATE. Figure 7.11 shows the fracture traces obtained from the fracture generation on a horizontal square window of 15m placed at the mid-level of the 30m cube. Out of the three fracture sets, the first two fracture sets are sub vertical and fracture set 3 has a mean dip angle of 30° (see Figure 7.1 and Table 7.2). Therefore, fracture sets 1 and 2 should intersect the horizontal window very well and fracture set 3 should intersect the window at a moderate level. According to Table7.2b, the mean strike values of the fracture sets 1, 2 and 3 are N 44° W, S 29° W, and S 56° E, respectively. Strike directions around these three mean strike values can be seen very well in Figure 7.11. Figure 7.12 shows the fracture traces obtained from the fracture generation on a vertical square window of size 15m having the strike direction same as the trend direction of borehole KAS02 (318°) and placed at the middle of the 30m cube. Fracture set 1 is almost vertical and strikes N 44° W. Therefore, mean strike of fracture set 1 is almost parallel to the vertical window. However, because of the orientation variability of fracture set 1, some of the fractures of fracture set 1 intersect the vertical window and produce traces around the vertical. Such traces can be seen very well on Figure 7.12. Fracture set 2 has a mean dip of 80° and a mean strike of S 29° W. Therefore, fracture set 2 should intersect the chosen vertical window very well and produce traces having high apparent dip angles. Figure 7.12 shows such traces very well. Fracture set 3 strikes S 56° E and dips 30° SW. Therefore, fracture set 3 should make sub-horizontal fracture traces on the chosen vertical window. Figure 7.12 shows sub-horizontal fracture traces very well. Figure 7.12 also shows that the traces appear on the figure come from 3 fracture sets. A 10m length of KAS02 borehole is simulated on Figure 7.12. The 1-D fracture frequency on this simulated borehole is about 3.3 fractures per m. This number compares very well with the observed 1-D fracture frequency of 3.08 fractures per m on actual KAS02 borehole (see Table 7.4). Fracture traces simulated on a 40m square vertical window produced a mean trace length value of 4.31 m and a coefficient of variation of 0.50. When the vertical window size was increased to 55m square, the mean trace length value increased to 4.79m keeping the value of coefficient of variation almost the same. This shows clearly that the mean trace length increases with window size. Note that for infinite size window, a mean trace length of 5m along with a coefficient of variation of 0.5 was used in modeling the fracture size. These numbers validate the used fracture size model. The above findings show that the fracture geometry features of the generated fracture system agree well with the fracture data used to model the 3-D stochastic fracture system.

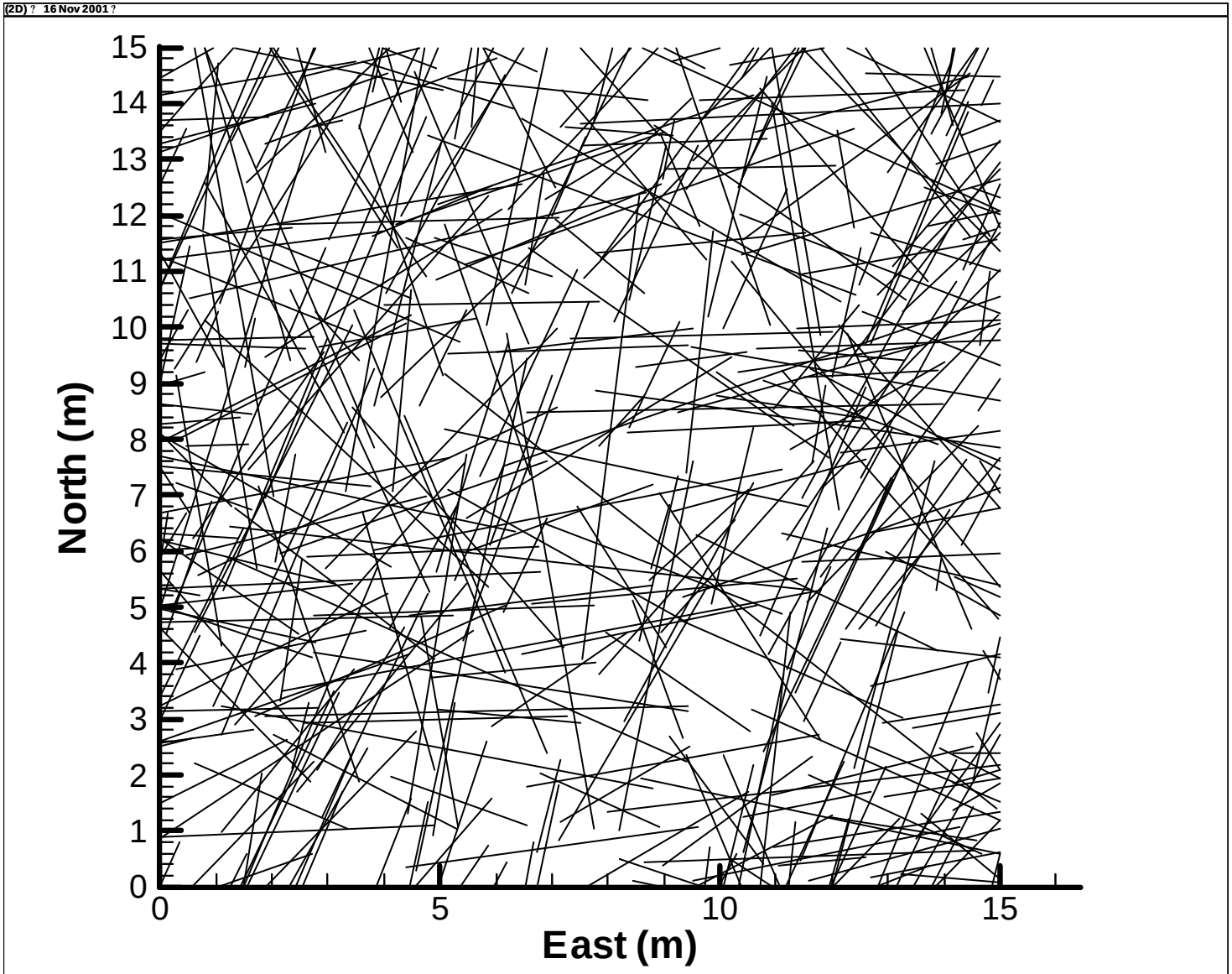

Fig. 7.11 Fracture traces obtained from fracture generation on a horizontal square window of size 15 m placed at the mid level of cube of 30m of mixed lithology rock mass (NGI box #49).

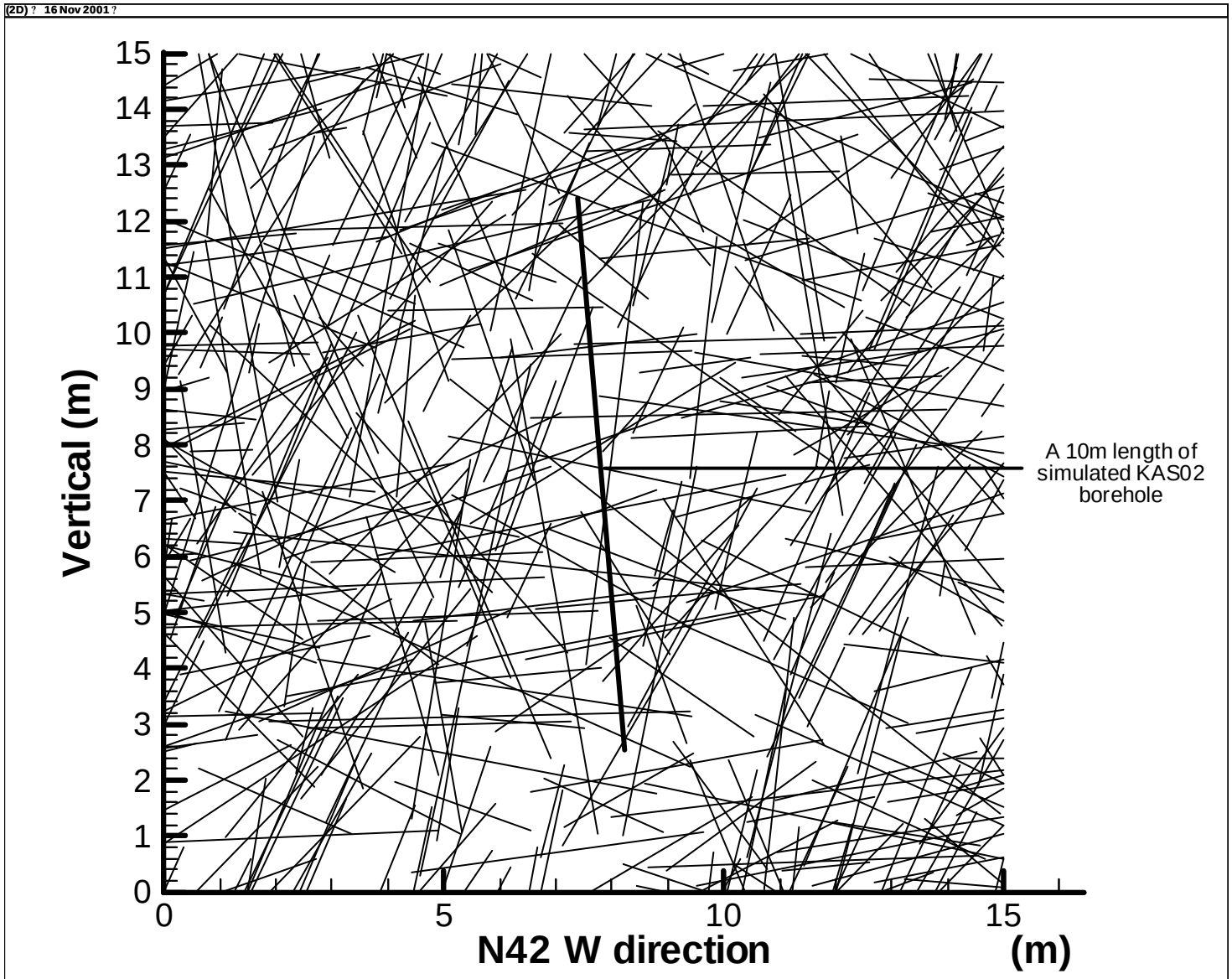

Fig. 7.12 Fracture traces obtained from fracture generation on a vertical square window of size 15 m having strike same as the trend direction of borehole KAS02 placed at the middle of 30m cube of mixed lithology rock mass (NGI box #49).

8. Conclusions

Three-dimensional Rectangular Cartesian Coordinate data provided for the NGI box were used to show the location of the NGI box in the three-dimensional space at the Äspö HRL. This box was divided into 480 blocks of 30m cubes. NGI provided the three-dimensional coordinates for the center of each cube. The orientation and location data given for the three boreholes KAS02, KA2598A and KA2511A were used to show the location of the boreholes in the three dimensional space with respect to the location of the NGI box. It was found that the borehole KA2511A only just touches the NGI box. The other two boreholes were found to intersect the NGI box. The lithology data provided for the boreholes KAS02 and KA2598A were used to select the following four 30m cubes from the NGI box, each having a different lithology which is given below: (a) NGI block number 409---Äspö diorite; (b) NGI block number 169----Småland granite; (c) NGI block number 5---fine-grained granite; (d) NGI block number 49----a mixed lithology consisting of about 49% Småland granite, 22% Äspö diorite, 15% greenstone and14% fine-grained granite.

Fracture data given for the boreholes KAS02 and KA2598A provided information on fracture orientation, spacing and 1-D fracture frequency. Raw fracture data were not provided for fracture trace length. However, some summarized information on fracture size was available through a technical report. In overall, the available information on fractures was limited with respect to both quality and quantity to build comprehensive stochastic 3-D fracture network models for the selected NGI blocks. The available fracture data were used to determine the number of fracture sets to represent each selected NGI block and then to develop statistical models of orientation, spacing and 1-D fracture frequency for the fracture sets of the selected NGI blocks incorporating corrections for sampling biases. Investigators previous experience on fracture trace length distribution and fracture size distribution in 3-D were used along with available summarized information on fracture size to develop statistical models to describe fracture size for the fracture sets of the selected NGI blocks. Also, for the selected NGI blocks 1-D fracture frequency in 3-D space and 3-D fracture frequency parameters were estimated. For each selected NGI block, fractures were generated in 3-D and fracture traces were predicted on vertical and horizontal cross sections drawn around the mid area of each block. Fracture geometry parameters estimated based on these predicted traces were then compared with fracture geometry parameter models used to build the fracture network in 3-D to validate the developed 3-D fracture network models for each NGI block. Validation attempts turned out to be successful. These selected NGI blocks with generated 3-D fracture networks will be used in a study later to estimate strength and deformability properties for the selected NGI blocks in 3-D.

References

Bingham, C., 1964. Distributions on the sphere and on the projective plane: unpbl. Doctoral dissertation. Yale Univ. 93 p.

Hermanson, J., Stigsson, M., Wei, Lingli, 1998?. A discrete fracture network model of the Äspö Zedex Tunnel section. A Technical Report submitted to Swedish Nuclear Fuel and Waste Management Co.

Kulatilake, P.H.S.W., 1985. Fitting Fisher distributions to discontinuity orientation data. Jour. of Geological Education, 33, 266-269.

Kulatilake, P.H.S.W., 1988. Stochastic joint geometry modeling: state-of-the-art. Proc. 29th US Symp. On Rock Mech., Minneapolis, Minnesota, 215-229.

Kulatilake, P.H.S.W., 1998. Software manual for FRACNTWK- a computer package to model discontinuity geometry in rock masses. Technical report submitted to Metropolitan Water District of Southern California.

Kulatilake, P.H.S.W., Chen, J., Teng, J., Shufang, X., and Pan G., 1996. Discontinuity geometry characterization for the rock mass around a tunnel close to the permanent shiplock area of the Three Gorges dam site in China. Int J Rock Mech and Min Sci., 33: 255-277.

Kulatilake, P.H.S.W., Um, J., Wang, M., Gao, H. and Chen, J. 1998. Stochastic discontinuity characterization for the metamorphic rock mass of the Arrowhead East Tunnel site, Inland Feeder Project. Technical Reports Vols.1 & 2 submitted to Metropolitan Water District of Southern California.

Kulatilake, P.H.S.W., Wathugala, D.N., Stephansson, O., 1990b. Three dimensional stochastic joint geometry modeling including a verification: a case study. Proceedings of the Int. Symp. on Rock joints, Loen, Norway, 67-74.

Kulatilake, P.H.S.W., Wathugala, D.N., Stephansson, O., 1993. Joint network modeling including a validation to an area in Stripa Mine, Sweden. Int. Jour. of Rock Mech. & Mining Science, 30, 503-526.

Kulatilake, P.H.S.W., Wu, T.H., 1984a. Sampling bias on orientation of discontinuities. Rock Mechanics and Rock Engineering, 17, 243-254.

Kulatilake, P.H.S.W., Wu, T.H., 1984b. Estimation of mean trace length of discontinuities. Rock Mechanics and Rock Engineering, 17, 215-232.

Kulatilake, P. H.S.W., Wu, T.H., 1986. Relation between discontinuity size and trace length. Proc. of the 27th U.S. Symp. on Rock Mech., 130-133.

Kulatilake, P.H.S.W., Wu, T.H., Wathugala, D.N., 1990a. Probabilistic modeling of joint orientation. Int. Jour. for Numerical and Analytical Methods in Geomechanics, 14, 325-350.

Mahtab, M.A., Yegulalp, T.M., 1984. A similarity test for grouping orientation data in rock mechanics. Proc. of the 25th U.S. Symp. on Rock Mech., 495-502.

Shanley, R. J., Mahtab, M.A., 1976. Delineation and analysis of clusters in orientation data. Mathematical Geology, 8, 9-23.

Terzaghi, R. 1965. Sources of error in joint surveys. Geotechnique, 15, 287-304.

Um, J., Morin M., Kulatilake, P.H.S.W., 2000. Discontinuity characterization and laboratory investigations conducted for the rock around and below the stationary crusher area on the north side of Esperanza pit. Technical Report submitted to Phelps Dodge Sierrita Inc., Arizona.

Wathugala, D.N., Kulatilake, P.H.S.W., Wathugala, G.W., Stephansson, O.A., 1990. A general procedure to correct sampling bias on joint orientation using a vector approach. Computer and Geotechnics, 10, 1-31.